Università degli Studi di Cagliari

Facoltà di Scienze

Dipartimento di Scienze Chimiche e Geologiche

Dottorato di Ricerca in Scienze e Tecnologie Chimiche

Settore Scientifico Disciplinare CHIM/02

XXVII Ciclo

Thermodynamical, structural, and dynamical characterization of solvent mixtures of technological interest: experimental and computational studies

PhD Thesis of:

Marianna Usula

Supervisor:

Dr. Silvia Porcedda

Coordinator:

Prof. Mariano Casu

Final Exam A.A. 2013-2014

ABSTRACT

N-methyl-2-pyrrolidone (NMP) and ionic liquids (ILs) are solvents with "green" characteristics, such as low volatility and low toxicity. They can be used as a valid alternative to the common organic solvents with a high environmental, health and safety impact. The aim of my research was to investigate their thermodynamical, structural, and dynamical properties, both in the neat state and in mixture, by using a combined approach of different experimental techniques together with computational ones.

In PAPER I, the structural effect of water on NMP over the whole concentration range were studied by using molecular dynamics (MD) simulations, wide-angle X-ray scattering experiments, and density measurements. The reason of why a density maximum is observed experimentally is explained. As an extension of the previous study we further investigated NMP-Water mixtures by a combined use of NMR spectroscopy, calorimetric measurements, and puckering analysis of MD simulations (PAPER II). These results provided additional information on the structural and dynamics changes of NMP taking place upon dilution.

In PAPER III and IV the results of volumetric and calorimetric measurements concerning some alkylammonium nitrate (XAN) ionic liquids + NMP and ethylammonium alkanoate (EAX) ionic liquids + Water binary mixtures are reported. Negative V^E and H^E values were obtained for all of the investigated systems in PAPER III and IV, indicating the presence of strong XAN + NMP and EAX + Water interactions.

List of Papers

I. **The Structural Organization of *N*-Methyl-2-Pyrrolidone + Water Mixtures: a Densitometry, X-Ray Diffraction, and Molecular Dynamics Study.** Marianna Usula, Francesca Mocci, Flaminia Cesare Marincola, Silvia Porcedda, Lorenzo Gontrani, and Ruggero Caminiti. *The Journal of Chemical Physics* 2014, 140 (12), 124503.

II. **NMR, Calorimetry, and Computational Studies of Aqueous Solutions of *N*-methyl-2-pyrrolidone.** Marianna Usula, Silvia Porcedda, Francesca Mocci, Lorenzo Gontrani, Ruggero Caminiti, and Flaminia Cesare Marincola**.** *The Journal of Physical Chemistry B* 2014, 118 (35), 10493-10502.

III. **Thermo-physical Properties of Ammonium-based Ionic Liquid + *N*-methyl-2-pyrrolidone Mixtures at 298.15 K.** Marianna Usula, Enrico Matteoli, Francesca Leonelli, Francesca Mocci, Flaminia Cesare Marincola, Lorenzo Gontrani, and Silvia Porcedda. *Fluid Phase Equilibria* 2014, 383, 49-54.

IV. **Ethylammonium Alkanoate-based Ionic Liquid + Water Mixtures: A Calorimetric and Volumetric Study at 298.15 K.** Marianna Usula, Natalia V. Plechkova, Alessandra Piras, and Silvia Porcedda. Submitted (November 2014) to *The Journal of Thermal Analysis and Calorimetry*.

Index

Chapter 1

Introduction

1. Introduction

The study of species in solution is one of the most important goals in chemistry. Indeed, solvents define a major part of the environmental performance of processes in chemical industry and also impact on cost, safety and health issues. However, as the introduction of cleaner technologies has become a major concern throughout both industry and academia, the search for alternatives to the most damaging solvents has become a high priority. An efficient way to reach this goal is to replace hazardous solvents with ones that show better EHS (environmental, health and safety) properties, commonly called "green solvents", such as organic solvents environmentally harmless or ionic liquids (ILs) that show low vapour pressure, and thus less emission to air.[1]

In the light of these considerations, as subject of my research I selected some compounds of technological interest with green characteristics, such as *a) N*-methyl-2-pyrrolidone (NMP) and *b)* room temperature ionic liquids (RTILs). In particular, the aim of this work was *i)* to understand the behaviour of NMP in water, since the presence of water influence notably its physicochemical properties; *ii)* to extend the RTILs proprieties database, and to understand the behaviour of neat ionic liquids and their mixtures with water or with NMP so as to test their applicability in substitution of neat ILs, which could have inadequate properties for a selected application.

1.1. *N*-methyl-2-pyrrolidone

Concurrently with the explosion of interest in ionic liquids, solvents with noteworthy properties quite close to ionic liquids were studied, tested

and used for several applications, such as *N*-methyl-2-pyrrolidone (Figure 1). Indeed, NMP exhibits very attractive properties such as high boiling point (477.45 K), low melting point (249.55 K), low volatility, low viscosity, large chemical and thermal resistance, and low toxicity that make it a highly useful solvent in a variety of chemical reactions. For instance, it is employed in process chemicals, coatings, engineering plastics, agricultural chemicals, electronic, and paint stripping and cleaning.[2] Among its many uses, the most interesting were discovered recently: thanks to its excellent solvating capabilities, NMP has been used to exfoliate graphene layers form graphite[3] and as solubility enhancer in the pharmaceutical industry.[4]

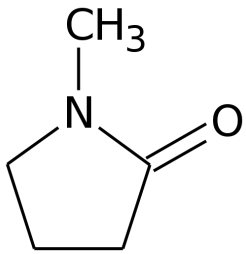

Figure 1. NMP structure.

NMP is often used as a selective solvent in combination with small amounts of water. It is well known that the presence of water in NMP has a significant impact on its properties, particularly on its solvent power and selectivity, in a number of processes. Thus, investigations of NMP-water mixtures are very important, not only scientifically but also industrially, because physico-chemical properties of NMP can be tuned by appropriate mixture composition.[5-6] The concentration dependence of different physico-chemical properties for this mixture, such as viscosity,[3–6] density,[6–8] and self-diffusion coefficients,[6] evidenced an inversion point on going from the NMP-rich region to the water-rich region. Although all these findings pointed out the presence of important interactions between water and NMP, a detailed understanding of the structural organization of this

system is still lacking.

In order to understand the macroscopic properties of NMP and, thus, to further develop its applications, it is essential to investigate the microscopic structure and dynamics of this system at molecular level. Recently, by combining energy dispersive X-ray diffraction experiments and molecular dynamics (MD) simulations with generalized AMBER force field, *Gontrani and Caminiti*[9] achieved a very good agreement between theoretical and experimental diffraction patterns of liquid NMP. The analysis of the radial distribution functions showed that the network of intermolecular C-H···O hydrogen bonds between methyl and carbonyl groups observed in the crystal structure[10] is partly preserved in the liquid structure. In 2009, *Carver et al.*[11] studied the structure of NMP extremely diluted in water by using experimental mutual diffusion coefficients complemented with MD simulations. The attention of *Carver et al.* was focused on the water behaviour in presence of NMP. Conversely, what is the behaviour of NMP in the presence of smaller percentage of water? In front of the aforementioned singular trends of the physico-chemical properties of this system, it was evident that its structural organization is strongly dependent on the water content.

Thanks to a combined use of calorimetric and density measurements, NMR spectroscopy, X-ray diffraction patterns, and MD simulations, my work provided highlighting information on the structural and dynamical changes of NMP taking place upon dilution. Furthermore, the reason why a maximum is present in the density curve is clarified by analysing the structural organization obtained by MD simulations.

1.2. Ionic Liquids

Ionic liquids (ILs) are substances belonging to molten salts which consist of large organic cations like ammonium, imidazolium or pyridinium (Figure 2) combined with anions of smaller size and more symmetrical shape such as $[NO_3]^-$, $[COO]^-$, $[BF_4]^-$, $[PF_6]^-$, $[CF_3SO_3]^-$, $[(CF_3SO_2)_2N]^-$ (Figure 3).[12]

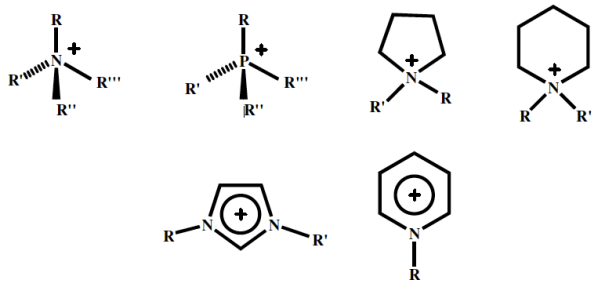

Figure 2. Some of the most common ionic liquid cations.

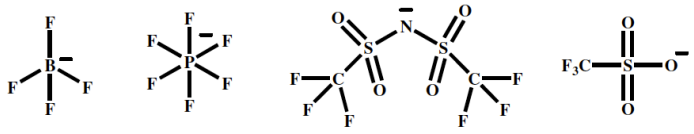

Figure 3. Some of the most common ionic liquid anions.

The significant size and the low degree of symmetry of cations result in a poor packing of this type of salts and hence most of these compounds are in the liquid state at ambient temperature. Interestingly, simply by changing the anion or cation portion a noticeable change of the properties of the ionic liquid as, for example, the viscosity, polarity, and density can be obtained. This ability has given them the appellative "*designer solvents*". Furthermore, their ionic nature gives them a vapour pressure extremely

low (often not measurable). Many ionic liquids are both air and moisture stable and having also a good thermal and chemical stability, they can be heated up to high temperatures. Thanks to all of these features, especially their non-volatile nature and good solvation properties for polar and apolar solvents, ILs attract much attention as a valid alternative to traditional volatile organic solvents *i.e.* they are largely used as solvents and catalysts in organic reactions such as in Heck,[13] Diels-Alder, Friedel-Crafts acylation and alkylation,[14] in chromatography,[15] in mass spectroscopy,[16] as lubricants,[17] and as support for the immobilization of enzymes.[18,19]

The number of ionic liquids that can be synthesized is extremely high (estimated greater than 10^{14}), then the synthesis and characterization of all possible ionic liquids is not a feasible approach to a rational and optimized use of these solvents. It is necessary to investigate ILs at the molecular level and to obtain, for each ionic liquid class, a structure-property correlation. This could be done using different experimental techniques together with computational studies.

Over the last years, the main goal of numerous research groups and industries was to investigate a great number of different ionic liquids for a range of novel applications.[20–29] The structure and dynamics of RTILs in the neat state or in binary mixtures with organic solvents or with water are largely studied using different experimental techniques such as X-ray diffraction (XRD), Infrared Spectroscopy (IR), Raman Spectroscopy, Multi Nuclear Resonance Spectroscopy (NMR), and Molecular Dynamics (MD) simulations. A short overview on how experimental techniques and computational studies has greatly contributed to the knowledge of the

structure and dynamics of some ionic liquids is given below.

Imidazolium- and alkylammonium-based ILs are among the most studied families of ionic liquids. Among the most recent revealing works, there is the study of six COOH-functionalized imidazolium ionic liquids crystal structures, where the presence of hydrogen bonds in the hydrophobic and hydrophilic ionic liquids were highlighted.[30] The presence of H-bonds is of paramount importance for ionic liquids because it can significantly influence a number of physical properties.[31] *Chen et al.*[32] studied the hydrogen-bonding interaction between 1-ethyl-3-methyl-imidazolium acetate ([EMIM][Ac]) and seven solvents (D_2O, CD_3OD, CD_3CN, d_6-DMSO, CD_3COCD_3, C_6D_6, and $CDCl_3$) by using AT-IR and NMR experiments. This study evidenced that along with the increasing of solvent concentration, the H-bonding interaction in the neat IL decreases, while the hydrogen bonding interaction between [EMIM][Ac] and solvent increases. *Marincola et al.*[33] studied by NMR spectroscopy the interaction of water with two imidazolium-based ionic liquids showing a packed structure where head-to-head, head-to-tail, and tail-to-tail contacts occur and where the site of maximal mobility restriction is at the polar head. *Remsing et al.*[34] combined NMR experiments with MD simulations to investigate the behaviour of 1-ethyl-3-methyl-imidazolium chloride in water and dimethylsulfoxide solvents. Both experimental and MD results revealed that in concentrate IL aqueous solutions, water molecules interact preferentially with the anion and the imidazolium ring, exchanging with Cl^- ions around the ring and thus weakening the interactions between cations and anions.

As far as the alkylammonium-based ionic liquids, the structure of ethyl- and *n*-propylammonium nitrate (EAN and PAN, respectively) was largely studied in different works[35–42] and a thorough description of the H-bonding interactions observed in their structure was provided. A recent paper by *Kirchner et al.*[43] and recent neutron scattering studies on EAN and PAN[44–46] showed the existence of structural heterogeneities on a 10 Å scale which are compatible with the existence of alkyl chain aggregation that is the driving force responsible for the formation of micellar aggregates in other structured liquids. ILs are largely used as solvent/catalyst in organic reactions leading high yields;[47] EAN is a useful polar stationary phase for gas-liquid chromatography[48] and it was used to enhance the recovery of denatured-reduced hen egg white lysozyme showing the ability to prevent aggregation of the denatured protein.[49] Greaves and co-workers[35] developed a high-throughput approach in order to prepare and dry a series of ILs from 48 Brønsted acid-base combinations. Visual screens were developed to identify which acid-base combinations formed protic ionic liquids (PILs), and of those, which PILs were likely to have high surface tensions. Alkylammoium alkanoate is another ionic liquid class which attracted the attention of the scientific community.[50–56] Ethyl-, *n*-propyl-, and *n*-butylammonium methanoate (EAM, PAM, and BAM, respectively) were synthesized and tested as mobile-phase for reversed phase liquid chromatography. EAM, which has a polarity similar to that of methanol or acetonitrile, has been indicated as suitable solvent to be used as mobile phase in liquid chromatography. [52,53,57] *Chhotaray et al.*, [54] reported density, viscosity, and velocity of sound values at different temperatures and

atmospheric pressure for five ILs: propylammonium methanoate or ethanoate and 3-hydroxy-propylammonium methanoate or ethanoate or trifluoroethanoate.

In addition to the numerous structural and dynamical studies of ILs, experimental and/or theoretical thermodynamic studies on pure ILs and their mixtures with organic solvents[58–64] or water[65–68] were reported. *Heintz*[58] reviewed the developments of thermodynamic and thermophysical studies of ILs + non-aqueous solvent mixtures including an overview on the experimental data available. The review is limited to systems having the most promising chance to be successfully used in different fields of chemistry and chemical engineering.

Characterization of mixtures containing ionic liquids and organic solvents or water is thus required to test their applicability in substitution of neat compounds which could have inappropriate properties for a selected application, *i.e.* limited solvent power range, high viscosity, etc.[12] In particular, since most of ILs are quite hygroscopic and the water has a significant impact on their properties, for a proper and safety use of ILs, it is necessary to investigate how water or other solvents affect their physico-chemical properties. [69]

Porcedda et al.[65] studied some thermophysical properties of EAN or PAN + Water mixtures; the positive excess enthalpy implicates a weaker interaction upon mixing. It can be stated that the intermolecular forces between the same kind of ions or molecules (IL–IL and water–water interactions) are stronger than those among dissimilar ones. As the hydrophobic/hydrophilic ratio increases, along with the length of the alkyl

chain in the ILs, the specific interactions IL–Water become less important. Diisopropylethylammonium methanoate + Water mixtures have been investigated by *Anouti et al.*, [55] to obtain density, heat capacity, refractive index, and excess quantities values. Another promising alkanoate-based IL for practical applications, because of its low toxicity, is 2-hydroxyethylammonium methanoate, which has been synthesized for the first time by Bicak in 2005.[50] Density and ultrasonic velocity of their mixtures with water or methanol or ethanol have been measured by *Iglesias et al*. [56] Recently, some studies have pointed out the interesting properties of NMP with some ILs.[62–64] A series of ammonium based ionic liquids, similar to those considered in this thesis, with *N*-methyl-2-pyrrolidone mixtures were studied by *Kavitha et al*.;[62–64] ILs + NMP showed structure-based and temperature dependent properties.

Despite the rapid and incessantly growth of scientific papers, a satisfactory knowledge of structural, dynamical, and thermophysical properties of liquid mixtures containing ILs, which is important for designing of any technological processes, it is far from being achieved. In order to improve the knowledge on these properties, a systematic study of different ILs was carried out by using calorimetry, densitometry, NMR, and FT-IR experiments.

The selected ILs for this work belong to the alkylammonium *i)* nitrate (Figure 4) and *ii)* alkanoate families (Figure 5). In detail, they are:

i) ethylammonium nitrate (EAN), *n*-propylammonium nitrate (PAN), *n*-butylammonium nitrate (BAN), and 2-methoxyethylammonium nitrate (MEOEAN).

ii) ethylammonium methanoate (EAM), ethylammonium propanoate (EAP), and ethylammonium butanoate (EAB).

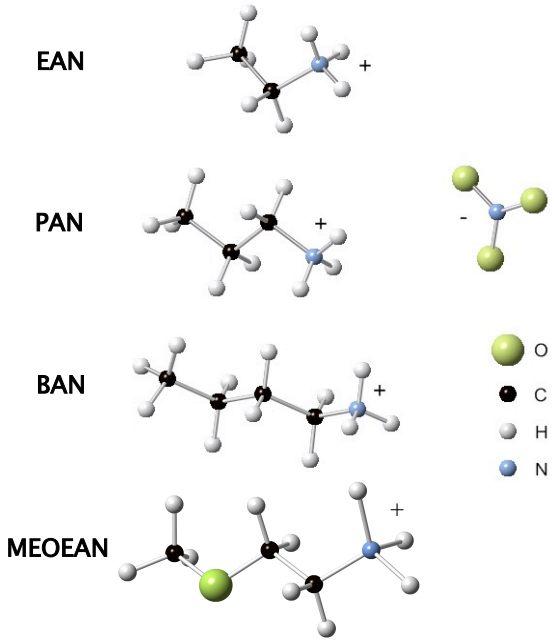

Figure 4. Alkylammonium nitrate ionic liquids selected for this work.

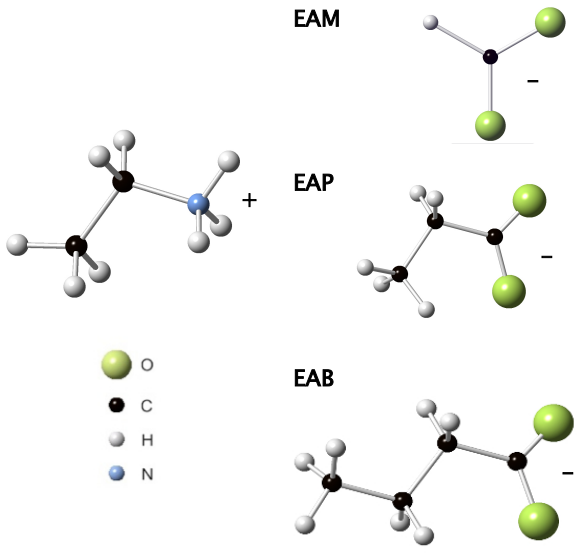

Figure 5. Etylammonium alkanoate ionic liquids selected for this work.

REFERENCES

(1) Scammells, P. J.; Scott, J. L.; Singer, R. D. Ionic Liquids: The Neglected Issues. *Aust. J. Chem.* **2005**, *58*, 155–169.

(2) *N*-Methyl-2-pyrrolidone Storage and Handling. BASF Intermediates. New Jersey. **1998**.

(3) Hernandez, Y.; Nicolosi, V.; Lotya, M.; Blighe, F. M.; Sun, Z.; Sukanta, D.; Mcgovern, I. T.; Holland, B.; Byrne, M.; Gun'ko, I. K.; et al. High-Yield Production of Graphene by Liquid-Phase Exfoliation of Graphite. *Nat. Nanotechnol.* **2008**, *3(9)*, 563-568.

(4) Sanghvi, R.; Narazaki, R.; Machatha, S. G.; Yalkowsky, S. H. Solubility Improvement of Drugs Using N-Methyl Pyrrolidone. *AAPS PharmSciTech* **2008**, *9*, 366–376.

(5) Chen, G.; Hou, Y.; Knapp, H. Diffusion Coefficients, Kinematic Viscosities, and Refractive Indices for Heptane + Ethylbenzene, Sulfolane + 1-Methylnaphtalene, Water + *N*,*N*-Dimethylformamide, Water + Methanol, Water + *N*-Formylmorpholine, and Water + *N*-Methylpyrrolidone. *J. Chem. Eng. Data* **1995**, *40*, 1005–1010.

(6) Ambrosone, L.; D'Errico, G.; Sartorio, R.; Vitagliano, V. Analysis of Velocity Cross-Correlation and Preferential Solvation for the System *N*-Methylpyrrolidone-Water at 20 °C. *J. Chem. Soc. Faraday Trans* **1995**, *91*, 1339–1344.

(7) Macdonald, D. D.; Dunay, D.; Hanlon, G.; Hyne, J. B. Propierties of the *N*-Methyl-2-Pyrrolidinone-Water System. *Can. J. Chem. Eng.* **1971**, *49*, 420–423.

(8) Henni, A.; Hromek, J. J.; Tontiwachwuthikul, P.; Chakma, A. Volumetric Properties and Viscosities for Aqueous *N*-Methyl-2-Pyrrolidone Solutions from 25 °C to 70 °C. *J. Chem. Eng. Data* **2004**, *49*, 231–234.

(9) Gontrani, L.; Caminiti, R. The Structure of Liquid *N*-Methyl Pyrrolidone Probed by X-Ray Scattering and Molecular Simulations. *J. Chem. Phys.* **2012**, *136*, 074505.

(10) Muller, G.; Lutz, M.; Harder, S. Methyl Group Conformation-Determining Intermolecular C-H···O Hydrogen Bonds: Structure of *N*-Methyl-2-Pyrrolidone. *Acta Crystallogr. Sect. B* **1996**, *52*, 1014–1022.

(11) Carver, T. J.; Drew, M. G. B.; Rodger, P. M. Molecular Dynamics Calculations of *N*-Methylpyrrolidone in Liquid Water. *Phys Chem. Chem. Phys.* **1999**, *1*, 1807–1816.

(12) *Ionic Liquids. Vol. 9*; Kirchner, B., Ed.; Springer: Leipzig, Germany, **2010**.

(13) Kirchhecker, S.; Antonietti, M.; Esposito, D. Hydrothermal Decarboxylation of Amino Acid Derived Imidazolium Zwitterions: A Sustainable Approach towards Ionic Liquids. *Green Chem.* **2014**, *16*, 3705.

(14) Welton, T. Room-Temperature Ionic Liquids: Solvents for Synthesis and Catalysis. *Chem. Rev.* **1999**, *99*, 2071–2083.

(15) Anderson, J. L.; Armstrong, D. W. High-Stability Ionic Liquids. A New Class of Stationary Phases for Gas Chromatography Stationary Phases. *Anal. Chem.* **2003**, *75*, 4851–4858.

(16) Sun, P.; Armstrong, D. W. Ionic Liquids in Analytical Chemistry. *Anal. Chim. Acta* **2010**, *661*, 1–16.

(17) Tang, S.; Baker, G. a; Zhao, H. Ether- and Alcohol-Functionalized Task-Specific Ionic Liquids: Attractive Properties and Applications. *Chem. Soc. Rev.* **2012**, *41*, 4030–4066.

(18) Greaves, T. L.; Weerawardena, A.; Krodkiewska, I.; Drummond, C. J. Protic Ionic Liquids: Physicochemical Properties and Behavior as Amphiphile Self-Assembly Solvents. *J. Phys. Chem. B* **2008**, *112*, 896–905.

(19) Park, S.; Kazlauskas, R. J. Biocatalysis in Ionic Liquids – Advantages beyond Green Technology. *Curr. Opin. Biotechnol.* **2003**, *14*, 432–437.

(20) Earle, M. J.; Esperança, J. M. S. S.; Gilea, M. A.; Lopes, J. N. C.; Rebelo, L. P. N.; Magee, J. W.; Seddon, K. R.; Widegren, J. A. The Distillation and Volatility of Ionic Liquids. *Nature* **2006**, *439*, 831–834.

(21) Constantinescu, D.; Weingärtner, H.; Herrmann, C. Protein Denaturation by Ionic Liquids and the Hofmeister Series: A Case Study of Aqueous Solutions of Ribonuclease A. *Angew. Chem. Int. Ed. Engl.* **2007**, *46*, 8887–8889.

(22) Plechkova, N. V; Seddon, K. R. Applications of Ionic Liquids in the Chemical Industry. *Chem. Soc. Rev.* **2008**, *37*, 123–150.

(23) Attri, P.; Venkatesu, P.; Kumar, A.; Byrne, N. A Protic Ionic Liquid Attenuates the Deleterious Actions of Urea on A-Chymotrypsin. *Phys. Chem. Chem. Phys.* **2011**, *13*, 17023–17026.

(24) Henderson, L. C.; Byrne, N. Rapid and Efficient Protic Ionic Liquid-Mediated Pinacol Rearrangements under Microwave Irradiation. *Green Chem.* **2011**, *13*, 813.

(25) Yue, Y.; Jiang, X.-Y.; Yu, J.-G.; Tang, K.-W. Enantioseparation of Mandelic Acid Enantiomers in Ionic Liquid Aqueous Two-Phase Extraction Systems. *Chem. Pap.* **2013**, *68*, 465–471.

(26) Hernoux-Villière, A.; Lévêque, J.-M.; Kärkkäinen, J.; Papaiconomou, N.; Lajunen, M.; Lassi, U. Task-Specific Ionic Liquid for the Depolymerisation of Starch-Based Industrial Waste into High Reducing Sugars. *Catal. Today* **2014**, *223*, 11–17.

(27) Suzuki, T.; Kono, K.; Shimomura, K.; Minami, H. Preparation of Cellulose Particles Using an Ionic Liquid. *J. Colloid Interface Sci.* **2014**, *418*, 126–131.

(28) Attri, P.; Venkatesu, P.; Kumar, A. Temperature Effect on the Molecular Interactions between Ammonium Ionic Liquids and *N*,*N*-Dimethylformamide. *J. Phys. Chem. B* **2010**, *114*, 13415–13425.

(29) Fojutowski, A.; Pernak, J.; Przybylska, W.; Stangierska, A.; Zabielska-Matejuk, J. Patent Number: PL395817-A1, **2013**.

(30) Xuan, X.-P.; Chang, L.-L.; Zhang, H.; Wang, N.; Zhao, Y. Hydrogen Bonds in the Crystal Structure of Hydrophobic and Hydrophilic COOH-Functionalized Imidazolium Ionic Liquids. *CrystEngComm* **2014**, *16*, 3040.

(31) Fumino, K.; Peppel, T.; Geppert-Rybczyńska, M.; Zaitsau, D. H.; Lehmann, J. K.; Verevkin, S. P.; Köckerling, M.; Ludwig, R. The Influence of Hydrogen Bonding on the Physical Properties of Ionic Liquids. *Phys. Chem. Chem. Phys.* **2011**, *13*, 14064–14075.

(32) Chen, S.; Vijayaraghavan, R.; MacFarlane, D. R.; Izgorodina, E. I. Ab Initio Prediction of Proton NMR Chemical Shifts in Imidazolium Ionic Liquids. *J. Phys. Chem. B* **2013**, *117*, 3186–3197.

(33) Marincola, F. C.; Piras, C.; Russina, O.; Gontrani, L.; Saba, G.; Lai, A. NMR Investigation of Imidazolium-Based Ionic Liquids and Their Aqueous Mixtures. *ChemPhysChem* **2012**, *13*, 1339–1346.

(34) Remsing, R. C.; Hernandez, G.; Swatloski, R. P.; Massefski, W. W.; Rogers, R. D.; Moyna, G. Solvation of Carbohydrates in N , N # -Dialkylimidazolium Ionic Liquids : A Multinuclear NMR Spectroscopy Study NMR Spectroscopy Study. *J. Phys. Chem. B* **2008**, *112*, 11071–11078.

(35) Greaves, T. L.; Ha, K.; Muir, B. W.; Howard, S. C.; Weerawardena, A.; Kirby, N.; Drummond, C. J. Protic Ionic Liquids (PILs) Nanostructure and Physicochemical Properties: Development of High-Throughput Methodology for PIL Creation and Property Screens Tamar. *Phys. Chem. Chem. Phys.* **2015**.

(36) Atkin, R.; Warr, G. G. The Smallest Amphiphiles: Nanostructure in Protic Room-Temperature Ionic Liquids with Short Alkyl Groups. *J. Phys. Chem. B* **2008**, *112*, 4164–4166.
(37) Niga, P.; Wakeham, D.; Nelson, A.; Warr, G. G.; Rutland, M.; Atkin, R. Structure of the Ethylammonium Nitrate Surface: An X-Ray Reflectivity and Vibrational Sum Frequency Spectroscopy Study. *Langmuir* **2010**, *26*, 8282–8288.
(38) Campetella, M.; Gontrani, L.; Bodo, E.; Ceccacci, F.; Marincola, F. C.; Caminiti, R. Conformational Isomerisms and Nano-Aggregation in Substituted Alkylammonium Nitrates Ionic Liquids: An X-Ray and Computational Study of 2-Methoxyethylammonium Nitrate. *J. Chem. Phys.* **2013**, *138*, 184506.
(39) Ridings, C.; Warr, G. G.; Andersson, G. G. Composition of the Outermost Layer and Concentration Depth Profiles of Ammonium Nitrate Ionic Liquid Surfaces. *Phys. Chem. Chem. Phys.* **2012**, *14*, 16088–16095.
(40) Hayes, R.; Imberti, S.; Warr, G. G.; Atkin, R. The Nature of Hydrogen Bonding in Protic Ionic Liquids. *Angew. Chem. Int. Ed. Engl.* **2013**, *52*, 4623–4627.
(41) Greaves, T. L.; Kennedy, D. F.; Weerawardena, A.; Tse, N. M. K.; Kirby, N.; Drummond, C. J. Nanostructured Protic Ionic Liquids Retain Nanoscale Features in Aqueous Solution While Precursor Brønsted Acids and Bases Exhibit Different Behavior. *J. Phys. Chem. B* **2011**, *115*, 2055–2066.
(42) Ishiguro, S.; Umebayashi, Y.; Kanzaki, R.; Fujii, K. Structure, Solvation, and Acid–base Property in Ionic Liquids. *Pure Appl. Chem.* **2010**, *82*, 1927–1941.
(43) Zahn, S.; Thar, J.; Kirchner, B. Structure and Dynamics of the Protic Ionic Liquid Monomethylammonium Nitrate ($[CH_3NH_3][NO_3]$) from Ab Initio Molecular Dynamics Simulations. *J. Chem. Phys.* **2010**, *132*, 124506.
(44) Song, X.; Hamano, H.; Minofar, B.; Kanzaki, R.; Fujii, K.; Kameda, Y.; Kohara, S.; Watanabe, M.; Ishiguro, S.; Umebayashi, Y. Structural Heterogeneity and Unique Distorted Hydrogen Bonding in Primary Ammonium Nitrate Ionic Liquids Studied by High-Energy X-Ray Diffraction Experiments and MD Simulations. *J. Phys. Chem. B* **2012**, *116*, 2801–2813.
(45) Hayes, R.; Imberti, S.; Warr, G. G.; Atkin, R. Amphiphilicity Determines Nanostructure in Protic Ionic Liquids. *Phys. Chem. Chem. Phys.* **2011**, *13*, 3237–3247.
(46) Zahn, S.; Thar, J.; Kirchner, B. Structure and Dynamics of the Protic Ionic Liquid Monomethylammonium Nitrate ($[CH_3NH_3][NO_3]$) from Ab Initio Molecular Dynamics Simulations. *J. Chem. Phys.* **2010**, *132*, 124506.
(47) Hu, Y.; Wei, P.; Huang, H.; Le, Z.; Chen, Z. Organic Reactions in Ionic Liquids: Ionic Liquid Ethylammonium Nitrate–Promoted Knoevenagel Condensation of Meldrum's Acid With Aromatic Aldehydes. *Synth. Commun.* **2005**, *35*, 2955–2960.
(48) Pacholec, F.; Butler, H. T.; Poole, F. Molten Organic Salt Phase for Gas-Liquid Chromatography. *Anal. Chem.* **1982**, *54*, 1938–1941.
(49) Summer, C. A.; Flowers, R. A. Protein Renaturation by the Liquid Organic Salt Ethylammonium Nitrate. *Protein Sci.* **2000**, *9*, 2001–2008.
(50) Bicak, N. A New Ionic Liquid: 2-Hydroxy Ethylammonium Formate. *J. Mol. Liq.* **2005**, *116*, 15–18.
(51) Welton, T. Ionic Liquids in Catalysis. *Coord. Chem. Rev.* **2004**, *248*, 2459–2477.

(52) Waichigo, M. M.; Riechel, T. L.; Danielson, N. D. Ethylammonium Acetate as a Mobile Phase Modifier for Reversed Phase Liquid Chromatography. *Chromatographia* **2004**, *61*, 17–23.
(53) Waichigo, M. M.; Danielson, N. D. Ethylammonium Formate as an Organic Solvent Replacement for Ion-Pair Reversed-Phase Liquid Chromatography. *J. Chromatogr. Sci.* **2006**, *44*, 607–614.
(54) Chhotaray, P. K.; Gardas, R. L. Thermophysical Properties of Ammonium and Hydroxylammonium Protic Ionic Liquids. *J. Chem. Thermodyn.* **2014**, *72*, 117–124.
(55) Anouti, M.; Caillon-Caravanier, M.; Dridi, Y.; Jacquemin, J.; Hardacre, C.; Lemordant, D. Liquid Densities, Heat Capacities, Refractive Index and Excess Quantities for {protic Ionic Liquids + water} Binary System. *J. Chem. Thermodyn.* **2009**, *41*, 799–808.
(56) Iglesias, M.; Torres, a.; Gonzalez-Olmos, R.; Salvatierra, D. Effect of Temperature on Mixing Thermodynamics of a New Ionic Liquid: {2-Hydroxy Ethylammonium Formate (2-HEAF) + short Hydroxylic Solvents}. *J. Chem. Thermodyn.* **2008**, *40*, 119–133.
(57) Waichigo, M. M.; Danielson, N. D. Comparison of Ethylammonium Formate to Methanol as a Mobile-Phase Modifier for Reversed-Phase Liquid Chromatography. *J. Sep. Sci.* **2006**, *29*, 599–606.
(58) Heintz, A. Recent Developments in Thermodynamics and Thermophysics of Non-Aqueous Mixtures Containing Ionic Liquids. A Review. *J. Chem. Thermodyn.* **2005**, *37*, 525–535.
(59) Diedrichs, A.; Gmehling, J. Measurement of Heat Capacities of Ionic Liquids by Differential Scanning Calorimetry. *Fluid Phase Equilib.* **2006**, *244*, 68–77.
(60) Gonzàlez, E. J.; Gonzàlez, B.; Calvar, N.; Domìnguez, A. Physical Properties of Binary Mixtures of the Ionic Liquid 1-Ethyl-3-Methylimidazolium Ethyl Sulfate with Several Alcohols at T=298.15, 313.15, and 328.15) K and Atmospheric Pressure. *J. Chem. Eng. Data* **2007**, *52*, 1641–1648.
(61) Kandil, M. E.; Marsh, K. N.; Goodwin, A. R. H. Measurement of the Viscosity, Density, and Electrical Conductivity of 1-Hexyl-3-Methylimidazolium Bis(trifluorosulfonyl)imide at Temperatures between (288 and 433) K and Pressures below 50 MPa. *J. Chem. Eng. Data* **2007**, *52*, 2382–2387.
(62) Kavitha, T.; Attri, P.; Venkatesu, P.; Rama Devi, R. S.; Hofman, T. Influence of Temperature on Thermophysical Properties of Ammonium Ionic Liquids with N-Methyl-2-Pyrrolidone. *Thermochim. Acta* **2012**, *545*, 131–140.
(63) Kavitha, T.; Attri, P.; Venkatesu, P.; Rama Devi, R. S.; Hofman, T. Temperature Dependence Measurements and Molecular Interactions for Ammonium Ionic Liquid with *N*-Methyl-2-Pyrrolidone. *J. Chem. Thermodyn.* **2012**, *54*, 223–237.
(64) Kavitha, T.; Attri, P.; Venkatesu, P.; Devi, R. S. R.; Hofman, T. Influence of Alkyl Chain Length and Temperature on Thermophysical Properties of Ammonium-Based Ionic Liquids with Molecular Solvent. *J. Phys. Chem. B* **2012**, *116*, 4561–4574.
(65) Porcedda, S.; Marongiu, B.; Schirru, M.; Falconieri, D.; Piras, A. Excess Enthalpy and Excess Volume for Binary Systems of Two Ionic Liquids + Water. *J. Therm. Anal. Calorim.* **2010**, *103*, 29–33.
(66) Rodrìguez, Héctor; Brennecke, J. F. Temperature and Composition Dependence of the Density and Viscosity of Binary Mixtures of Water + Ionic Liquid. *J. Chem. Eng. Data* **2006**, *51*, 2145–2155.

(67) García-Miaja, G.; Troncoso, J.; Romaní, L. Excess Enthalpy, Density, and Heat Capacity for Binary Systems of Alkylimidazolium-Based Ionic Liquids + water. *J. Chem. Thermodyn.* **2009**, *41*, 161–166.

(68) Guan, W.; Li, L.; Wang, H.; Tong, J.; Yang, J. Studies on Thermochemical Properties of Ionic Liquids Based on Transition Metal. *J. Therm. Anal. Calorim.* **2008**, *94*, 507–510.

(69) Seddon, K. R.; Stark, A.; Torres, M.-J. Influence of Chloride, Water, and Organic Solvents on the Physical Properties of Ionic Liquids. *Pure Appl. Chem.* **2000**, *72*, 2275–2287.

Chapter 2

Experimental Section

2. Experimental Section

2.1. Materials

Compounds, structures, and abbreviations of materials used in this thesis are reported in Table 1.

N-methyl-2-pyrrolidone (purity > 99.5 %) was purchased from Sigma-Aldrich. Ethylammonium nitrate and *n*-propylammonium nitrate (purity > 97 %) were purchased from Iolitec. 2-methoxy-ethylammonium nitrate and *n*-butylammonium nitrate were prepared by F. Leonelli (Università "La Sapienza" – Roma) following a previously reported procedure.[1,2] Solvents (LC-MS grade), 2-methoxyethylamine (99 %) and *n*-butylamine were purchased from Aldrich. Nitric acid (65 % w/w) was purchased from Carlo Erba.

Alkylammonium nitrate ionic liquids (XAN) and NMP were dried for 5 days at room temperature under high vacuum ($6 \cdot 10^{-2}$ Torr) over P_2O_5 before using.

Ethylammonium alkanoate (EAX) ionic liquids were synthesised during my research stay at the QUILL laboratories of the Queen's University Belfast in the frame of the Erasmus PLACEDOC program. The adopted procedure is the following: alkylcarboxylic acid (methanoic, > 98 % puriss. Glacial, Riedel-de Haën; propanoic, ≥ 99.5 %, Sigma Aldrich; butanoic, ≥ 99 %, Sigma Aldrich) was added dropwise to an equimolar amount of an aqueous ethylamine solution (70 % in water, FlukaChemika) in a one-neck one-litre round-bottom flask, cooled with liquid N_2 (as the reaction is exothermic). The flask was kept closed after each acid addition, and cooled by adding more liquid N_2 when necessary. The reaction is fairly exothermic

and maintaining the temperature low is important. After all the acid had been added, the reaction was left to warm up to room temperature for approximately two hours, and then stirred at room temperature for one hour. Water was removed by freeze-drying technique at 0.03 mbar pressure. After a 12 h cycle, the water content was checked by Karl-Fischer (KF) titration. The result showed over 3 w/w % water content, so the freeze-drying cycle was repeated twice more, until no decrease in the water content was observed. The resulting ethylammonium methanoate, EAM (97 % yield); ethylammonium propanoate, EAP (97 % yield); and ethylammonium butanoate, EAB (98 % yield) are extremely hygroscopic light yellow liquids, therefore they were kept under N_2 atmosphere, in a glove box until use.

The ILs with NMP or with water mixtures were prepared by mass as follow: *i)* for ILs (1) + NMP (2) mixtures the proper amounts of ILs and NMP were weighted with an analytical balance (± 0.0001 g) in screw-cap glass vials in a glove-bag under nitrogen atmosphere; *ii)* for ILs (1) + water (2) mixtures, the procedure was analogous to the previous one but the proper amounts of water to give different compositions samples were added after removing the vials from the bag.

For density determinations, all materials were degassed for about 2 h by means of an ultrasonic device (WVR model USC100T - 45 kHz, 30 W).

For NMR analysis, mixtures were moved to a nitrogen-filled glove-bag where it was transferred to a 5 mm NMR tube.

Table 1
Compounds: name with abbreviation, source, purity, final water content, and purification and analysis methods.

Chemical name (abbreviation)	Source	Purity / %	Purification method	Final water content /mole fraction	Analysis method
N-methyl-2-pyrrolidone (NMP)	Sigma-Aldrich	>99.5	dehydration *in vacuo*	< 0.02	^{1}H-NMR
ethylammonium nitrate (EAN)	Iolitec	>97	dehydration *in vacuo*	< 0.02	^{1}H-NMR
n-propylammonium nitrate (PAN)	Iolitec	>97	dehydration *in vacuo*	< 0.02	^{1}H-NMR
n-butylammonium nitrate (BAN)	synthesis	-	dehydration *in vacuo*	< 0.01	^{1}H-NMR
2-methoxyethylammonium nitrate (MEOEAN)	synthesis	-	dehydration *in vacuo*	< 0.01	^{1}H-NMR
ethylammonium methanoate (EAM)	synthesis	-	dehydration *in vacuo*	< 0.006	KF titration
ethylammonium propanoate (EAP)	synthesis	-	dehydration *in vacuo*	< 0.006	KF titration
ethylammonium butanoate (EAB)	synthesis	-	dehydration *in vacuo*	< 0.006	KF titration

2.2. Characterizations

2.2.1. Lewis acidity measurement and data treatment

An efficient employment of ionic liquids in scientific research and technical applications requires a deep knowledge on their physico-chemical properties, which are extremely connected with the IL-IL and/or IL-solute interactions. These interactions and their strength, influenced by intermolecular van der Waals forces, intermolecular Coulomb interactions, and ability of a solvent to form hydrogen bonds, can be quantified by using the so-called "donor–acceptor concept" approach developed by Victor Gutmann.[3,4] He defined the acceptor number (AN), as a measure for the

electrophilic properties of a solvent, specifically the ability to accept electron pairs. The Gutmann AN[4] is a well-established quantitative measure of Lewis acidity and it could help to predict the intermolecular interactions of nucleophiles and other electron-rich substrates with the IL cations. It is determined from the ^{31}P-NMR chemical shift of a triethylphosphine oxide (TEPO) probe molecule, dissolved in the respective pure solvent.[4] RTIL-TEPO complexes induce a change in the chemical shift in the ^{31}P-NMR spectrum, which is directly proportional to the AN. To obtain precise data, the ^{31}P NMR chemical shifts are measured at several concentrations of TEPO as recommended by Gutmann, because the chemical shifts are affected by concentration of TEPO and the magnetic permeability of the solvent. These data are then extrapolated to infinite dilution, δ_{inf} (^{31}P chemical shift at infinite dilution of TEPO). The AN value is calculated by using the following equation:

$$AN = 2.348\ \delta_{inf} \qquad 1)$$

The proportionality constant in eq. 1 has been empirically determined from the endpoints of hexane (AN = 0) and 10^{-3} M solution in 1,2-dichloroethane of antimony(V) chloride (AN = 100).

Sample preparation was done in the glove-box. Three samples (≈ 1 g) of each alkylammonium alkanoate were weighed into a sample vial (10 cm^3) containing a magnetic stirring bar. The vial was left on the balance, and TEPO wasc added (approximately 3, 5 or 7 mol % per mol of ionic liquid cation). After a 5 hours-long stirring of the sample to ensure the complete dissolution, the liquids were loaded into NMR tubes (5 mm, borosilicate glass), each containing a capillary with DMSO-d$_6$. The tubes were closed,

taken out of the glove-box immediately prior to measurement. ^{31}P-NMR spectra were acquired at 121.452 MHz using a Bruker 300 spectrometer. All samples were measured at 300.15 K.

2.2.2. Volumetric measurements and data treatment

The density, or more precisely mass density of a sample, is one of its most important and easily-measured physical properties. It is defined as the mass of a sample divided by its volume and its values are currently expressed in the SI units kg m^{-3} and more often in the submultiple g cm^{-3}.[5] Densities are widely used to identify pure substances and to characterize and estimate the composition of many kinds of mixtures. The densities of the liquid mixtures and the pure compounds were measured, at 298.15 K, by means of a vibrating tube densitometer (model DMA 58-Anton Paar - Gratz, Austria). Accuracy in the temperature was better than ±0.01 K. Density precision and accuracy were ±0.00001 and ±0.00005 g/cm^3, respectively. The instrument was calibrated before each experimental run using dry air and distilled water as references. Solutions were prepared by weight in septum-capped vials of approximately 2 cm^3 using needles and syringes to transfer liquids. The molar volumes, V_m, were obtained from:

$$V_m = \frac{(x_1 M_1 + x_2 M_2)}{\rho_{mix}} \qquad 2)$$

The excess molar volumes, V^E, defined as the difference between real and ideal mixing volume at a given temperature, can be calculated as the difference between the mixture molar volume and the volume of the

necessary amounts of pure liquids, from the molar mass, M_k, and the density, ρ_k, the mole fraction, x_k, of the component k (k = 1 or 2):

$$V^{\mathrm{E}} = V_{\mathrm{m}} - \frac{(x_1 M_1)}{\rho_1} - \frac{(x_2 M_2)}{\rho_2} \qquad 3)$$

V^{E} data were fitted by means of the Redlich-Kister (RK) equation having the form:

$$V^{\mathrm{E}} = x_1 x_2 \sum_{i=0}^{n-1} \mathrm{a}_i (x_1 - x_2)^i \qquad 4)$$

The absolute standard deviation of the fit, $\sigma(V^{\mathrm{E}})$, was calculated by the following equation:

$$\sigma(V^{\mathrm{E}}) = \sqrt{\frac{\Sigma(V^{\mathrm{E}}_{j,\mathrm{calc}} - V^{\mathrm{E}}_{j,\mathrm{exp}})^2}{N - n}} \qquad 5)$$

where N is the number of experimental points and n is the number of coefficients.

Excess molar volumes at infinite dilution, $\overline{V}_k^{\mathrm{E},\infty}$, of each component k, is defined as the difference between the molar volumes at infinite dilution and in the neat state: $\overline{V}_k^{\mathrm{E},\infty} = \overline{V}_k^{\infty} - V_k^*$. Their values were calculated from the RK parameters by means of the following equation:

$$\overline{V}_k^{\mathrm{E},\infty} = \sum_{i=0}^{n} (-1)^k a_i \qquad 6)$$

Furthermore, from the standard deviations of the above RK parameters we calculated the SD, and the uncertainties, u (u = 2·SD), of the excess molar

volumes at equimolar composition, $V_{0.5}^{\mathrm{E}}$, and of the partial molar volumes of each component at infinite dilution, $\bar{V}_k^{\mathrm{E},\infty}$.

The procedure was checked by comparison of our experimental V^{E} data of the water + ethanol system with reliable literature data.[6] We found a difference lower than 0.8 % in the whole composition range.

2.2.3. Calorimetric measurements and data treatment

Heats of mixing coinciding with excess enthalpies, $\Delta H = H^{\mathrm{E}}$, are important for understanding molecular interactions because they are related to the structure and the interaction energy of the particles (molecules and/or ions) in the pure substance and in the mixture.[7] They are also important for the design of industrial processes, since they can be used directly in energy balance calculations and give information about Gibbs energy and hence about phase equilibrium. Heats of mixing and their derivatives with respect to pressure and temperature relate to the volumetric properties and heat capacity of mixtures.

$$\left(\frac{\partial H^{\mathrm{E}}}{\partial p}\right)_T = V^E - T\left(\frac{\partial V^{\mathrm{E}}}{\partial T}\right)_P \qquad 7)$$

$$\left(\frac{\partial H^{\mathrm{E}}}{\partial T}\right)_P = C_P^{\mathrm{E}} \qquad 8)$$

Eq. 7 sets a relationship between the pressure dependence of H^{E} and V^{E}; the larger the V^{E} the larger is the effect of pressure on H^{E}. Eq. 8 can be used as a consistency test of excess molar enthalpies measured over extended

temperature and pressure ranges by comparing with calorimetric measurements of excess heat capacities.

Heats of solution were collected through a heat flow calorimeter by Thermometric (model 2277, Thermal Activity Monitor - Järfälla, Sweden) at 298.15 K (±0.01 K). Experiments were conducted by adding a pure component, via Hamilton gas-tight syringes of capacity in the range of (250.0 to 1000) μL driven by Cole-Parmer (model 74900 - Vernon Hills, Illinois, USA) pumps, to an ampoule of 1 or 4 cm^3 capacity initially charged with the other component or with a stock mixture of them. With this system, we were able to make accurate injections starting from a minimum of 1 μL, with precision 0.5 %, and to measure accurate heat effects as small as 0.01 J, with sensitivity 0.5 μW. We chose this technique instead of mixing-flow calorimetry to avoid errors due to incomplete mixing and to obtain more precise values of the partial molar enthalpy at infinite dilution.[5]

The experimental solution heats, Q_{exp}, released by the additions of very small quantities of the titrant, n_k, practically represent partial molar excess enthalpies, $\overline{H}_k^{E}$:

$$\overline{H}_k^{E} \cong Q / n_k \qquad 9)$$

The partial molar excess enthalpies is defined as the difference between the partial molar enthalpy of a given component, $\overline{H}_k$, and the molar enthalpy of the same compound in the pure state, H_k^*.

From the eq. 9, calculated values of the solution heats, Q_{calc}, can be obtained, being $\overline{H}_{k,calc}^{E}$ accounted for by proper differentiation of the

equation $H^E = f(x)$, such as the Redlich-Kister (RK) one (eq. 10)[8] or the modified Margules one (eq. 11):[8]

$$\frac{H^E}{RT} = x_1 x_2 \sum_{k=1}^{n} c_k \left(x_1 - x_2\right)^{k-1} \qquad 10)$$

$$\frac{H^E}{RT} = x_1 x_2 \left(A_{12} x_2 + A_{21} x_1 - \frac{\alpha_{12}\alpha_{21} x_1 x_2}{\alpha_{12} x_1 + \alpha_{21} x_2 + \eta x_1 x_2} \right) \qquad 11)$$

A standard least squares procedure identifies the best values of parameters at the minimum of the objective function $OF = \Sigma\left(Q_{\text{exp}} - Q_{\text{calc}}\right)^2$. Proper allowance was made for the heat involved in the phase composition changes brought about by the vapour-liquid equilibration after each addition. An exhaustive description of the apparatus, the experimental procedure, and the data treatment, can be found in literature.[9, 10]

From the standard deviations of the RK or Margules equation we calculated the uncertainties, u, on H^E at equimolar mixtures and on partial molar enthalpies of each component at infinite dilution, $\overline{H}_k^{E,\infty}$.

The reliability of the whole procedure was checked by measuring the H^E, in the whole range of concentration, of the system Benzene (1) + Cyclohexane (2). Comparison with reliable literature[11] data revealed a discrepancy lower than 2 %. The uncertainty in the observed heat, Q, as determined by the reproducibility of the experiments and by integration of the peak area, can be evaluated as 0.5 %.

2.2.4. NMR Spectroscopy

The analysis of ^{1}H NMR spectra is routinely used to verify the purity of ILs obtained by synthesis. The shielding constants are sensitive to molecular conformations, the chemical environment (especially when hydrogen bonds can be formed), and interactions between cations and anions. Therefore, both ^{1}H chemical shifts of neat compounds and their mixtures were used to study intermolecular interactions in the systems under investigations. Complementary information was obtained by the analysis of ^{13}C chemical shifts and spin-lattice relaxation times.

As stated elsewhere,[12–17] the investigation of aggregation behaviour by means of NMR spin relaxation rate measurements relies on the dependence of the rates on the dynamics of molecular reorientation as expressed by the spectral density function $J(\omega)$.[18] For proton-carrying ^{13}C nuclei in medium-sized molecules, the spin relaxation is usually dominated by the dipole-dipole interaction with directly bonded protons. If the protons are subjected to broadband decoupling and the cross-correlations between different interactions can be neglected, the ^{13}C spin–lattice relaxation is a simple exponential process, characterized by a single time constant, T_1, called the spin–lattice relaxation time. Neglecting the contributions from protons that are not directly bonded, the dipolar contribution to the spin–lattice relaxation rate ($1/T_1^{DD}$) and the nuclear Overhauser enhancement (NOE) are given by Equations 12 and 13, respectively:

$$\frac{1}{T_1^{DD}} = N\frac{\mu_0^2\gamma_H^2\gamma_C^2\hbar^2}{160\pi^2 r_{CH}^6}\left(J(\omega_H-\omega_C)+3J(\omega_C)+6J(\omega_H+\omega_C)\right) \quad 12)$$

$$NOE = \frac{\gamma_H}{\gamma_C}\frac{6J(\omega_H+\omega_C)-J(\omega_H-\omega_C)}{J(\omega_H-\omega_C)+3J(\omega_C)+6J(\omega_H+\omega_C)} \quad 13)$$

where N is the number of attached protons; γ_H, γ_C and ω_H, ω_C are the gyromagnetic ratios and Larmor frequencies of proton and carbon, respectively; $\hbar$ is the reduced Planck constant; r_{CH} is the carbon–proton distance (fixed at 1.09 Å for our analysis); μ_0 is the permittivity of free space. Provided the motion is isotropic, $J(\omega)$ is given by:

$$J(\omega) = \frac{2\tau_c}{1+\omega^2\tau_c^2} \quad 14)$$

where τ_C is the correlation time for the motion of the C-H axis and approximates the time required for rotation of the molecule through 1 radian.

When the contribution of T_1^{DD} to the measured T_1 is 100 %, the NOE value reaches a maximum of 1.988 ($=\gamma_H/2\gamma_X$). For ^{13}C nuclei where DD relaxation competes with other mechanisms, the contribution of the dipole-dipole mechanism can be calculated if the experimental NOE (NOE_{exp}) is determined as:

$$\%\ \text{DD relaxation} = \frac{NOE_{exp}}{1.988}\times 100 \quad 15)$$

Experimental details. ^1H NMR spectra were obtained with a Varian Unity INOVA 500 spectrometer operating at the proton resonance frequency of 499.84 MHz, while ^{13}C NMR spectra were recorded using a Varian Unity INOVA 400 spectrometer with ^{13}C resonance frequency of 100.57 MHz.

Locking was performed using an inserted capillary tube filled with D_2O. All experiments were carried out at 300 K.

^1H spectra were acquired using 16 scans, a spectral width of 3000 Hz, a relaxation delay of 15 s, and a 90° pulse of 8.5 μs. Chemical shifts were referred to the signal of the residual water of D_2O in the capillary tube (δ = 4.78 ppm).

Two-dimensional adiabatic ROESY spectra were acquired with a standard pulse sequence[19,20] over a sweep width of 3000 Hz using 2048 data points in the t_2 dimension and 256 increments in the t_1 dimension. A total of 16 scans were collected for each t_1 increment with an acquisition time of 0.15 s followed by an additional relaxation delay of 2 s. A mixing time of 200 ms was used for all samples. The ROESY data set was processed by applying a shifted square sine-bell function in both dimensions and zero-filling to 2048×2048 real data points prior to the Fourier transformation.

The ^{13}C spin–lattice relaxation times (T_1) were measured by the inversion recovery method. A total of 16 scans were collected and 16-18 variable delays were used. The relaxation delay was at least five times greater than the longest T_1. The reported values are averages of three measurements with an estimated precision of 5 %.

$^{13}C\{^1H\}$ nuclear Overhauser enhancement (*NOE*) factors were determined from the ratios of peak intensities in a spectrum obtained with continuously applied composite pulse decoupling and in a spectrum where the *NOE* was suppressed by gating the decoupler on only during acquisition. For both spectra, a delay of at least 10 T_1 was allowed between acquisition pulses. The *NOE* measurements were reproducible within ±10 %.

2.3. Molecular dynamics simulations

MD simulations are a powerful method for obtaining detailed molecular information on a large variety of systems from the microscopic point of view. The method uses a force field to describe the interaction between atoms. A largely used force field for different kind of molecules those of AMBER and can be written as follow:[21]

$$V_{total} = \sum_{bonds} k_r \left(r - r_{eq}\right)^2 + \sum_{angles} k_\theta \left(\theta - \theta_{eq}\right)^2 + \sum_{torsions} \frac{V_n}{2}\left(1 + \cos\left(n\phi - \gamma\right)\right) + \sum_{i<j}\left(\frac{A_{ij}}{R_{ij}^{12}} - \frac{B_{ij}}{R_{ij}^{6}} + \frac{q_i q_j}{\varepsilon R_{ij}}\right) \quad 16)$$

where K_r, K_θ, V_n are the force constants for the bond lengths, r. θ and ϕ are bond and torsional angles, respectively. A_{ij} and B_{ij} are force constants for the Lennard-Jones potential describing the van der Waals interaction, and q_i and q_j the charges of atoms i and j in the electrostatic contribution to the total potential energy, with the dielectric constant of the medium, ε. R_{ij} is the distance between atoms i and j.

MD simulations of the NMP + Water system were performed with the AMBER 11 package[22] (both CPU and GPU versions of PMEMD)[23] using a cubic box containing about 11000 atoms of the pure liquid (NMP or water) or of the NMP + Water mixtures. Several systems with different x_1 were simulated covering the whole composition range (x_1 = 0.81; 0.67; 0.57; 0.37; 0.22; 0.18; 0.08).

The adopted simulation protocol is described below. Bound and van der Waals force field parameters for NMP were taken from *Gontrani and Caminiti,*[24] and the rigid four site TIP4PEW model was used for water.[25] It is known that depending on the solvent, the atomic partial charges are

expected to vary; the use of a proper set of charge is fundamental to ensure that molecular simulations produce reliable results.[26,27] Three set of charges for NMP were evaluated for the simulation of NMP + Water system: charges in Set1 were taken from ref. 13; charges in Set2 were obtained from QM calculations taking into account the polarization effect of water; charges in Set3 were obtained by interpolation of charges in Set1 and Set2. Charges in Set2 were calculated using Restrained Electrostatic Potential (RESP)[28] procedure using the Hartree-Fock theory level with 6-31G basis set, which was also used for charges in Set1, and modelling the effect of water with a polarizable continuum model (PCM). We used the current implementation in Gaussian 09 of PCM,[29] performing a reaction field calculation using integral equation formalism IEF-PCM model.[30–32] Ideally, charges in Set2 are the charges in an infinitely dilute water solution (i.e. for x_1=0), while charges in Set1 have been shown to reproduce correctly the structural properties of pure NMP (x_1=1). Charges in Set3 were obtained for intermediate values of NMP mole fraction, by a linear fitting of charges in Set1 and Set2 for each value of x_1.

The starting spatial configurations of pure liquids were created with the *tleap* program of the AMBER 11 package. The molecules of NMP + Water mixtures were packed in a simulation cubic box of side 55 Å using PACKMOL program.[33] Every pair of atoms of different molecules was separated by, at least 2 Å, and the molecules centres were distributed inside the cube at random starting positions. Each of the systems was equilibrated with a first short *NVT ensemble* run (260 ps) followed by a *NPT ensemble* run (3 ns) with the same pressure and temperature to be used in the production

step (1 atm, 300 K) using the Berendsen algorithm[34] with time constants of 1 ps in the initial phase of equilibration, and 3 ps in the last part. Periodical removal (every 10 ps) of the centre of mass velocity was done in order to minimize the "flying ice cube" phenomenon.[35] 3 ns of *NPT* equilibration were sufficient to reach the statistical equilibrium as assessed by inspecting the convergence of the thermodynamic properties. All simulations were carried out using a time step of 2 fs and SHAKE constraints[36] on hydrogen atoms (tolerance=0.00005); a cut-off radius of 9 Å was used in calculating the non-bonded interactions. Electrostatic interactions were calculated by the particle mesh Ewald method[37] as implemented in AMBER 11, with a cubic B-spline interpolation order and 0.00001 tolerance for the direct space sum cutoff. The length of production run was of 80 ns for each system, and absolutely no variation in selected RDFs calculated from 10 ns portions of the trajectory was observed in any of the systems (data not shown).

In order to extract structural information from the large set of coordinates obtained during simulations, the most common type of analysis has been done by calculating the radial distribution functions (RDFs) or pair correlation functions, usually indicated as $g(r)$. The RDF of a site B with respect to a site A is the probability to find atom B at a distance r from atom A (normalized with the bulk density of B):

$$g_{AB} = \frac{\rho_B\left(r|r_A=0\right)}{\rho_B} = \left(\frac{V}{N_B}\right)\frac{N_B\left(r_A,\Delta\right)}{V_B\left(r_A,\Delta\right)} \qquad 17)$$

where $\rho_B\left(r|r_A=0\right)$ is the conditional distance dependent density of site B at the distance r_A from site A; r_B is the bulk density; N_B (r, Δ) is the average

number of B which can be found in the volume V_B (r, Δ) of the spherical slice between (r_A – 0.5Δ) and (r_A + 0.5Δ). Integration of the RDFs to the first minimum gives a coordination number, which is an average number of neighbors in the first coordination sphere. It becomes hydration number if the RDF is calculated between a solute and the solvating water molecules.

Spatial distribution functions (SDFs) can be considered as the extension of RDFs to three dimensions thereby giving orientational information of the structure. Fixing a local coordinate system in the reference molecule, or on a portion of it, spatial pairwise correlations are calculated within the local frame as vectors (not as plain distances as in the RDF). Apart from this difference, SDF is defined in the same way as RDF, and can be calculated in the Cartesian space as:

$$\mathrm{S}_{AB}(i,j,k) = \left\langle \frac{1}{N_A} \sum_{n_A=1}^{N_A} \sum_{n_B=1}^{N_B} I_{i,j,k} \left[R_{n_A}^{A} \left(\vec{r}_{n_B}^{B} - \vec{r}_{n_A}^{A} \right) \right] \right\rangle \qquad 18)$$

where $R_{n_A}^{A}$ is a rotational transformation matrix from laboratory frame to molecular frame fixed on molecule A and $I_{i,j,k}$ is used to collect the three-dimensional spatial populations of site B.

The analysis of normalized RDF and SDF was done using an in house modified version of the Tranal program of the Mdynamix Package.[38]

REFERENCES

(1) Gontrani, L.; Bodo, E.; Triolo, A.; Leonelli, F.; Angelo, P. D.; Migliorati, V.; Caminiti, R. The Interpretation of Diffraction Patterns of Two Prototypical Protic Ionic Liquids: A Challenging Task for Classical Molecular Dynamics Simulations. *J. Phys. Chem. B* **2012**, *116*, 13024–13032.

(2) Campetella, M.; Gontrani, L.; Bodo, E.; Ceccacci, F.; Marincola, F. C.; Caminiti, R. Conformational Isomerisms and Nano-Aggregation in Substituted Alkylammonium Nitrates Ionic Liquids: An X-Ray and Computational Study of 2-Methoxyethylammonium Nitrate. *J. Chem. Phys.* **2013**, *138*, 184506.

(3) Gutmann, V. Empirical Parameters for Donor and Acceptor Properties of Solvents. *Electrochim. Acta* **1976**, *21*, 661–670.

(4) V. Gutmann. *The Donor Acceptor Approach to Molecular Interaction*; Plenum: New York, **1978**; p. 1978.

(5) Porcedda, S.; Usula, M.; Marongiu, B. *Physical-Chemical Properties of Ionic Liquid-Containing Mixtures. In: The Structure of Ionic Liquids, Soft and Biological Matter.*; Caminiti, R.; Gontrani, L., Eds.; Springer International Publishing Switzerland, **2014**; pp. 171–191.

(6) Marsh, K.N. ; Richards, A. E. Marsh. *Aust. J. Chem.* **1980**, *33*, 2121–2132.

(7) Grolier, J. P. E.; Wormald, C. J.; Fontaine, J. C.; Sosnkowska-Kehian; Groelier, J.P.E.; Wormald, C.J.; Fontaine, C.J.; Sosnokowska-Kehiaian, K.; Kehiaian, H. V. *Numerical Data and Functional Relationships in Science and Technology. Volume 10 Heats of Mixing and Solutions.*; Keiahian, H. V., Ed.; Springer: Landolt-Bornstein, **2004**.

(8) Abbott, M. M.; Van Ness, H. C. Vapor-Liquid Equilibrium: Part III. Data Reduction with Precise Expressions for GE. *AIChE J.* **1975**, *21*, 62–71.

(9) Matteoli, E.; Lepori, L.; Spanedda, A. Thermodynamic Study of Heptane + Amine Mixtures. *Fluid Phase Equilib.* **2003**, *212*, 41–52.

(10) Matteoli, E.; Gianni, P.; Lepori, L. Thermodynamic Study of Heptane + Secondary, Tertiary and Cyclic Amines Mixtures. Part IV. Excess and Solvation Enthalpies at 298.15K. *Fluid Phase Equilib.* **2011**, *306*, 234–241.

(11) Marsh, K. N. Excess Enthalpies of Benzene + cyclohexane Mixtures. *Int. Data Ser. Sel. Data Mix. Ser. A* **1973**, 1–5.

(12) Antony, J. H.; Dölle, A.; Mertens, D.; Wasserscheid, P.; Carper, W. R.; Wahlbeck, P. G. ^{13}C NMR Relaxation Rates in the Ionic Liquid 1-Methyl-3-Nonylimidazolium Hexafluorophosphate. *J. Phys. Chem. A* **2005**, *109*, 6676–6682.

(13) Carper, W. R.; Wahlbeck, P. G.; Dolle, A. NMR Relaxation Rates: Separation of Dipolar and Chemical Shift Anisotropy Effects. *J. Phys. Chem. A* **2004**, *108*, 6096–6099.

(14) Heimer, N. E.; Wilkes, J. S.; Wahlbeck, P. G.; Carper, W. R. C NMR Relaxation Rates in the Ionic Liquid 1-Ethyl-3-Methylimidazolium Butanesulfonate. *J. Phys. Chem. A* **2006**, *110*, 868–874.

(15) Imanari, M.; Tsuchiya, H.; Seki, H.; Nishikawa, K.; Tashiro, M. Characterization of the Molecular Reorientational Dynamics of the Neat Ionic Liquid 1-Butyl-3-Methylimidazolium Bromide in the Super Cooled State Using ^{1}H and ^{13}C NMR Spectroscopy. *Magn. Reson. Chem.* **2009**, *47*, 67–70.

(16) Marincola, F. C.; Piras, C.; Russina, O.; Gontrani, L.; Saba, G.; Lai, A. NMR Investigation of Imidazolium-Based Ionic Liquids and Their Aqueous Mixtures. *ChemPhysChem* **2012**, *13*, 1339–1346.

(17) Mocci, F.; Laaksonen, A.; Wang, Y.-L.; Saba, G.; Lai, A.; Cersare Marincola, F. *CompChem and NMR Probing Ionic Liquids. In: The Structure of Ionic Liquids, Soft and Biological Matter.*; Caminiti, R.; Gontrani, L., Eds.; Springer International Publishing Switzerland, **2014**; pp. 95–124.
(18) Abragam, A. *Principles of Nuclear Magnetism*; Oxford Science Pubblications, London, **1961**.
(19) Hansen, D. F.; Kay, L. E. Improved Magnetization Alignment Schemes for Spin-Lock Relaxation Experiments. *J. Biomol. NMR* **2007**, *37*, 245–255.
(20) Bax, A. D.; Davis, D. G. Practical Aspects of Two-Dimensional Transverse NOE Spectroscopy. *J. Magn. Reson.* **1985**, *63*, 207–213.
(21) Cornell, W.D.; Cieplak, P.; Bayly, C.I.; Gould, I.R.; Merz, K.M. Jr.; Ferguson, D.M.; Spellmeyer, D.C.; Fox, T.; Caldwell, J.W.; Kollman, P.A. A second generation force field for the simulation of proteins, nucleic acids, and organic molecules. *J. Am. Chem. Soc.* **1995**, *117*, 5179–5197.
(22) Case, D. A.; Darden, T. A.; Cheatham III, T. E.; Simmerling, C. L.; Wang, J.; Duke, R. E.; Luo, R.; Walker, R. C.; Zhang, W.; Merz, K. M.; et al. *AMBER 11*, Univ. California, San Francisco, **2010**.
(23) Goetz, A. W.; Williamson, M. J.; Xu, D.; Poole, D.; Le Grand, S.; Walker, R. C. Routine Microsecond Molecular Dynamics Simulations with AMBER on GPUs. 1. Generalized Born. *J. Chem. Theory Comput.* **2012**, *8*, 1542–1555.
(24) Gontrani, L.; Caminiti, R. The Structure of Liquid *N*-Methyl Pyrrolidone Probed by X-Ray Scattering and Molecular Simulations. *J. Chem. Phys.* **2012**, *136*, 074505.
(25) Horn H. W; Swope W. C; Pitera J. W; Madura J. D; Dick T. J; Hura G. L; Head-Gordon, T. Development of an Improved Four-Site Water Model for Biomolecular Simulations: TIP4P-Ew. *J. Chem. Phys.* **2004**, *120*, 9665–9678.
(26) Jämbeck, J. P. M. .; Mocci, F.; Lyubartsev, A. P.; Laaksonen, A. Partial Atomic Charges and Their Impact on the Free Energy of Solvation. *J. Comput. Chem.* **2013**, *34*, 187–197.
(27) Mobley, D. L.; Dumont, E.; Chodera, J. D; Dill, K. A. Comparison of Charge Models for Fixed-Charge Force Fields: Small-Molecule Hydration Free Energies in Explicit Solvent. *J. Phys. Chem. B* **2007**, *111*, 2242–2254.
(28) Bayly, C. I.; Cieplak, P.; Cornell, W.; Kollman, P. A. *J. Phys. Chem. B* **1993**, *97*, 10269–10280.
(29) Scalmani, G.; Frisch, M. J. *J. Chem. Phys.* **2010**, *132*, 114110.
(30) Cances, M.-T.; Menucci, B.; Tomasi, J.*J. Chem. Phys.* **1997**, *107*, 3032.
(31) Cossi, M.; Barone, V.; Menucci, B.; Tomasi, J. *Chem. Phys. Lett.* **1998**, *286*, 253.
(32) Mennucci, B.; Tomasi, J. *J. Chem. Phys.* **1997**, *106*, 5151.
(33) Martínez, L.; Andrade, R.; Birgin, E. G.; Martínez, J. M. Software News and Update Packmol: A Package for Building Initial Configurations. *J. Comput. Chem.* **2009**, *30*, 2157–2164.
(34) Berendsen, H. J. C.; Postma, J. P. M.; van Gunsteren, W. F.; DiNola, A.; Haak, J. R. *J. Chem. Phys.* **1984**, *81*, 3684–3690.
(35) Harvey, S. C.; Tan, R. K. Z.; Cheatham, T. E. *J. Comput. Chem.* **1998**, *19*, 726–740.
(36) Ryckaert, J. P.; Ciccoti, G.; Berendsen, H. J. C.*J. Comp. Phys.* **1977**, *23*, 327–341.
(37) Essmann, U.; Perera, L.; Berkowwitz, M. L.; Darden, T.; Lee, H.*J. Chem. Phys.* **1995**, *103*, 8577–8593.
(38) Lyubartsev, A.; Laaksonen, A. *Comput. Phys. Commun.* **2000**, *128*, 565–589.

Chapter 3

Results

3. Results

3.1. *N*-methyl-2-pyrrolidone

The results of a combined approach of MD simulations, wide-angle X-ray scattering experiments, and density measurements, to investigate the structural effect of water on NMP over the whole concentration range is reported in PAPER I.[1]

A very good agreement between computed and experimental density values and diffraction patterns was obtained, and the analysis of the MD trajectories allowed us to explain why a density maximum is observed experimentally for this system (Figure 3.1 bottom). The simulations indicated that water molecules can occupy "empty cavities" of NMP network, *i.e.* spatial regions which are not accessible to the heavy atoms of the solvating NMP molecules, but are accessible to water molecules (Figure 3.1 top). Each cavity can host only two water molecules; therefore the addition of water to NMP leads to an increase in density up to a water:NMP molar ratio of 2:1. Further addition of water molecules alters the NMP network and the density decreases the as the water content increases.

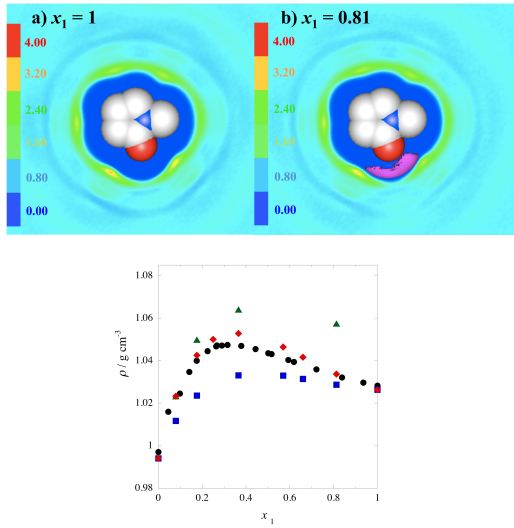

Figure 3.1. Top: cross-section representation of the SDFs of heavy atoms of selected NMP molecules a) in the neat state; b) at x_1 =0.81. Bottom: experimental (●) and computed (Set1, ■; Set2, ▲; Set3, ◆) densities, ρ.

As an extension of the previous study,[1] we further investigated NMP-Water mixtures by a combined use of NMR spectroscopy, calorimetric measurements, and puckering analysis of MD simulations (PAPER II).[2] These results provided additional information on the structural and dynamics changes of NMP taking place upon dilution:

i) the calorimetric study evidenced the presence of strong interactions between NMP and water and revealed that, under comparable conditions, the solvation of NMP by water results in an interaction stronger than the solvation of water by NMP.

ii) the changes of ^{1}H and ^{13}C chemical shifts and 2D ROESY spectra upon dilution suggested a preferential location of water nearby the carbonyl group of NMP and the formation of hydrogen bonding between these two molecules. In parallel, observation of correlation times by ^{13}C NMR spectroscopy evidenced a different dynamic behaviour moving from the NMP-rich region to the water-rich region, characterized by a maximum value at about 0.7 water mole fraction (Figure 3.2). This maximum corresponds to the concentration at which the highest density is observed.

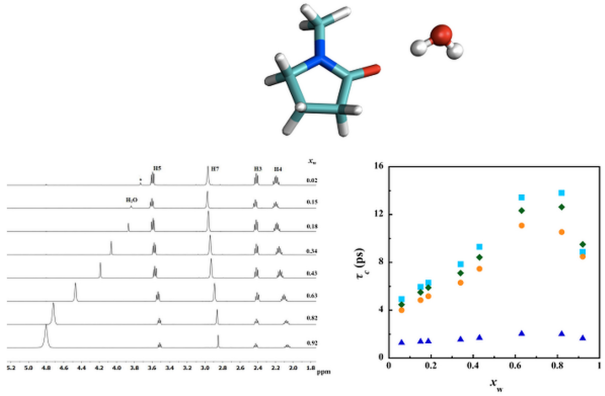

Figure 3.2. Left: ^{1}H NMR spectra of dried NMP and its aqueous mixtures at different water mole fractions. Right: rotational correlation times, τ_c, for NMP as a function of the water mole fraction.

iii) Puckering analysis of MD simulations showed that the NMP conformations distribution is not affected by the interactions with water molecules over the entire concentration range.

3.2. Room Temperature Ionic Liquids

In PAPER III[3] are reported the results concerning some alkylammonium nitrate (XAN) ionic liquids + NMP mixtures that were investigated over the whole concentration range by using density and calorimetric measurements with the purpose to understand the effect of XAN alkyl chain length on their mixing properties with NMP. The main information from the density measurements is that the increase of the alkyl chain length of the XAN cation inhibits the compaction of neat XAN. Negative and similar V^E values for each XAN + NMP system were found, indicating that the alkyl chain length does not significantly influence the mixture compaction. Negative H^E values (Figure 3.3) were obtained for all of the investigated systems; a clear indication for the presence of strong attractive interaction between the components; in addition, it can be highlighted that the mixing process of these ammonium nitrate ionic liquids is more exothermic for ILs with short alkyl chain than

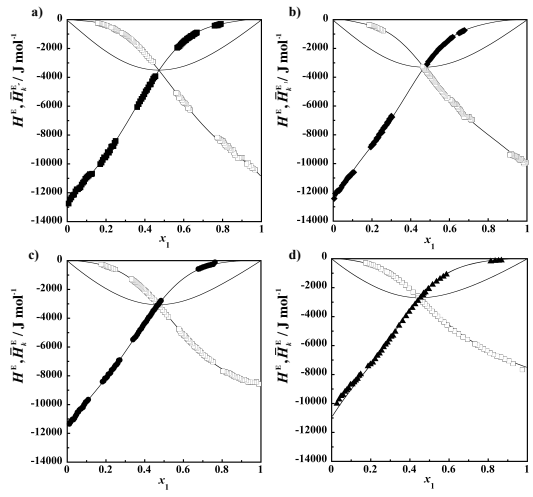

Figure 3.3. Excess molar enthalpies and partial molar enthalpies of XAN + NMP systems as function of the IL mole fraction. a) EAN; b) PAN; c) BAN; d) MEOEAN.

for those with long ones. In general, the dissolution of XAN by the NMP solvent was found to result in stronger interactions with respect to those accompanying the NMP dissolution by the ionic liquids. MEOEAN showed a different behaviour compared to the other selected alkylammonium nitrate ionic liquids:

i) the addition of a polar group to the shorter alkyl chain considered promotes a greater compaction of the neat ionic liquids than EAN, PAN and BAN.

ii) when MEOEAN is mixed with the organic solvent NMP, the methoxy group inhibits the interactions between the ions of XAN and NMP.

In the supplementary data, the NMR results are reported. The ^{1}H and ^{13}C chemical shift analysis evidenced the presence of hydrogen bond network between the polar head of the cation and NMP solvent. Complementary information on the XAN + NMP interaction was assessed by ^{13}C NMR relaxation measurements. The carbons in the NMP ring and those of the methylenic groups in XAN show an inversion point of R_1 in the mole fraction range of 0.6-0.8, and it is more pronounced for BAN ionic liquid. This inversion point is not observed for CH_3 carbons both in XAN and in NMP, probably due to the rotational contribution.

Further information about the structure and dynamic of these systems can be improved with a study from the microscopic point of view through MD simulations.

Furthermore, volumetric results of XAN + Water mixtures were reported. Negative V^E values were found for each system, like in NMP systems (PAPER III),[3] indicating the presence of strong attractive

interactions between ionic liquids and water solvent, greater than in neat compounds. The V^E curves of each system showed a comparable trend so they are not affected by the alkyl chain length. Even in this case, MEOEAN + Water system, showed the smallest reduction of volume.

In PAPER IV,[4] EAX + Water mixtures were studied by using density and calorimetric measurements. Density values of neat EAX decreases as the alkyl chain length of the anion increases, which can be attributed to an increase in steric hindrance as the chains become more voluminous (Figure 3.4 left).

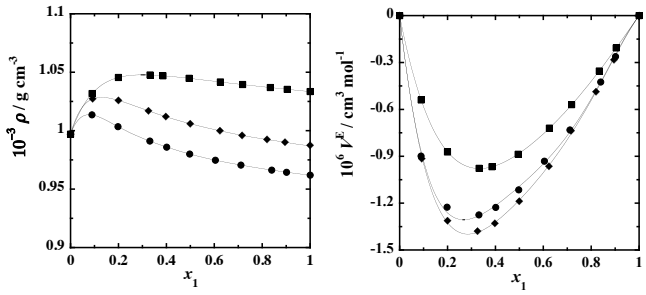

Figure 3.4. Experimental densities, ρ, (left) and excess molar volumes, V^E, (right) of EAX (1) + Water (2) mixtures as a function of x_1.

EAX + Water mixtures can be classified as "contractive" binary mixtures because of negative V^E values. By comparing V^E trends, it is evident that the addition of the first -CH_2 group to the alkyl chain of the methanoate anion causes a relevant increase in compaction of the mixture, while a further extension of the alkyl chain has an opposite effect even if it is quite moderate (Figure 3.4 right). In regards to calorimetric results, the negative excess enthalpies found for each system suggest the presence of attractive interactions between the mixture constituents stronger than the interactions acting in pure liquids. $H^E_{x=0.5}$ values for each investigated system are quite close indicating that the alkyl chain length of the anion does not

significantly influence the mixing process. In agreement with V^E results, the addition of the first -CH_2 group to the alkyl chain of the methanoate anion favourites a greater interaction between the components, while a further increase in length of the alkyl chain inhibits this interaction.

In the supplementary data, FT-IR spectra of EAX + Water systems are reported. The ν_3 and ν_1 water band shifts to lower wavenumber when water interacts with the solvent, indicating that the water molecules interact via H-bonding with the ionic liquids.

EAX ionic liquids are investigated in NMP mixtures by using density and calorimetric measurements. Excess molar volumes are negative and quite small in absolute value. V^E curves show a minimum at different x_1: EAM in the region of lower values of the more polar component, the IL; EAP approximately at equimolar composition; EAB in the IL-rich region. These results demonstrate that the anion affected significantly the IL-NMP interactions. Calorimetric measurements showed that EAP and EAB when are mixed with NMP generate a weak endothermic effect in the NMP-rich region, while in the IL-rich region the mixing is exothermic. In the case of the EAM + NMP system, it was found a moderate exothermic mixing effect in the whole concentration range. By comparing H^E values of the three systems, it can be observed that a longer alkyl chain in the carboxylic anion prevent the IL-solvent interaction, while a shorter alkyl chain favoured it.

In view of these results, it can be noticed that NMP is unable to exert strong attractive interactions towards EAX as, for example water does (PAPER IV), probably because of the well-known different capability to interact via hydrogen bonding.

REFERENCES

(1) Usula, M.; Mocci, F.; Cesare Marincola, F.; Porcedda, S.; Gontrani, L.; Caminiti, R. The Structural Organization of N-Methyl-2-Pyrrolidone + Water Mixtures: A Densitometry, X-Ray Diffraction, and Molecular Dynamics Study. *J. Chem. Phys.* **2014**, *140*, 124503.

(2) Usula, M.; Porcedda, S.; Mocci, F.; Gontrani, L.; Caminiti, R.; Cesare Marincola, F. NMR, Calorimetry, and Computational Studies of Aqueous Solutions of N-Methyl-2-Pyrrolidone. *J. Phys. Chem. B* **2014**, *118*, 10493–10502.

(3) Usula, M.; Matteoli, E.; Leonelli, F.; Mocci, F.; Marincola, F. C.; Gontrani, L.; Porcedda, S. Thermo-Physical Properties of Ammonium-Based Ionic Liquid + N-Methyl-2-Pyrrolidone Mixtures at 298.15K. *Fluid Phase Equilib.* **2014**, *383*, 49–54.

(4) Usula, M.; Plechkova, N. V; Piras, A.; Porcedda, S. Ethylammonium Alkanoate-Based Ionic Liquid + Water Mixtures : A Calorimetric and Volumetric Study at 298.15 K. Submitted to *J. Therm. Anal. Calorim.* **2015**.

Chapter 4

Conclusions

4. Conclusions and Perspectives

In this contribution it is shown how experimental studies together with computational ones can provide useful information on the structure of liquid systems in general, and can greatly improve the knowledge of molecular structural changes upon a solvent dilution. My attention was focused on solvents with interesting green characteristics and attractive proprieties to be used as valid alternatives to the common organic solvents. In particular, *N*-methyl-2-pyrrolidone and alkylammonium nitrate and alkanoate ionic liquids were considered.

The study of NMP + Water system reported in PAPER I and II is an example of how a combined approach of MD simulations and different experimental techniques contributed to understand a particular structural NMP organization in aqueous mixtures, which is the cause of a density maximum at the NMP:Water molar ratio of 1:2.

Room temperature ionic liquids are one of the most promising class of material that in the last decades were used in several applications. Their performance is strongly influenced by physicochemical characteristics such as alkyl chain and cation/anion head nature, for the neat ILs, and by the polar/apolar nature of additive solvents in binary mixtures. As it could be expected, the physicochemical proprieties of both families of ionic liquids investigated in this work are significantly influenced by the ion nature or by the alkyl chain length. In particular, structural modification in the anion and in the cation affected significantly the IL-solvent interactions. In general, as can be seen in PAPER III and IV, a longer alkyl chain length in the cation (XAN) or in anion (EAX) generates a decrease in density

indicating that the compaction of neat ionic liquids in bearing longer alkyl chains is hindered. The addition of a polar group (methoxy-) to the shorter alkyl chain in the considered XAN ionic liquids promotes a greater compaction of the neat ionic liquids than the other XAN.

XAN ionic liquids showed a better affinity for NMP solvent, while EAX ones for water solvent.

The results presented in this work provide valuable new information on XAN and EAX ionic liquids and their mixtures with water or NMP, and allow us to dispose quantities, obtained in a direct and reliable way, that are necessary for the chemical plants design.

Of course the use of a combined experimental and computational approach, as it has been done for the NMP + Water system, would be important for a better understanding of structural and dynamical changes in ILs, especially those that occurs upon solvent dilution. Therefore, we intend to continue the experimental studies of these IL + solvent mixtures by using different experimental techniques and MD simulations with the goal to obtain a in-depth knowledge of these systems from the microscopic point of view.

PAPER I

Reprinted with the permission:

The Structural Organization of *N*-Methyl-2-Pyrrolidone + Water Mixtures: a Densitometry, X-Ray Diffraction, and Molecular Dynamics Study.

M. Usula, F. Mocci, F. Cesare Marincola, S. Porcedda, L. Gontrani, and R. Caminiti.

Citation: *The Journal of Chemical Physics* **140**, 124503 (2014)

DOI: 10.1063/1.4869235

Published by the **AIP Publishing**

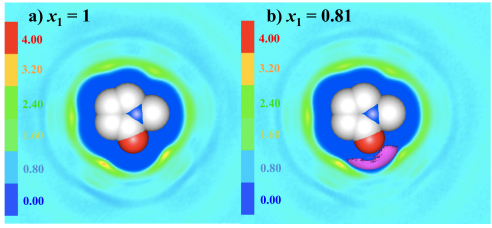

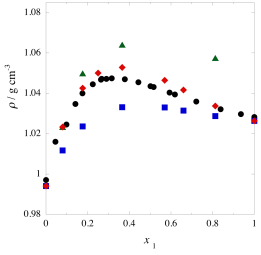

AIP | The Journal of Chemical Physics

The structural organization of N-methyl-2-pyrrolidone + water mixtures: A densitometry, x-ray diffraction, and molecular dynamics study

M. Usula, F. Mocci, F. Cesare Marincola, S. Porcedda, L. Gontrani, and R. Caminiti

Citation: The Journal of Chemical Physics **140**, 124503 (2014); doi: 10.1063/1.4869235
View online: http://dx.doi.org/10.1063/1.4869235
View Table of Contents: http://scitation.aip.org/content/aip/journal/jcp/140/12?ver=pdfcov
Published by the AIP Publishing

The structural organization of *N*-methyl-2-pyrrolidone + water mixtures: A densitometry, x-ray diffraction, and molecular dynamics study

M. Usula,[1] F. Mocci,[1,2,a)] F. Cesare Marincola,[1] S. Porcedda,[1] L. Gontrani,[3,4,b)] and R. Caminiti[4]

[1]*Dipartimento di Scienze Chimiche e Geologiche, Università degli Studi di Cagliari, S.S. 554 Bivio Sestu, 09042 Monserrato, Italy*
[2]*Department of Materials and Environmental Chemistry, Arrhenius Laboratory, Stockholm University, S-106 91 Stockholm, Sweden*
[3]*CNR – Istituto di Struttura della Materia, Area della Ricerca di Roma Tor Vergata, Via del Fosso del Cavaliere 100, I-00133 Roma, Italy*
[4]*Dipartimento di Chimica, Università di Roma "La Sapienza," P.le Aldo Moro 5, I-00185 Roma, Italy*

(Received 9 November 2013; accepted 10 March 2014; published online 25 March 2014)

A combined approach of molecular dynamics simulations, wide angle X-ray scattering experiments, and density measurements was employed to study the structural properties of *N*-methyl-2-pyrrolidone (NMP) + water mixtures over the whole concentration range. Remarkably, a very good agreement between computed and experimental densities and diffraction patterns was achieved, especially if the effect of the mixture composition on NMP charges is taken into account. Analysis of the intermolecular organization, as revealed by the radial and spatial distribution functions of relevant solvent atoms, nicely explained the density maximum observed experimentally. © *2014 AIP Publishing LLC*. [http://dx.doi.org/10.1063/1.4869235]

I. INTRODUCTION

N-methyl-2-pyrrolidone, NMP, is a heterocyclic compound having a five-membered ring structure with a lactam functionality (Fig. 1). It is hygroscopic, aprotic, and strongly polar solvent with high boiling point (477.45 K), low melting point (249.55 K), low volatility, low viscosity, and a mild amine odour. Furthermore, it has large chemical and thermal resistance and low toxicity. All of these characteristics make NMP a highly useful solvent in a variety of chemical reactions where an inert medium is required. Indeed, NMP is employed in a wide range of industrial applications,[1] such as chemicals processing, coatings, engineering plastics, agricultural chemicals, electronic, paint stripping and cleaning, and many others. Among its many uses, the most singular has been discovered recently: thanks to its excellent solvating capabilities, NMP has been used to exfoliate graphene layers from graphite.[2]

NMP is often used as a selective solvent in combination with small amounts of water (W). Since the presence of water has a significant effect on the solvent properties of NMP, particularly on its selectivity and efficacy in a number of processes,[3] a wide interest has been turned to the physicochemical characterization of these mixtures. However, despite the numerous data in the literature,[3–11] the structure and organization of NMP in water mixtures is still not clear. For instance, the density and the viscosity of NMP (1) + W (2) mixtures showed an interesting trend as a function of the composition, having a maximum at $x_1 \approx 0.3$. This peculiar behavior has been suggested to be due to the simple formation of complexes or hetero-associates species of the type (NMP $\times$ $2H_2O$).[10] Usually, the curve representing density with respect to composition is monotonic, nonlinear; but in few cases a point of maximum is found, such as, to cite a few, a series of cyclic amide or ethanolamine in water mixtures.[12] However, to the best of our knowledge the origin of this phenomenon at microscopic level is not known yet. NMP in pure state or in extremely dilute aqueous solution was studied through molecular dynamics (MD) simulations.[13,14] In 2012, Gontrani and Caminiti[13] studied the structure of NMP in liquid state by using X-ray diffraction complemented with interpretative models built with MD simulations. Although X-ray data were employed successfully in the study of pure liquids[15] and electrolyte solutions[16] in the past, the literature about structural studies of water solutions of organic liquids is still scarce, apart from some studies on water-alcohol mixtures.[17–21] The very good agreement between experimental and calculated patterns found in Ref. 13 suggested that the use of a simple two-body force field is appropriate for the NMP system. In 2009, Carver *et al.*[14] studied the structure of NMP extremely diluted in water by using experimental mutual diffusion coefficients complemented with MD simulations. The analysis showed the presence of four well-defined solvation shells around the NMP. In particular, they found that only 2.5 water molecules were bound to the carbonyl oxygen and 15.5 waters were found in the first solvation shell of the methyl group. The attention of Carver *et al.*[14] was focused on the water behavior in presence of NMP. Conversely, what is the behavior of NMP in the presence of smaller percentage of water? In front of the aforementioned singular trends of the physical-chemical properties of this system, it is evident that its structural organization is strongly dependent on the water content.

The aim of this study is to investigate the structural organization of NMP + W mixtures over the whole concentration

a)Electronic mail: fmocci@unica.it
b)Electronic mail: lorenzo.gontrani@gmail.com

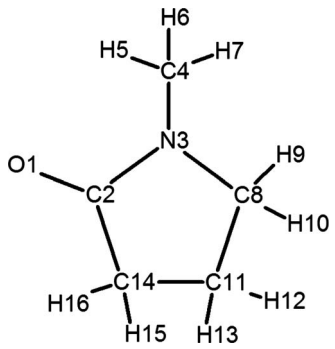

FIG. 1. Atom numbering scheme of *N*-methyl-2-pyrrolidone (NMP).

range, contributing to cover the concentration gap left open by previous studies,[14] with X-ray diffraction and densitometry techniques complemented with computed models built with MD simulations. The performance of MD simulations in predicting the experimental densities and X-ray diffraction patterns is discussed, and the reason why a maximum is present in the density curve is clarified by analysing the structural organization obtained by MD simulations.

II. EXPERIMENTAL

A. Materials

N-methyl-2-pyrrolidone (purity > 97%) was purchased from Sigma-Aldrich and was dried in vacuum ($p = 2 \times 10^{-2}$ mbar) for 24 h.

B. Density measurements

NMP + W mixtures were prepared by weight in septum-capped vials of approximately 2 cm^3 using needles and syringes to transfer liquids. Before weighting, NMP was degassed for about 2 h by means of an ultrasonic device (WVR model USC100T – 45 kHz, 30 W), while pure water was used immediately after distillation.

The densities (ρ) of the liquid mixtures and the pure compounds were measured at 298.15 K by means of a vibrating tube densitometer (model DMA 58, Anton Paar, Gratz, Austria). Accuracy in the temperature was better than ±0.01 K. Density precision and accuracy were ±0.00001 and ±0.00005 g/cm^3, respectively. Each density measurement was performed in duplicate. The instrument was calibrated before each experimental run using dry air and distilled water as references.

C. X-ray diffraction

NMP + W mixtures were prepared by weight as follow: first, the proper amounts of NMP were weighted with an analytical balance in screw-cap glass vials in a glove-bag under nitrogen atmosphere; then, the vials were removed to the glove-bag and suitable amounts of water were added to give mole fraction x_1 of: 0.08; 0.18; 0.22; 0.37; 0.57; 0.66; 0.81. The mixtures were transferred into the capillary tube for X-ray measurements and sealed with wax. Data used for the elaboration of X-ray patterns are reported in Table I.

The wide angle X-ray scattering experiments were performed using the noncommercial energy-scanning diffractometer built in the Department of Chemistry at the University "La Sapienza" of Rome (Patent no. 01126484, June 23, 1993). For a detailed description of instrument, technique, and the experimental protocol of the data acquisition phase, the reader is referred to Refs. 22–25.

In this experiment, the 0–2ϑ instrument geometry (only one of the two diffractometer arms can move) was used. In such a setup, higher diffracted intensities can be recorded. The appropriate measuring time (i.e., number of counts) was chosen to obtain scattering variable (Q) spectra with high signal-to-noise ratio (600 000 counts on average). The diffraction patterns acquired at the different angles are then joined to obtain a continuous spectrum in Q. Only five diffraction angles are enough to cover a Q-spectrum ranging from 0.1 to 20 $Å^{-1}$. The total intensity of the radiation scattered by a sample in a diffraction experiment, after the correction for systematic effects (polarization, absorption, incoherent and multiple scattering) and rescaling to absolute units (electron units per stoichiometric unit), can be expressed as the sum of two terms

$$I(Q)_{E.U.} = \sum_{i=1}^{N} x_i f_i^2 + i(Q). \quad (1)$$

The first term represents the independent atomic scattering from the atoms in a stoichiometric unit, while $i(Q)$ is the "total structure function" and constitutes the structurally sensitive part of the scattering intensity, being due to the interference contributions from different atoms.

TABLE I. Mole fraction of NMP x_1, density ρ, stoichiometric volume SV, NMP and water molar concentration, and molar concentration of each chemical element in the mixtures. Molar concentrations are expressed as mol/dm^3.

Mixture	x_1	ρ (g/cm^3)	SV ($Å^3$)	[NMP]	[water]	[O]	[N]	[C]	[H]
(a)	0.81	1.0332	165.9869	10.004	2.310	12.305	10.004	50.020	94.638
(b)	0.66	1.0376	173.4963	9.571	4.930	14.431	9.571	47.855	95.999
(c)	0.57	1.0410	179.8866	9.231	6.967	16.198	9.231	46.155	97.013
(d)	0.37	1.0476	205.7407	8.071	13.742	21.813	8.071	40.355	100.123
(e)	0.22	1.0445	256.4906	6.474	22.355	28.829	6.474	37.025	102.976
(f)	0.18	1.0396	293.0697	5.666	26.527	32.193	5.666	28.33	104.048
(g)	0.08	1.0267	497.3145	3.339	38.396	41.735	3.339	16.695	106.843

The variable Q is the magnitude of the transferred momentum, and depends on the scattering angle (2ϑ), according to the relation $Q = 4\pi\ (\sin\vartheta/\lambda) = \text{cost} * E * \sin\vartheta$, with cost = 1.014 Å^{-1}/keV, if E is expressed in keV and Q in Å^{-1}. The function $i(Q)$ is related to the radial distribution functions (RDF) descriptive of the structure, according to the formula

$$i\,(Q) = \sum_{i=1}^{N}\sum_{j=1}^{N} x_i x_j f_i f_j H_{ij}(Q), \tag{2}$$

where we have introduced the partial structure functions H_{ij} defined in terms of radial distribution functions by the Fourier integral

$$H_{ij}(Q) = \rho_0 \int_0^{\infty} 4\pi r^2 (g_{ij}(r) - 1)) \frac{sin\,(Qr)}{Qr} dr \tag{3}$$

(ρ_0 is the bulk number density).

By inverting this Fourier transform, we get

$$g_{ij}\,(r) - 1 = \frac{1}{(2\pi)^3 \rho_0} \int_0^{\infty} 4\pi\, Q^2 H_{ij}(Q) \frac{sin\,(Qr)}{Qr} dQ. \tag{4}$$

Thus, if the $n(n + 1)/2$ pair distribution functions $g_{ij}(r)$ are calculated from a theoretical simulation, the partial structure factors, and, ultimately, $i(Q)$ can be achieved. Therefore, the link between experimental data and molecular modelling is particularly important, considering the fact that from a X-ray diffraction experiment a "total scattering" quantity is obtained (i.e., a linear combination of H_{ij}, Eq. (2)) and that the deconvolution into its components is not directly feasible. The structure functions, both the one derived from experimental diffraction patterns and that obtained from theoretical radial distribution functions were multiplied by a modification function $M(Q)$, a sharpening factor, necessary to improve the curve resolution at high Q, and then Fourier-transformed in the distance domain, according to the relation

$$\begin{aligned} Diff(r) &= D(r) - 4\pi r^2 \rho_0 = 4\pi r^2 \rho_0 (G(r) - 1) \\ &= \frac{2r}{\pi} \int_0^{\infty} Q i(Q) M(Q) \sin(rQ) dQ. \end{aligned} \tag{5}$$

The differential correlation function Diff(r) function contains only the structural contribution to the distribution function, since the uniform distribution component, corresponding to the second term of the subtraction, or to 1, is dropped. For a comprehensive report of all the formulas, see Refs. 26 and 27.

Summarizing, the comparison between experimental and model data for a given NMP/W solution will be carried out using both $Qi(Q)M(Q)$ (reciprocal space) and Diff(r) (direct space). If a comparison among the various systems is sought, a very useful function is the so-called "atomic" structure function $f(Q)$, where $i(Q)$ is normalized by the independent atomic scattering, the first term of the right sum in Eq. (1). With this further normalization, the scaling arising from species concentration is removed and the scattering functions are more easily comparable, though the dependence on scattering factors cannot be completely eliminated, since the total functions are scattering factor-weighted sums of partial functions.[26,27]

D. Computational details

Molecular dynamics simulations were performed with the AMBER 11 package[28] (both CPU and GPU versions of PMEMD)[29] using a cubic box containing about 11 000 atoms of the pure liquid (NMP or water) or of the NMP + W mixtures. Several systems with different x_1 were simulated covering the whole composition range. More specifically, in addition to the simulations of the two pure liquids, seven simulations of the mixtures were performed with the following x_1 values: 0.81; 0.67; 0.57; 0.37; 0.22; 0.18; 0.08.

The adopted simulation protocol is described below. Bound and van der Waals force field parameters for NMP were taken from Gontrani and Caminiti,[13] and the rigid four site TIP4PEW model was used for water.[30] It is known that depending on the solvent the atomic partial charges are expected to vary; the use of a proper set of charge is fundamental to ensure that molecular simulations produce reliable results.[31,32] Three sets of charges for NMP were evaluated for the simulation of NMP/W system: charges in Set1 were taken from Ref. 13; charges in Set2 were obtained from QM calculations taking into account the polarization effect of water; charges in Set3 were obtained by interpolation of charges in Set1 and Set2. Charges in Set2 were calculated using Restrained Electrostatic Potential (RESP)[33] procedure using the Hartree-Fock theory level with 6-31G basis set, which was also used for charges in Set1, and modelling the effect of water with a polarizable continuum model (PCM). We used the current implementation in Gaussian 09 of PCM,[34] performing a reaction field calculation using integral equation formalism IEF-PCM model.[35–37] Ideally, charges in Set2 are the charges in an infinitely dilute water solution (i.e., for $x_1 = 0$), while charges in Set1 have been shown to reproduce correctly the structural properties of pure NMP (NMP mole fraction equal to 1). Charges in Set3 were obtained for intermediate values of NMP mole fraction, by a linear fitting of charges in Set1 and Set2 for each value of x_1. The three sets of partial atomic charges are reported in Table II.

The starting spatial configurations of pure liquids were created with the *tleap* program of the AMBER 11 package. The molecules of NMP + W mixtures were packed in a simulation cubic box of side 55 Å using PACKMOL program.[38] Every pair of atoms of different molecules was separated by, at least, 2 Å, and the molecules centers were distributed inside the cube at random starting positions. Each of the systems was equilibrated with a first short *NVT ensemble* run (260 ps) followed by a *NPT ensemble* run (3 ns) with the same pressure and temperature to be used in the production step (1 atm, 300 K) using the Berendsen algorithm[39] with time constants of 1 ps in the initial phase of equilibration, and 3 ps in the last part. Periodical removal (every 10 ps) of the centre of mass velocity was done in order to minimize the "flying ice cube" phenomenon.[40] 3 ns of *NPT* equilibration were sufficient to reach the statistical equilibrium as assessed by inspecting the convergence of the thermodynamic properties, as

TABLE II. Partial atomic charges used in the three sets of MD simulations. The mole fraction of NMP is denoted as x_1.

	Set1	Set2	Set3						
Atom type	all x_1	all x_1	$x_1 = 0.08$	$x_1 = 0.18$	$x_1 = 0.22$	$x_1 = 0.37$	$x_1 = 0.57$	$x_1 = 0.66$	$x_1 = 0.82$
O1	−0.61897	−0.71551	−0.71551	−0.69850	−0.69377	−0.68014	−0.66044	−0.65174	−0.63658
C2	0.61137	0.64648	0.64648	0.64026	0.63853	0.63356	0.62636	0.62318	0.61764
N3	−0.13761	−0.12354	−0.12354	−0.12595	−0.12662	−0.12855	−0.13134	−0.13257	−0.13472
C4	−0.24240	−0.29921	−0.29921	−0.28931	−0.28655	−0.27861	−0.26714	−0.26207	−0.25324
H5	0.10784	0.12658	0.12658	0.12330	0.12387	0.11976	0.11596	0.11428	0.11136
H6	0.10784	0.12658	0.12658	0.12330	0.12387	0.11976	0.11596	0.11428	0.11136
H7	0.10784	0.12658	0.12658	0.12330	0.12387	0.11976	0.11596	0.11428	0.11136
C8	−0.10358	−0.10252	−0.10252	−0.10270	−0.10275	−0.10290	−0.10312	−0.10321	−0.10338
H9	0.07067	0.09096	0.09096	0.08739	0.08639	0.08353	0.07939	0.07756	0.07437
H10	0.07067	0.09096	0.09096	0.08739	0.08639	0.08353	0.07939	0.07756	0.07437
C11	−0.02696	−0.02805	−0.02805	−0.02788	−0.02783	−0.02770	−0.02751	−0.02742	−0.02727
H12	0.03663	0.05124	0.05124	0.04867	0.04796	0.04591	0.04294	0.04163	0.03934
H13	0.03663	0.05124	0.05124	0.04867	0.04796	0.04591	0.04294	0.04163	0.03934
C14	−0.15957	−0.23324	−0.23324	−0.22027	−0.21665	−0.20626	−0.19122	−0.18458	−0.17301
H15	0.06981	0.09572	0.09572	0.09116	0.08989	0.08623	0.08094	0.07861	0.07454
H16	0.06981	0.09572	0.09572	0.09116	0.08989	0.08623	0.08094	0.07861	0.07454

shown in Figure S1 of the supplementary material.[46] All simulations were carried out using a time step of 2 fs and SHAKE constraints[41] on hydrogen atoms (tolerance = 0.00005); a cutoff radius of 9 Å was used in calculating the non-bonded interactions. Electrostatic interactions were calculated by the particle mesh Ewald method[42] as implemented in AMBER 11, with a cubic B-spline interpolation order and 0.00001 tolerance for the direct space sum cutoff. The length of production run was of 80 ns for each system, and absolutely no variation in selected RDFs calculated from 10 ns portions of the trajectory was observed in any of the systems (data not shown).

We investigated the structural properties of these systems in the whole concentration range through the analysis of normalized RDF and SDF (Radial and Spatial Distribution Function) calculated using the *Tranal* program of the Mdynamix Package.[43] Integration of the first peak of the appropriate RDF allowed calculating the number of water molecules in the first solvation shell of selected atoms.

III. RESULTS AND DISCUSSION

A. Theoretical calculations and density measurements

Three sets of MD simulations (Set1, Set2, Set3) were carried out differing in the charges used for NMP. The average density values at 298 K obtained in the three sets of MD simulations, together with the experimental values, are plotted as function of x_1 in Fig. 2. It can be seen that the density values obtained in Set1 simulations reproduce somehow the experimental trend. For this set, the comparison with experimental values is clearly very good at high NMP mole fractions, but at lower NMP concentrations the values from the simulations are systematically lower than experimental ones. The discrepancy is larger in the region where the maximum is observed. Results from Set2 are in good agreement with experimental data in the region of low NMP concentrations; however, the agreement worsens at higher NMP contents with computed density values higher than the experimental one. This indicates that charges used in Set2, obtained considering pure water as solvent (see Sec. II D), are suitable for simulations at low NMP contents, but are too polarized for reproducing the behavior of the mixtures when the content of NMP solvating NMP itself increases. For this reason, we carried out an additional set of simulation, Set3, using the partial atomic charges obtained by a linear fitting between the charges in Set1 and Set2. The average densities obtained in Set3 not only reproduce very well the experimental trend but also have absolute values quite close to the experimental ones over the whole concentration range.

The agreement between experimental and computed data validated the use of MD simulations to understand the origin of the peculiar density trend from the microscopic point of

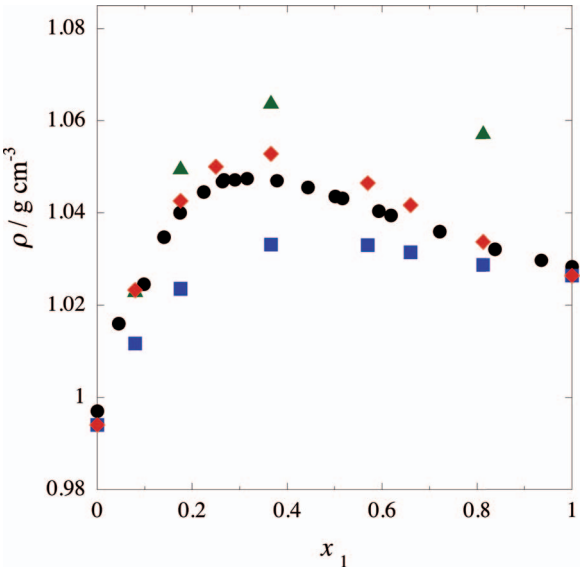

FIG. 2. Experimental (black circles) and theoretical (Set1, blue squares; Set2, green triangles; Set3, red diamonds) densities, ρ, of NMP (1) + W (2) mixtures at 298 K.

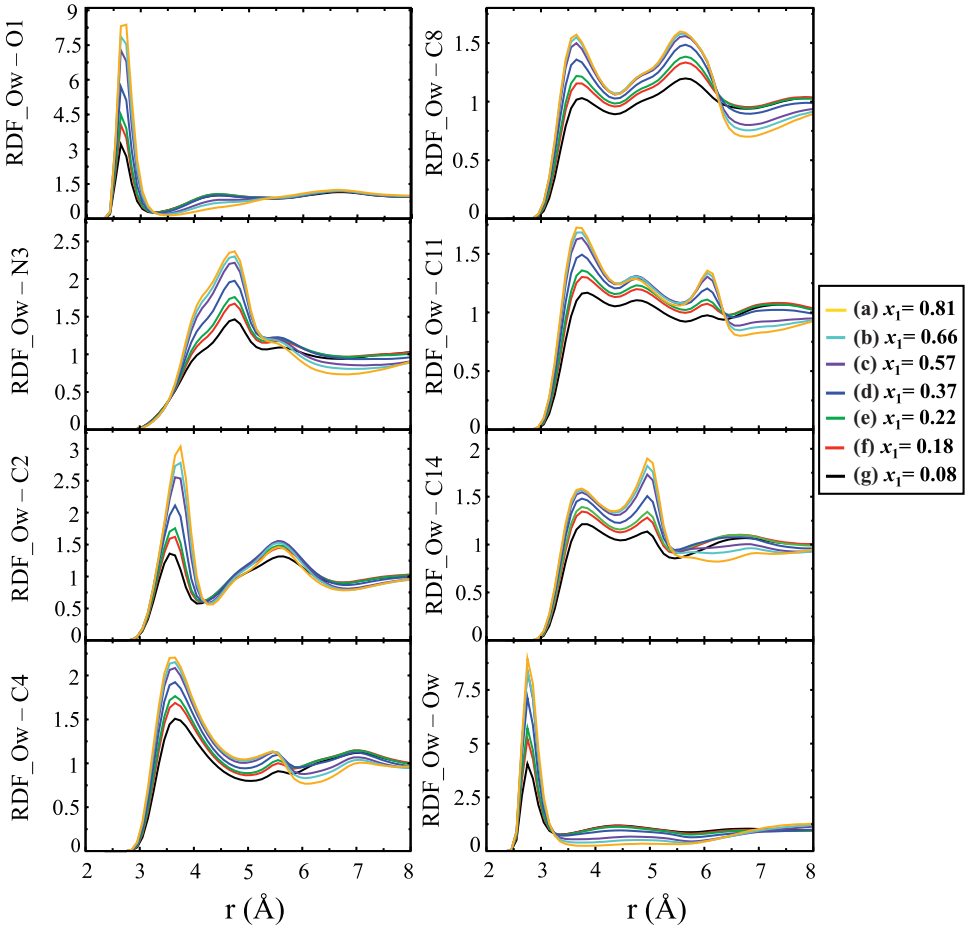

FIG. 3. RDFs between the water oxygen (Ow) with selected atoms of NMP and with other water oxygen atoms in NMP (1) + W (2) mixtures at different x_1 values.

view. To reach this goal, we analysed the radial and spatial distribution functions obtained from the Set3 simulations. In Fig. 3, the RDFs of the oxygen of water (Ow) with selected atoms of NMP and of other water molecules are shown. As can be seen, the most intense first maxima were observed in the RDFs of the carbonyl (O1 and C2), and the methyl (C4) groups. It can also be noticed that the intensity of these maxima increases with increasing NMP mole fraction. It is interesting to highlight that the RDFs of N3 and C14 exhibit a second maximum more intense than the first one at high NMP concentrations. These observations are consistent with the presence of H-bonds between water and the carbonyl group of NMP, and possibly with the methyl group. When the water content is reduced, these interactions prevail on those of water with other NMP atoms, and the second maximum of N3 and C14 can therefore be attributed to the water molecules bound to the carbonyl and methyl groups. Similar considerations can be done for the third maximum in C11 and C8 RDFs. To support the RDFs interpretation, representative distances between selected NMP atoms and the oxygen of a water molecule coordinating the carbonyl oxygen are represented in Figure 4.

The number of water molecules bound to the carbonyl oxygen, to the methyl group, and to the oxygen of water, calculated by integrating the first peak of O1, C4, and Ow RDFs, are shown in Fig. 5. As it can be expected, this number decreases with increasing NMP mole fraction. In particular, the decrease is approximately linear for the water molecules bound to the carbonyl oxygen and to other water molecules, while those bound to the methyl group decrease more rapidly at mole fraction up to $x_1 = 0.4$.

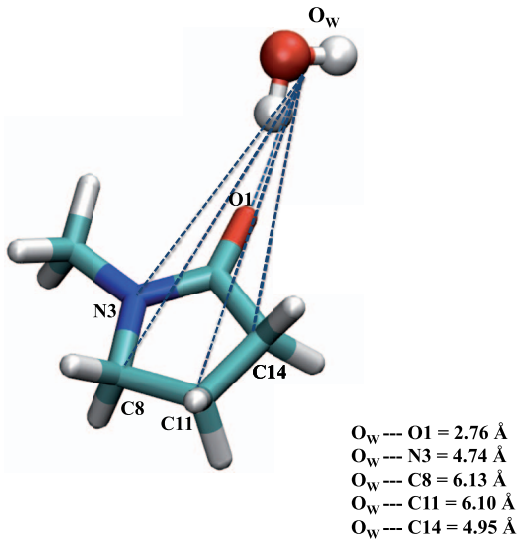

FIG. 4. Distances between selected NMP atoms and the oxygen atom of a water molecule hydrogen bonded to the carbonyl group.

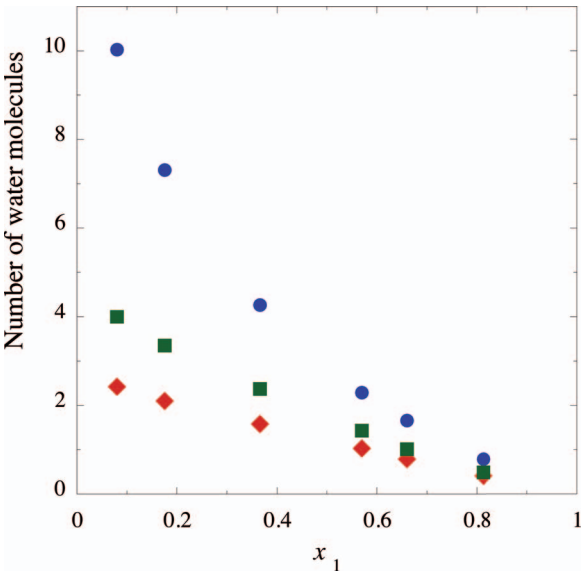

FIG. 5. Number of water molecules in the first hydration shell of (a) the carbonyl oxygen of NMP (red diamonds), (b) methyl carbon of NMP (blue circles), and (c) water oxygen (green squares).

Previous studies[44] have shown that in order to properly describe the spatial arrangement of molecules in solution, it is quite useful to visualize the SDFs of the solvating molecules around a selected molecular type or a fragment. SDFs are three-dimensional functions, and therefore to represent them their dimensionality should be reduced. This is commonly done by representing *isodensity surfaces* (or isosurfaces), i.e., surfaces that connect points with a given value of probability to find the particle(s) for which the SDF is calculated. Another common way to reduce the dimensionality is through the *cross-section* representations, i.e., plotting the value assumed by the SDFs on a selected two-dimensional surface, very often a plane. In normalized SDFs, the value of 1 corresponds to the bulk value, and to visualize the intermolecular spatial organization values higher than 1 should be selected. To identify regions where the probability is lower than in the bulk, the cross-section representations are more useful.

In Fig. 6 are displayed the isodensity surfaces of the SDFs of different atom types around a reference molecule of NMP, calculated from the trajectories of the pure NMP system (Fig. 6(a)), and from the Set3 trajectories of all the simulated mole fractions (Figs. 6(b)–6(h)). In Fig. 7 are shown the cross sections of the SDFs calculated on the same set of trajectories for all of the NMP heavy atoms. Visual inspection of SDFs nicely explains the NMP + W organization and the increase in density observed experimentally when adding water to NMP. In Fig. 6(a), it can be seen how neat NMP solvates itself. The spatial region with higher probability of finding the methyl carbon (C4) and the methylenic carbon in β-position with respect to the amide group (C11) were found close to the carbonyl oxygen of the reference molecule. The SDFs of the carbonyl oxygen (O1) has higher values in three different regions close to the reference molecule: on the left and on the right side of the amide group, and on the opposite side of the carbonyl group. As shown in Fig. 6(b), when a small amount of water is added, $x_1 = 0.81$, water molecules coordinate mainly to the oxygen of the carbonyl group. It is interesting to highlight that at low water content, water molecules can coordinate to the carbonyl oxygen without excessively perturbing NMP SDFs adopted in the NMP neat state (Figs. 6(a)–6(d) and 7(a)–7(d)), thus resulting in an increase of the density as observed experimentally. This arrangement is possible because, as can be seen by comparing Fig. 6(a) with Fig. 6(b) and Fig. 7(a) with Fig. 7(b), the water molecule size fit perfectly with the "empty cavity" observed in the SDFs of solvating NMP molecules in proximity of the carbonyl group. As "empty cavity" we refer to the spatial region which is not accessible to the heavy atoms of the solvating NMP molecules, but is accessible to water molecules. Instead, the addition of more than two water molecules for each NMP molecule (Figs. 6(f)–6(h)) leads to significant modifications of the SDFs adopted in the NMP neat state, and to the decrease in density, as it is expected when adding water to a liquid with higher density. Another proof that water molecules occupy a region not accessible to the heavy atoms of NMP is given by the RDFs between the carbonyl oxygen and each of the heavy atoms in the system (Fig. 8 and Fig. S2 of the supplementary material[46]). The peak of the first maximum of O1-Ow RDF is found in a region where the probability of finding any of the NMP atoms is zero. The same behavior is observed at all mole fractions shown in Fig. S2 of the supplementary material.[46]

It is important to note that even if the "cavity" can host only two water molecules, this does not imply that the water molecules in that region are somehow in a cage or isolated from other water molecules. The same water molecule can coordinate two carbonyl groups as hydrogen donor, and at the same time it can form other hydrogen bonds as an acceptor, as illustrated in the example shown in Fig. S3 of the supplementary material[46] and as indicated by the number of coordinating water molecules for both Ow and O1 reported in Fig. 5.

B. X-ray diffraction

Experimental and model patterns calculated from Set3 trajectories of $i(Q)$ and $Diff(r)$ for each mixture at different mole fractions of NMP are shown in Figs. 9 and 10, respectively; model patterns of $i(Q)$ and $Diff(r)$ calculated from each set of MD simulations (see Sec. II D) are reported in the supplementary material (Figs. S4 and S5[46]). The changes in the structure of the NMP + W mixtures are more easily visible in the cumulative plot (Fig. 11) of the atomic structure function $f(Q)$. All the experimental functions were calculated using in-house written codes. The X-ray model patterns (structure function and radial distribution function) were calculated on 4000 frames sampled regularly in the diffusive part of the trajectory. As it can be seen, a good agreement between experimental and simulated data obtained from the Set3 trajectories (see Sec. II D) was achieved, for all distance and Q ranges. Such agreement indicates that the model is reliable and appropriate to capture the overall structural information about these mixtures.

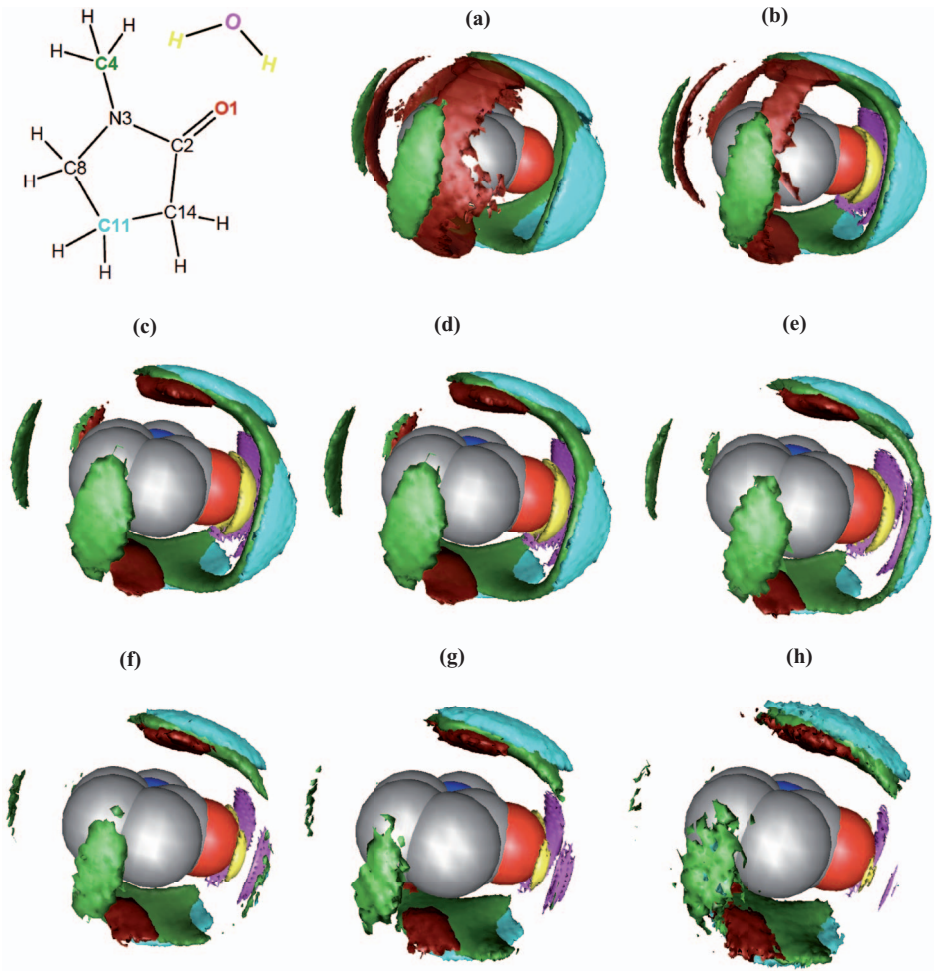

FIG. 6. (a) $x_1 = 1$, (b) $x_1 = 0.81$, (c) $x_1 = 0.66$, (d) $x_1 = 0.57$, (e) $x_1 = 0.37$, (f) $x_1 = 0.22$, (g) $x_1 = 0.18$, (h) $x_1 = 0.08$: Isodensity surfaces of the SDFs of selected NMP atoms in NMP (1) + W (2) mixtures at different x_1 values. Isodensity surface value is 3 for the NMP atoms and 13 for water atoms. Colour scheme used for the SDFs: magenta: Ow; yellow: Hw1 and Hw2; red: O1; green: C4; ciano: C11. 2D structures of NMP and water are reported for visual aid, with atom colours matching those used in the SDFs representation.

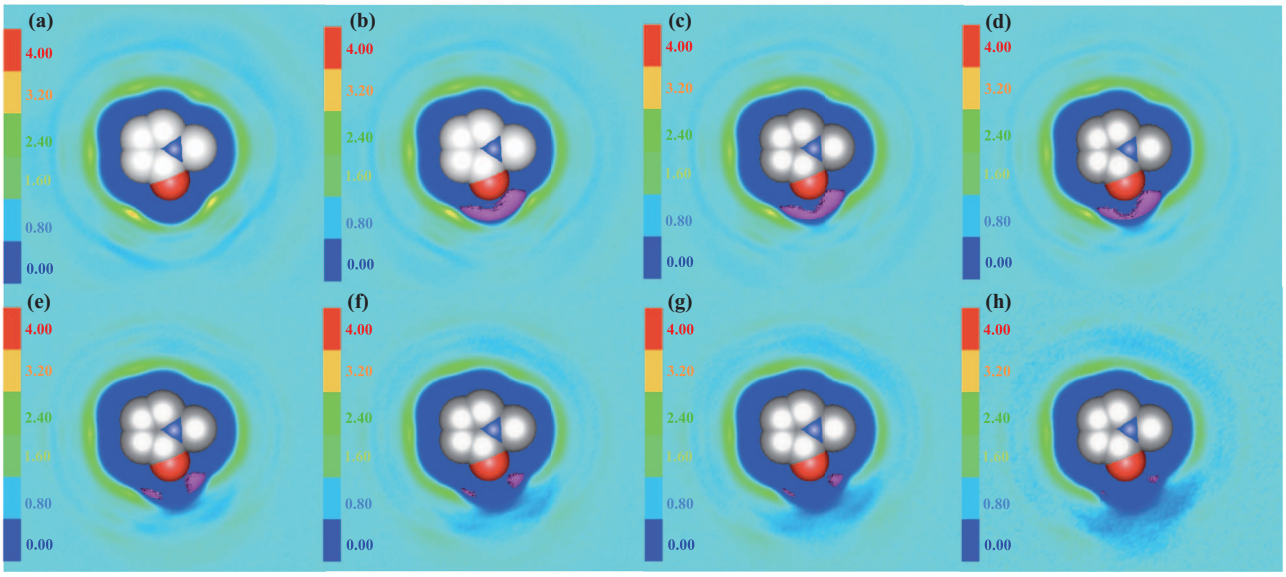

FIG. 7. (a) $x_1 = 1$, (b) $x_1 = 0.81$, (c) $x_1 = 0.66$, (d) $x_1 = 0.57$, (e) $x_1 = 0.37$, (f) $x_1 = 0.22$, (g) $x_1 = 0.18$, (h) $x_1 = 0.08$: Cross-section representation of the SDF of heavy atoms of NMP in NMP (1) + W (2) mixtures at different x_1 values. The cross-section is that of the plane defined by O1–C2–N2, which also corresponds to the plane of the average NMP structure.

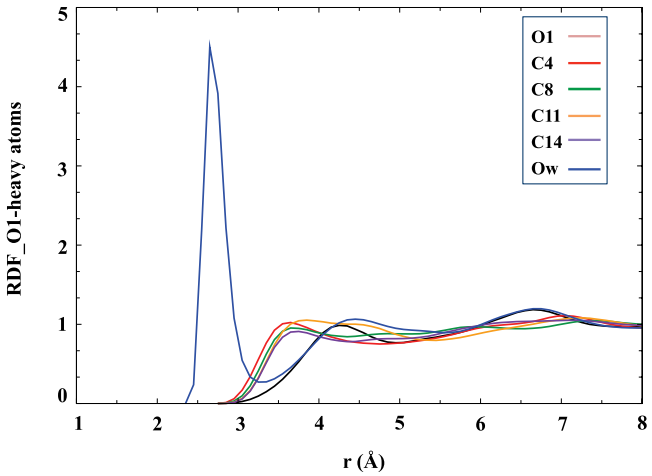

FIG. 8. RDFs between the NMP oxygen and heavy atoms of NMP or water in NMP (1) + W (2) mixture at $x_1 = 0.81$.

The patterns showed the broad peaks typically found in liquids, with a moderate degree of ordering suggested by the intensity of the peaks. In the most diluted mixture, the two signals falling at 2 and 3 Å^{-1} in $i(Q)$ (water "doublet" peak), which were attributed to O–O and O–H intermolecular correlations of the hydrogen-bond network of liquid water,[45] are clearly evident. The two peaks decrease in intensity as NMP content increases until they merge into a single signal at 1.5 Å^{-1}, similar to what is found for neat NMP. As the water content decreases the structure function becomes similar to that found for neat NMP.[13]

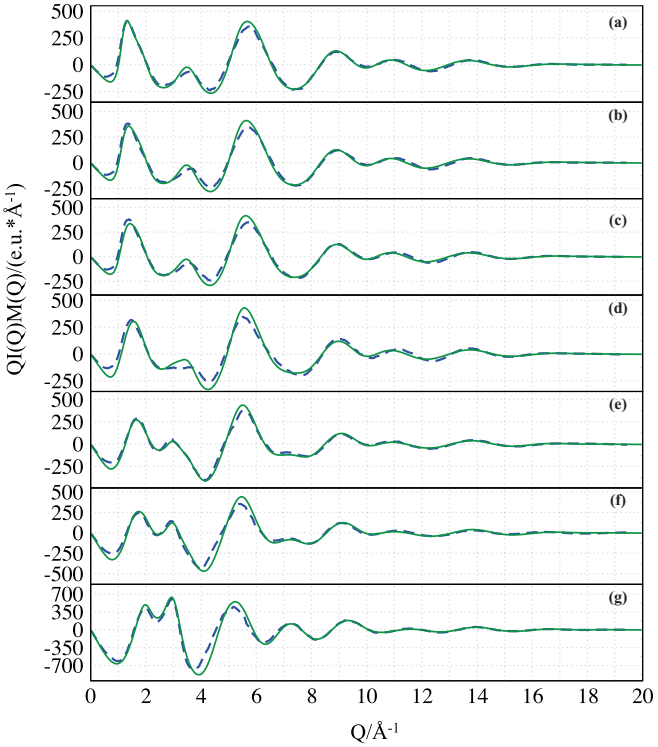

FIG. 9. (a) $x_1 = 0.81$, (b) $x_1 = 0.66$, (c) $x_1 = 0.57$, (d) $x_1 = 0.37$, (e) $x_1 = 0.22$, (f) $x_1 = 0.18$, (g) $x_1 = 0.08$: Total structure function $Qi(Q)M(Q)$. Experimental (dashed, blue) and model from Set3 trajectories (continuous, green) for NMP (1) + W (2) mixtures at different x_1 values.

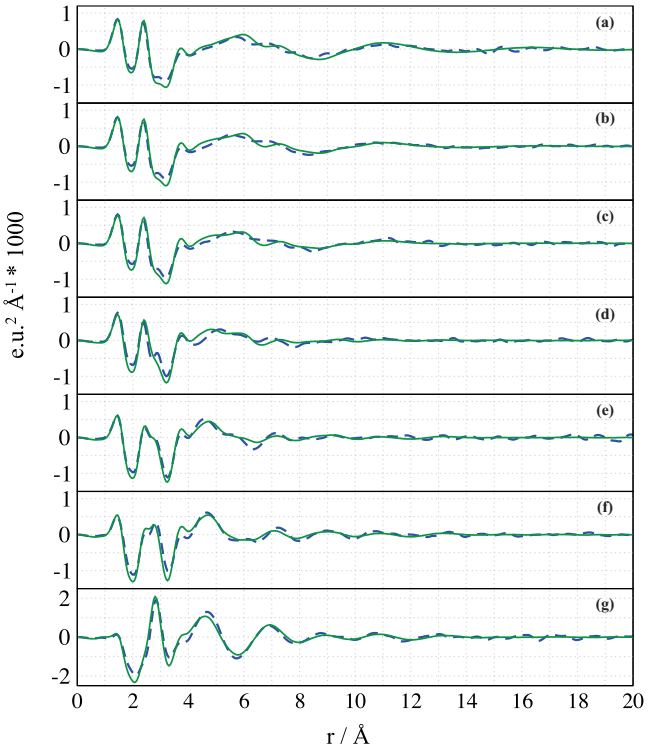

FIG. 10. (a) $x_1 = 0.81$, (b) $x_1 = 0.66$, (c) $x_1 = 0.57$, (d) $x_1 = 0.37$, (e) $x_1 = 0.22$, (f) $x_1 = 0.18$, (g) $x_1 = 0.08$: Differential correlation function $Diff(r)$. Experimental (dashed, blue) and model from Set3 trajectories (continuous, green) for NMP (1) + W (2) mixtures at different x_1 values.

The results shown comply very nicely with the volumetric data and with the SDF plots discussed above, since the addition of water to NMP up to $x_1 = 0.37$ (Figs. 9(a)–9(d)) does not affect very much the relative balance of structural correlations and the resulting X-ray structure functions very much, apart from a small gradual drift of the 9 Å^{-1} and 6 Å^{-1} peaks towards lower Q values, due to the loss of NMP ring intermolecular contacts. This result indicates that NMP overall structure is only slightly perturbed up to $x_1 = 0.37$. At smaller NMP concentrations (Figs. 9(e)–9(g)), the new intermolecular contacts originated by the water molecules that cannot be allocated inside NMP structure ("pure" water) tend to dominate. This picture is mirrored in the radial patterns of Fig. 10, which show how NMP intramolecular fingerprints, i.e., the two molecular peaks at 1.5 and 2.2 Å of the ring (1,2 and 1,3 contacts) and the 1,4 peak around 3.7 Å (contributed by (N)CH_3–O and by the larger N–C and O–C distances) are hardly noticeable at mole fractions larger than 0.37. At the same time, the oxygen–oxygen water shell structure peaks come out (at 2.85, 4.7, and 7 Å).

The structure pattern just described is even more evident in the $f(q)$ functions (Fig. 11). It can be seen how the peaks generally undergo only slight modifications in the first three solutions. Focusing on the 2.5–3.5 Å^{-1} range, in particular, the most concentrated solutions show a negative peak, the central region around 0.37 shows a plateau, while increasing the water content, the characteristic peak around 2.9 Å^{-1}, mostly originated by O–H intermolecular correlations,[45] builds up.

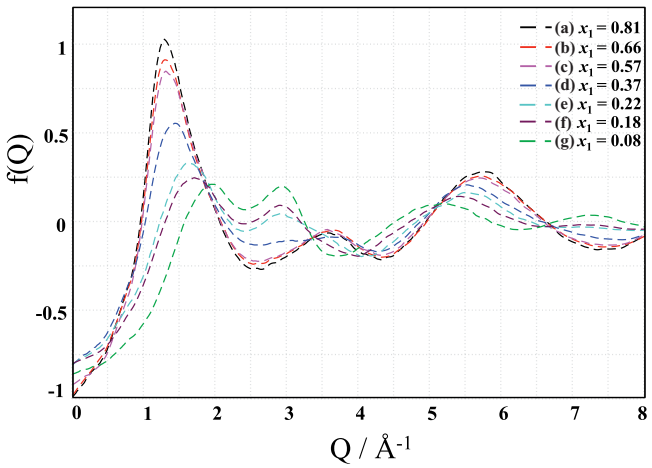

FIG. 11. Total structure function f(Q) for NMP (1) + W (2) mixtures at different x_1 values.

IV. CONCLUSIONS

The structure of *N*-methyl-2-pyrrolidone + water mixtures was investigated by combining density measurements, X-ray diffraction, and molecular dynamics simulations. Three sets of MD simulations were carried out differing in the charges used for NMP. In order to reproduce the experimental density trend of this binary system over the whole composition range of concentration, it was important to consider that the variation in the solvation around NMP affects the charge polarization. The sets of charges, which well reproduce the neat NMP or NMP in diluted aqueous solution, were found to be not perfectly suited for simulating the behavior at intermediate concentration. This lack is certainly of importance when the simulations are used, as in our case, to understand the presence of a density maximum at intermediate concentration. However, a simple linear fitting of the charges that well reproduces the density at the terminal parts of the curve is capable to correct this weakness. As regards the X-ray patterns, all of simulated data were appropriate to reproduce the experimental trend. The very good agreement between measured and calculated densities or X-ray patterns suggests that the models employed are appropriate for this system. Analysis of SDFs of relevant NMP and water atoms around NMP clarifies the origin of the density maximum. In fact, by comparing the SDFs calculated from the neat NMP trajectory and those calculated from the mixtures trajectories, it could be observed that water molecules can occupy a cavity of the NMP network, which is empty in neat NMP. The mentioned cavity can host only two water molecules; therefore, the addition of water to NMP leads to an increase in density up to the molecular ratio of 2:1. Further addition of water alters the NMP network and the density decreases increasing the water content.

The X-ray results are in very good agreement with the volumetric data and with the SDF plots: the addition of water to NMP up to $x_1 = 0.37$ does not affect the relative balance of structural correlations and the resulting x-ray structure functions, and at smaller NMP mole fractions, the new intermolecular interactions originated by the water molecules that cannot be allocated inside the structure of NMP ("pure" water) dominate.

ACKNOWLEDGMENTS

This research was financially supported by PRIN (2009 WHPHRH). M.U. gratefully acknowledges Sardinia Regional Government for the financial support of her Ph.D. scholarship (P.O.R. Sardegna F.S.E. 2007–2013). F.M. thanks Aaatto Laaksonen for helpful discussions and for the computing resources he made available, and Carl Trygger Foundation for funding for Visiting Professorship. M.U., F.M., and L.G. wish to thank Giuseppe Saba for insightful comments and technical assistance; L.G. acknowledges support from Italian FIRB (RBFR086BOQ).

[1] *N-Methyl-2-pyrrolidone Storage and Handling* (BASF Intermediates, 1998).
[2] Y. Hernandez, V. Nicolosi, M. Lotya, F. M. Blighe, Z. Sun, D. Sukanta, I. T. Mcgovern, B. Holland, M. Byrne, I. K. Gun'ko, J. J. Boland, P. Niraj, G. Duesberg, R. Krishnamurthy, R. Goodhue, J. Hutchison, V. Scardaci, A. C. Ferrari, and J. N. Coleman, Nat. Nanotechnol. **3**(9), 563 (2008).
[3] O. Noll, K. Fischer, and J. Gmehling, J. Chem. Eng. Data **41**, 1434 (1996).
[4] L. Ambrosone, G. D'Errico, R. Sartorio, and V. Vitagliano, J. Chem. Soc. Faraday Trans. **91**, 1339 (1995).
[5] M. Bernauer and V. Dohnal, Fluid Phase Equilib. **282**, 100 (2009).
[6] V. Dohnal, A. H. Roux, and V. Hynek, J. Sol. Chem. **23**, 889 (1994).
[7] K. Fischer and J. Gmehling, Fluid Phase Equilib. **119**, 113 (1996).
[8] D. D. Macdonald, D. Dunay, G. Hanlon, and J. B. Hyne, Can. J. Chem. Eng. **49**, 420 (1971).
[9] A. Blanco, A. Garcìa-Abuin, D. Gòmez-Diaz, J. M. Navaza, and I. Vidal-Tato, J. Chem. Eng. Data **55**, 962 (2010).
[10] A. Henni, J. J. Hromek, P. Tontiwachwuthikul, and A. Chakma, J. Chem. Eng. Data **49**, 231 (2004).
[11] A. Blanco, A. García-Abuín, D. Gómez-Díaz, and J. M. Navaza, J. Chem. Eng. Data **57**, 1009 (2012).
[12] J. P. E. Groelier, C. J. Wormald, C. J. Fontaine, K. Sosnokowska-Kehiaian, and H. V. Kehiaian, *Heats of Mixing and Solutions* (Springer-Verlag, 2005), Subvolume A.
[13] L. Gontrani and R. Caminiti, J. Chem. Phys. **136**, 074505 (2012).
[14] T. J. Carver, M. G. B. Drew, and P. M. Rodger, Phys Chem. Chem. Phys. **1**, 1807 (1999).
[15] L. Gontrani, F. Ramondo, G. Caracciolo, and R. Caminiti, J. Mol. Liq. **139**(1), 23–28 (2008); L. Gontrani, O. Russina, F. Lo Celso, R. Caminiti, G. Annat, and A. Triolo, J. Phys. Chem. B **113**(27), 9235–9240 (2009); E. Bodo, L. Gontrani, R. Caminiti, N. V. Pleckova, K. R. Seddon, and A. Triolo, *ibid.* **114**(49), 16398–16407 (2010); O. Russina, L. Gontrani, B. Fazio, D. Lombardo, A. Triolo, and R. Caminiti, Chem. Phys. Lett. **493**(4), 259–262 (2010).
[16] R. Caminiti, G. Licheri, G. Piccaluga, and G. Pinna, J. Chem. Phys. **68**, 1967 (1978); J. Appl. Cryst. **12**(1), 34–38 (1979); J. Chem. Phys. **69**(1), 1 (1978); Chem. Phys. Lett. **47**(2), 275–278 (1977); R. Caminiti, A. Musinu, G. Paschina, and G. Pinna, J. Appl. Cryst. **15**(5), 482–487 (1982).
[17] K. Nishikawa, H. Hayashi, and T. Iijima, J. Phys. Chem. **93**, 6559 (1989).
[18] J.-H. Guo, Y. Luo, A. Augustsson, S. Kashtanov, J.-E. Rubensson, D. K. Shuh, H. Ågren, and J. Nordgren, Phys. Rev. Lett. **91**, 157401 (2003).
[19] K. Nishikawa and T. Iijima, J. Phys. Chem. **97**, 10824 (1993).
[20] H. D. Bale, R. E. Shepler, and D. K. Sorgen, Phys. Chem. Liq. Int. J. **1**, 181 (1968).
[21] K. Nishikawa and T. Iijima, J. Phys. Chem. **94**, 6227–6231 (1990).
[22] M. Carbone, R. Caminiti, C. Sadun, D. Chimica, R. La, and P. A. Moro, J. Mater. Chem. **6**, 1709 (1996).
[23] V. Rossi Albertini, L. Bencivenni, R. Caminiti, F. Cilloco, and C. Sadun, J. Macromol. Sci., Phys. B **35**(2), 199–213 (1996).
[24] P. Ballirano, R. Caminiti, C. Ercolani, A. Maras, and M. A. Orru, J. Am. Chem. Soc. **120**, 12798 (1998).
[25] D. Atzei, T. Ferri, C. Sadun, P. Sangiorgio, and R. Caminiti, J. Am. Chem. Soc. **123**, 2552 (2001).
[26] D. A. Keen, J. Appl. Cryst. **34**, 172 (2001).
[27] R. Caminiti, G. Licheri, G. Piccaluga, and G. Pinna, Rev. Inorg. Chem. **1**, 333 (1979).
[28] D. A. Case, T. A. Darden, T. E. Cheatham III, C. L. Simmerling, J. Wang, R. E. Duke, R. Luo, R. C. Walker, W. Zhang, K. M. Merz, B. Roberts,

B. Wang, S. Hayik, A. Roitberg, G. Seabra, I. Kolossváry, K. F. Wong, F. Paesani, J. Vanicek, J. Liu, X. Wu, S. R. Brozell, T. Steinbrecher, H. Gohlke, Q. Cai, X. Ye, M.-J. Hsieh, G. Cui, D. R. Roe, D. H. Mathews, M. G. Seetin, C. Sagui, V. Babin, T. Luchko, S. Gusarov, A. Kovalenko, and P. A. Kollman, AMBER 11, University of California, San Francisco, 2010.

[29]A. W. Goetz, M. J. Williamson, D. Xu, D. Poole, S. Le Grand, and R. C. Walker, J. Chem. Theory Comput. **8**, 1542 (2012).

[30]H. W. Horn, W. C. Swope, J. W. Pitera, J. D. Madura, T. J. Dick, G. L. Hura, and T. Head-Gordon, J. Chem. Phys. **120**, 9665 (2004).

[31]J. P. M. Jämbeck, F. Mocci, A. P. Lyubartsev, and A. Laaksonen, J. Comput. Chem. **34**, 187 (2013).

[32]D. L. Mobley, E. Dumont, J. D. Chodera, and K. A. Dill, J. Phys. Chem. B **111**, 2242 (2007).

[33]C. I. Bayly, P. Cieplak, W. Cornell, and P. A. Kollman, J. Phys. Chem. B **97**, 10269 (1993).

[34]G. Scalmani and M. J. Frisch, J. Chem. Phys. **132**, 114110 (2010).

[35]M.-T. Cances, B. Menucci, and J. Tomasi, J. Chem. Phys. **107**, 3032 (1997).

[36]M. Cossi, V. Barone, B. Menucci, and J. Tomasi, Chem. Phys. Lett. **286**, 253 (1998).

[37]B. Mennucci and J. Tomasi, J. Chem. Phys. **106**, 5151 (1997).

[38]L. Martínez, R. Andrade, E. G. Birgin, and J. M. Martínez, J. Comput. Chem. **30**, 2157 (2009).

[39]H. J. C. Berendsen, J. P. M. Postma, W. F. van Gunsteren, A. DiNola, and J. R. Haak, J. Chem. Phys. **81**, 3684 (1984).

[40]S. C. Harvey, R. K. Z. Tan, and T. E. Cheatham III, J. Comput. Chem. **19**, 726 (1998).

[41]J. P. Ryckaert, G. Ciccoti, and H. J. C. Berendsen, J. Comput. Phys. **23**, 327 (1977).

[42]U. Essmann, L. Perera, M. L. Berkowitz, T. Darden, and H. Lee, J. Chem. Phys. **103**, 8577 (1995).

[43]A. Lyubartsev and A. Laaksonen, Comput. Phys. Commun. **128**, 565 (2000).

[44]D. L. Bergman, L. Laaksonen, and A. Laaksonen, J. Mol. Graph. Model. **15**, 301–306 (1997); A. Vishnyakov, A. P. Lyubartsev, and A. Laaksonen, J. Phys. Chem. A **105**, 1702–1710 (2001); P. G. Kusalik, D. Bergman, and A. Laaksonen, J. Chem. Phys. **113**(18), 8036 (2000); A. Vishnyakov, A. Laaksonen, and G. Widmalm, J. Mol. Graph. Model. **19**, 338–342 (2001); A. Laaksonen, P. G. Kusalik, and I. M. Svishchev, J. Phys. Chem. A **101**(33), 5910–5918 (1997); P. G. Kusalik, A. Laaksonen, I. M. Svishchev, P. B. Balbuena, and J. M. Seminario, *Molecular Dynamics: From Classical to Quantum Methods*, Theoretical and Computational Chemistry Vol. 7 (Elsvevier, New York, 1999), Chap. 3, pp. 61–97; I. M. Svishchev and P. G. Kusalik, J. Chem. Phys. **99**(4), 3049–3058 (1993).

[45]T. Head-Gordon and M. E. Johnson, Proc. Natl. Acad. Sci. U.S.A. **103**, 7973 (2006).

[46]See supplementary material at http://dx.doi.org/10.1063/1.4869235 for Figures S1–S5.

Supplementary Data of

The Structural Organization of *N*-Methyl-2-pyrrolidone + Water Mixtures: A Densitometry, X-ray Diffraction and Molecular Dynamics Study

M. Usula[1], F. Mocci[1,2,a)], F. C. Marincola[1], S. Porcedda[1], L. Gontrani[3,4,b)], R. Caminiti[4]

[1] *Dipartimento di Scienze Chimiche e Geologiche - Università degli Studi di Cagliari, S.S. 554 Bivio Sestu, 09042 Monserrato (Italy)*

[2] *Department of Materials and Environmental Chemistry, Arrhenius Laboratory, Stockholm University, S-106 91, Stockholm (Sweden)*

[3] *CNR – Istituto di Struttura della Materia, Area della Ricerca di Roma Tor Vergata, Via del Fosso del Cavaliere 100, I-00133 Roma (Italy)*

[4] *Dipartimento di Chimica - Università di Roma "La Sapienza", P.le Aldo Moro 5, I-00185 Roma (Italy)*

[a)] Electronic mail: fmocci@unica.it;

[b)] Electronic mail: lorenzo.gontrani@gmail.com

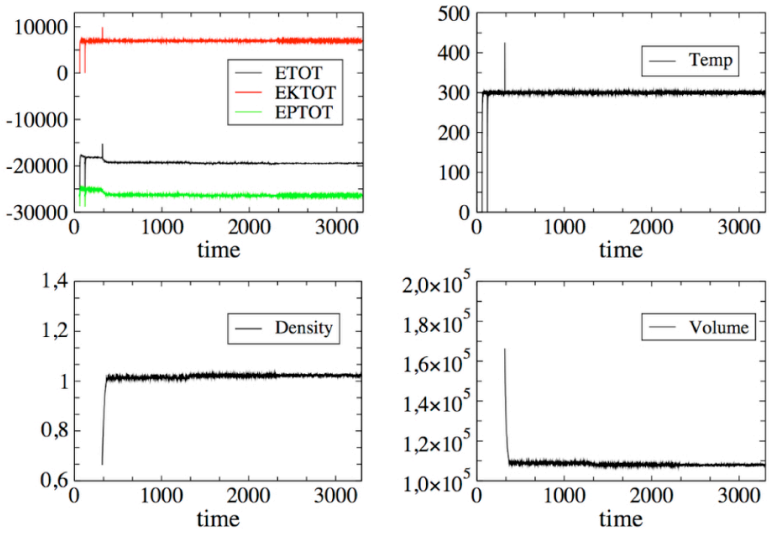

FIG. S1. Temporal variation of the thermodynamic properties of a representative NMP-water system at x_1=0.81 during the equilibration phase. After an initial part (0-260 ps) of *NVT* equilibration, the MD simulations were performed under *NPT* conditions.

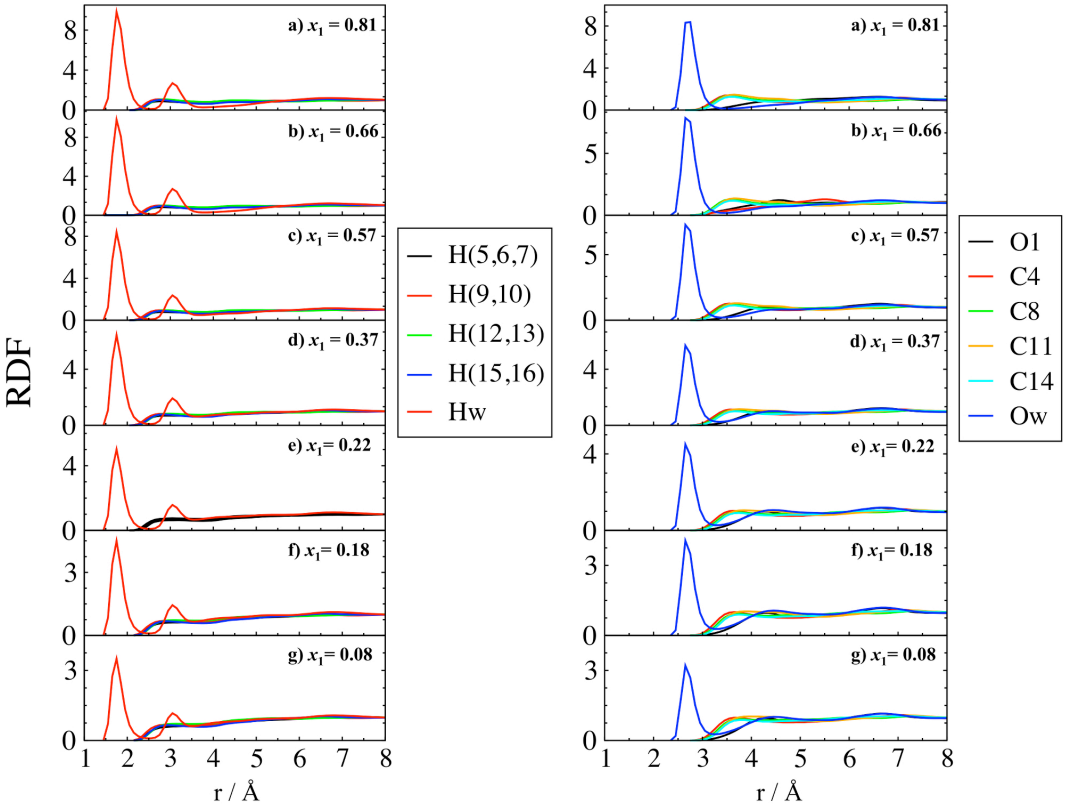

FIG S2. RDFs between the NMP oxygen and 1) H atoms of NMP or water (plots on left); 2) heavy atoms of NMP or water (plots on right) in NMP (1) + W (2) mixture at different x_1 values.

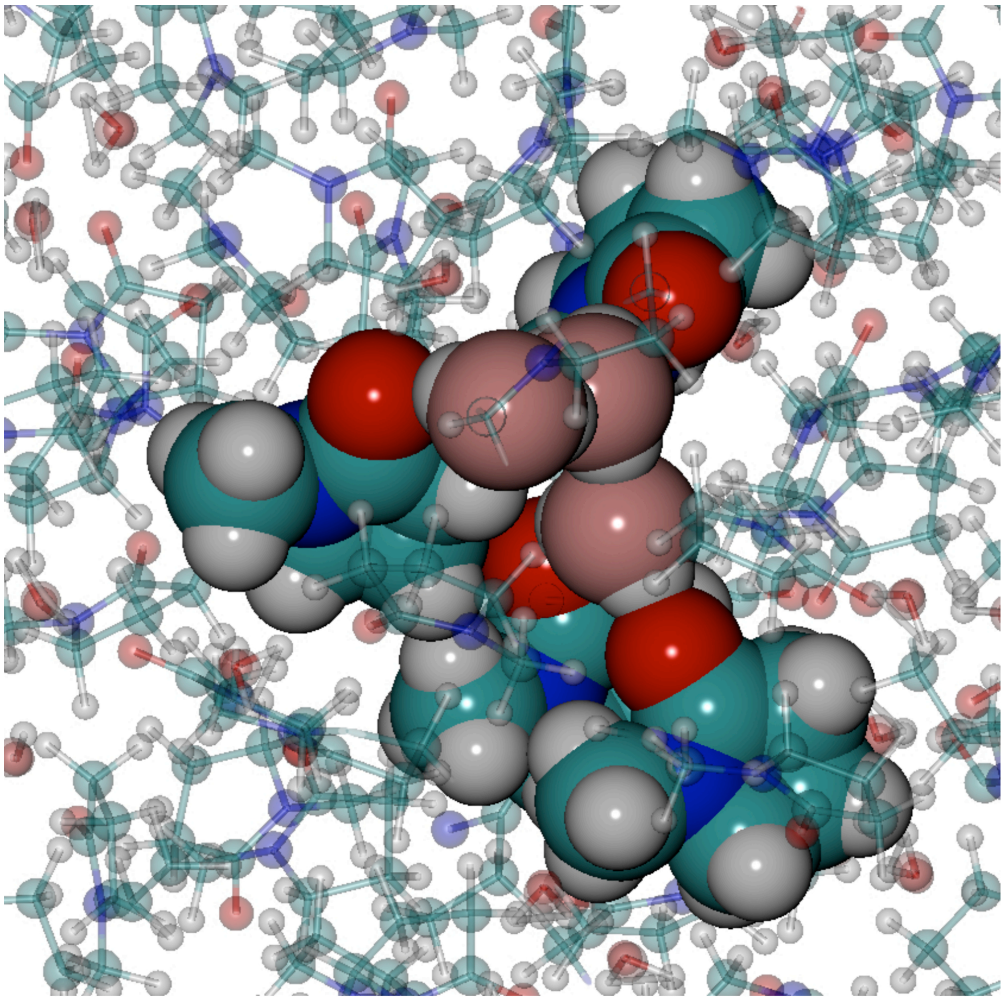

FIG S3. An example of water molecules coordinated to the carbonyl group of NMP. The ball representation of atoms of selected molecules has been scaled to the van der Waals radius. Colour code: cyan: carbon, white: hydrogen, blue: nitrogen, red: NMP oxygen; pink: water oxygen. The first water molecule from the bottom coordinates two carbonyl groups as hydrogen donor; at the same time it forms an hydrogen bonds as an acceptor with a water molecule coordinating the oxygen of a nearby NMP molecule. The latter water molecule is acceptor of hydrogen bond from other water molecules, which coordinates yet another carbonyl group. This example illustrates how, even if only one water molecule is found in the volume not accessible to other NMP molecules, each water molecule can be coordinated to one or more water molecules.

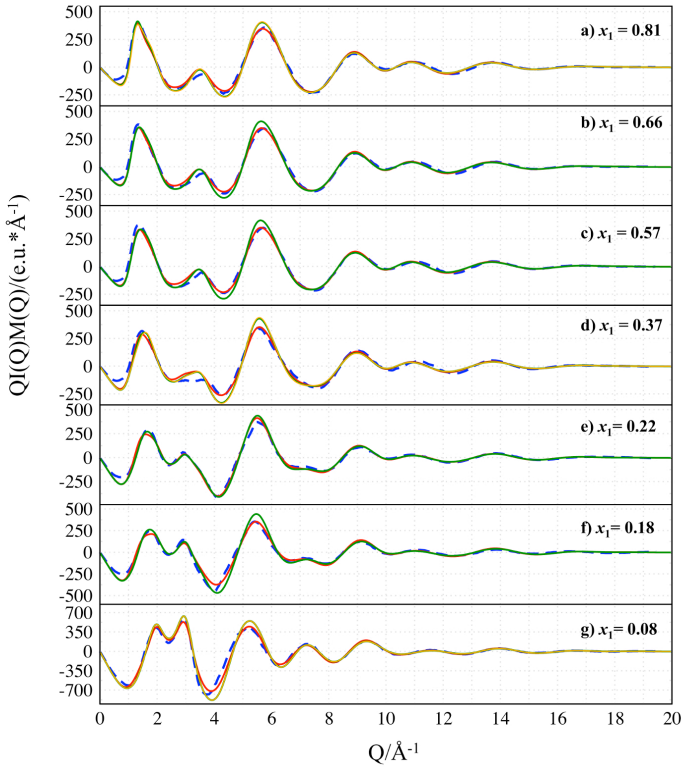

FIG S4. Total structure function *I(Q)*. Experimental (dashed, blue) and model (continuous: red, Set1; orange, Set2; green, Set3) for NMP (1) + W (2) mixtures at different x_1 values.

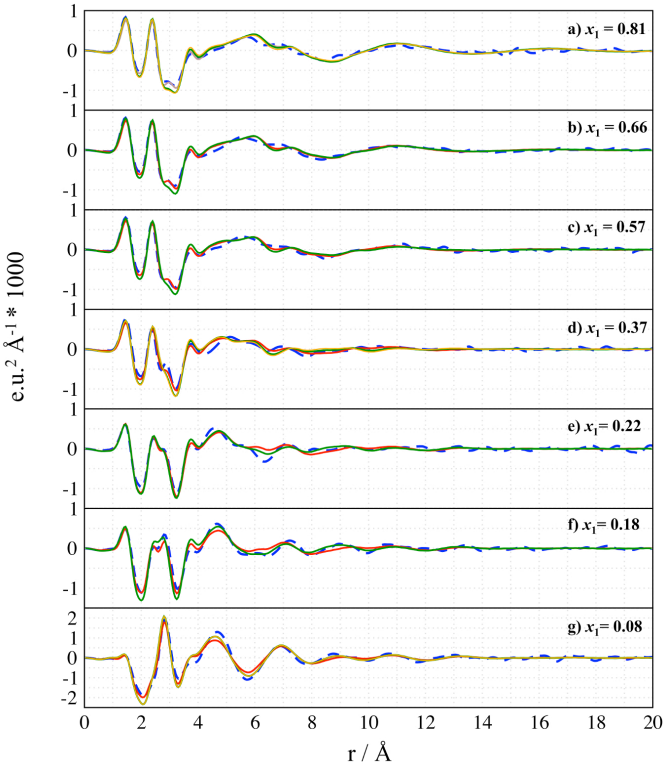

FIG S5. Differential correlation function Diff(r). Experimental (dashed, blue) and model (continuous: red, Set1; orange, Set2; green, Set3) for NMP (1) + W (2) mixtures at different x_1 values.

PAPER II

Reprinted with the permission:

NMR, Calorimetry, and Computational Studies of Aqueous Solutions of *N*-Methyl-2-pyrrolidone.

M. Usula, S. Porcedda, F. Mocci, L. Gontrani, R. Caminiti, and F. Cesare Marincola.

Citation: The Journal of Physical Chemistry B 118, 10493-10502 (2014)

DOI: 10.1021/jp505286z

Published by the **ACS Publications**

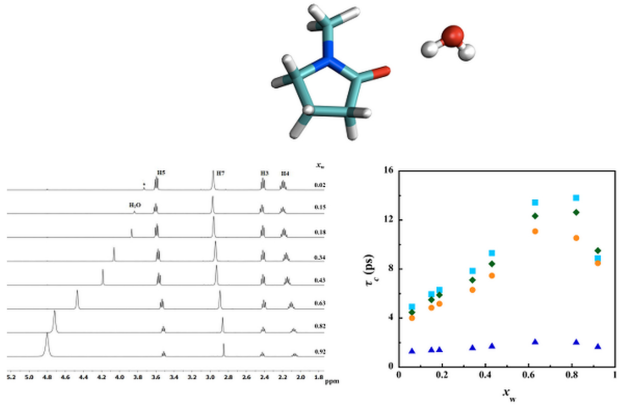

THE JOURNAL OF PHYSICAL CHEMISTRY B

Article

pubs.acs.org/JPCB

NMR, Calorimetry, and Computational Studies of Aqueous Solutions of *N*-Methyl-2-pyrrolidone

Marianna Usula,[†] Silvia Porcedda,[†] Francesca Mocci,[†,‡] Lorenzo Gontrani,[§,∥] Ruggero Caminiti,[∥] and Flaminia Cesare Marincola*[,†]

[†]Dipartimento di Scienze Chimiche e Geologiche, Università degli Studi di Cagliari, S.S. 554 Bivio Sestu, 09042 Monserrato, Italy

[‡]Department of Materials and Environmental Chemistry, Arrhenius Laboratory, Stockholm University, S-106 91 Stockholm, Sweden

[§]CNR − Istituto di Struttura della Materia, Area della Ricerca di Roma Tor Vergata, Via del Fosso del Cavaliere 100, I-00133 Roma, Italy

[∥]Dipartimento di Chimica, Università di Roma "La Sapienza", P.le Aldo Moro 5, I-00185 Roma, Italy

Supporting Information

ABSTRACT: *N*-Methyl-2-pyrrolidone (NMP) is a solvent with applications in different industrial fields. Although largely employed in aqueous mixtures, little is known on the structural and dynamic properties of this system. In order to improve the knowledge on NMP aqueous solutions, useful to the development of their applications, NMR spectroscopy, calorimetric titration, and puckering analysis of molecular dynamics (MD) simulations were employed in this work. Our calorimetric study evidenced the presence of strong interactions between NMP and water and revealed that, under comparable conditions, the solvation of NMP by water results in an interaction stronger than the solvation of water by NMP. Overall, the changes of ^{1}H and ^{13}C chemical shifts and 2D ROESY spectra upon dilution suggested a preferential location of water nearby the carbonyl group of NMP and the formation of hydrogen bonding between these two molecules. In parallel, observation of correlation times by ^{13}C NMR spectroscopy evidenced a different dynamic behavior moving from the NMP-rich region to the water-rich region, characterized by a maximum value at about 0.7 water mole fraction. MD simulations showed that the NMP conformation remains the same over the whole concentration range. Our results were discussed in terms of changes in the NMP assembling upon dilution.

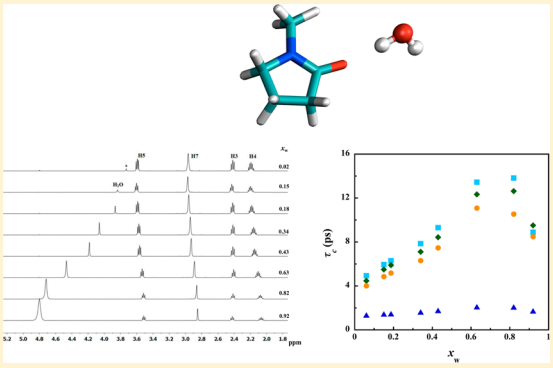

1. INTRODUCTION

Over the past years, considerable interest has been manifested in the use of *N*-methyl-2-pyrrolidone (NMP) as a solvent for industrial applications. Indeed, NMP (Figure 1) exhibits very fascinating properties, such as high boiling point (477.45 K), low melting point (249.55 K), low volatility, low viscosity, large chemical and thermal resistance, and low toxicity, that make it a highly useful solvent in a variety of chemical reactions where an inert medium is required. For instance, it is employed in processing chemicals, coatings, engineering plastics, agricultural chemicals, electronics, paint stripping and cleaning, etc.[1] In addition, NMP is also an attractive solubility enhancer in the pharmaceutical industry.[2]

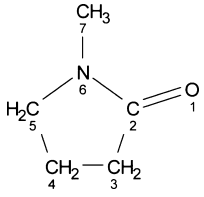

Figure 1. Structure and atom numbering of NMP.

It is well-known that the presence of water in NMP has a significant impact on its properties, particularly on its solvent power and selectivity, in a number of processes. Thus, investigations of NMP−water mixtures are very important, not only scientifically but also industrially, because physicochemical properties of NMP can be tuned by appropriate mixture composition.[3−6] The concentration dependence of different physicochemical properties for this mixture, such as viscosity,[3−6] density,[4−6] and self-diffusion coefficients,[4] evidenced a different behavior on going from the NMP-rich region to the water-rich region. Although all these findings pointed out the presence of important interactions between water and NMP, a detailed understanding of the structural organization of this binary system is still lacking.

In order to understand the macroscopic properties of NMP and, thus, to further develop its applications, it is essential to

Received: May 29, 2014
Revised: August 6, 2014
Published: August 14, 2014

   dx.doi.org/10.1021/jp505286z | *J. Phys. Chem. B* 2014, 118, 10493−10502

investigate the microscopic structure and dynamics of this system at a molecular level. Recently, by combining energy dispersive X-ray diffraction experiments and molecular dynamics (MD) simulations with the generalized AMBER force field, we have achieved a very good agreement between theoretical and experimental diffraction patterns of liquid NMP.[7] The analysis of the radial distribution functions showed that the network of intermolecular C−H···O hydrogen bonds between methyl and carbonyl groups observed in the crystal structure[8] is partly preserved in the liquid structure. Later, we employed a combined approach of MD simulations, wide-angle X-ray scattering experiments, and density measurements to investigate the structural effect of water on NMP over the whole concentration range.[9] A very good agreement between computed and experimental density values and diffraction patterns was obtained, and analysis of the MD trajectories allowed us to explain why a density maximum is observed experimentally for this system. The simulations indicated that water molecules can occupy "empty cavities" of the NMP network, i.e., spatial regions which are not accessible to the heavy atoms of the solvating NMP molecules but are accessible to water molecules. Each cavity can host only two water molecules; therefore, the addition of water to NMP leads to an increase in density up to a water:NMP molar ratio of 2:1. Further added water molecules alter the NMP network and the density decreases, increasing the water content.

As an extension of our previous studies,[7,9] in the present work, we further investigated NMP−water mixtures over the whole concentration range by a combined use of NMR spectroscopy, calorimetric measurements, and puckering analysis of MD simulations. The results provided additional information on the structural and dynamics changes of NMP taking place upon dilution.

2. EXPERIMENTAL SECTION

2.1. Sample Preparation. *N*-Methyl-2-pyrrolidone (purity >99.5%) was purchased from Sigma-Aldrich. NMP was dried for 5 days at room temperature under a high vacuum (6×10^{-2} Torr) over P_2O_5. The residual water content, estimated by ^{1}H NMR spectroscopy, was 0.18% w/w (0.02 mole fraction of water, x_w). From now on, this sample will be referred to as dried, despite the presence of water.

For NMR analysis, dried NMP was moved to a nitrogen-filled glovebag where it was transferred to a 5 mm NMR tube. Aqueous solutions were prepared by weighing samples of NMP in screw-cap glass vials in the glovebag, removing the samples from the bag, and adding proper amounts of water to give mole fractions of water, x_w, of 0.15, 0.18, 0.34, 0.43, 0.63, 0.82, and 0.92.

2.2. Calorimetric Measurements and Data Treatment. Heats of solution were collected through a heat flow calorimeter by Thermometric (Järfälla, Sweden - Thermal Activity Monitor, model 2277) at 298.1 K (±0.1 K). Experiments were conducted by adding a pure component, via Hamilton gastight syringes of capacity ranging from 250.0 to 1000 μL driven by Cole-Parmer pumps (Vernon Hills, Illinois, USA - model 74900), to an ampule of 4 cm^3 capacity initially charged with the other component or with a stock mixture of them. With this system, we were able to make accurate injections starting from a minimum of 1 μL, with precision 0.5%, and to measure accurate heat effects as small as 0.01 J, with a sensitivity of 0.5 μW. We chose this technique instead of mixing-flow calorimetry to avoid errors due to incomplete mixing and to obtain direct experimental values of the partial molar enthalpy in the whole concentration range.[10]

The experimental solution heats, Q_{exp}, released by the additions of very small quantities of the titrant, n_j, practically represent partial molar enthalpies, $\bar{H}_j$ ($\bar{H}_j \cong Q/n_j$). Calculated values of the solution heats, Q_{calc}, can be obtained by proper differentiation of the equation $H^E = f(x)$, such as the Redlich−Kister (RK) one:

$$\frac{H^E}{RT} = x_1 x_2 \sum_{k=1}^{n} c_k (x_1 - x_2)^{k-1} \quad (1)$$

A standard least-squares procedure identifies the best values of c_k parameters at the minimum of the objective function OF = $\sum(Q_{exp} - Q_{calc})^2$. Proper allowance was made for the heat involved in the phase composition changes brought about by the vapor−liquid equilibration after each addition. An exhaustive description of the apparatus, the experimental procedure, and the data treatment can be found in the literature.[11,12]

The reliability of the whole procedure was checked by measuring the H^E of the benzene + cyclohexane system in the whole concentration range. Comparison with literature data[13] revealed a discrepancy lower than 2%. The uncertainty in the observed heat, Q, as determined by the reproducibility of the experiments and by integration of the peak area, was evaluated as 0.5%.

2.3. NMR Spectroscopy. ^{1}H NMR spectra were obtained with a Varian Unity INOVA 500 spectrometer operating at a proton resonance frequency of 499.84 MHz, while ^{13}C NMR spectra were recorded using a Varian Unity INOVA 400 spectrometer with a ^{13}C resonance frequency of 100.57 MHz. Locking was performed using an insert capillary tube filled with D_2O. All experiments were carried out at 300 K.

^{1}H spectra were acquired using 16 scans, a spectral width of 3000 Hz, a relaxation delay of 15 s, and a 90° pulse of 8.5 μs. Chemical shifts were referred to the signal of the residual water of D_2O in the capillary tube (δ = 4.78 ppm).

Two-dimensional adiabatic ROESY spectra were acquired with a standard pulse sequence[14,15] over a sweep width of 3000 Hz using 2048 data points in the t_2 dimension and 256 increments in the t_1 dimension. A total of 16 scans were collected for each t_1 increment with an acquisition time of 0.15 s followed by an additional relaxation delay of 2 s. A mixing time of 200 ms was used for all samples. The ROESY data set was processed by applying a shifted square sine-bell function in both dimensions and zero-filling to 2048 × 2048 real data points prior to the Fourier transformation.

The ^{13}C spin−lattice relaxation times (T_1) were measured by the inversion recovery method. A total of 16 scans were collected, and 16−18 variable delays were used. The relaxation delay was at least 5 times greater than the longest T_1. The reported values are averages of three measurements with an estimated precision of 5%.

^{13}C{^{1}H} nuclear Overhauser enhancement (NOE) factors were determined from the ratios of peak intensities in a spectrum obtained with continuously applied composite pulse decoupling and in a spectrum where the NOE was suppressed by gating the decoupler on only during acquisition. For both spectra, a delay of at least 10 T_1 was allowed between acquisition pulses. The NOE measurements were reproducible within ±10%.

^{13}C NMR Relaxation Data Analysis. As stated elsewhere,[16−21] the investigation of aggregation behavior by means of NMR spin relaxation rate measurements relies on the dependence of the rates on the dynamics of molecular reorientation as expressed by the spectral density function $J(\omega)$.[22] For proton-carrying ^{13}C nuclei in medium-sized molecules, the spin relaxation is usually dominated by the dipole−dipole interaction with directly bonded protons. If the protons are subjected to broadband decoupling and the cross-correlations between different interactions can be neglected, the ^{13}C spin−lattice relaxation is a simple exponential process, characterized by a single time constant, T_1, called the spin−lattice relaxation time. Neglecting the contributions from protons that are not directly bonded, the dipolar contribution to the spin−lattice relaxation rate $(1/T_1^{DD})$ and the nuclear Overhauser enhancement (NOE) are given by eqs 2 and 3, respectively:

$$\frac{1}{T_1^{DD}} = N\frac{\mu_0^2\gamma_H^2\gamma_C^2\hbar^2}{160\pi^2 r_{CH}^6}(J(\omega_H - \omega_C) + 3J(\omega_C) + 6J(\omega_H + \omega_C)) \quad (2)$$

$$NOE = \frac{\gamma_H}{\gamma_C}\frac{6J(\omega_H + \omega_C) - J(\omega_H - \omega_C)}{J(\omega_H - \omega_C) + 3J(\omega_C) + 6J(\omega_H + \omega_C)} \quad (3)$$

where N is the number of attached protons; γ_H, γ_c and ω_H, ω_c are the gyromagnetic ratios and Larmor frequencies of proton and carbon, respectively; $\hbar$ is the reduced Planck constant; r_{CH} is the carbon−proton distance (fixed at 1.09 Å for our analysis); and μ_0 is the permittivity of free space. Provided the motion is isotropic, $J(\omega)$ is given by

$$J(\omega) = \frac{2\tau_c}{1 + \omega^2\tau_c^2} \quad (4)$$

where τ_c is the correlation time for the motion of the C−H axis and approximates the time required for rotation of the molecule through 1 rad.

When the contribution of T_1^{DD} to the measured T_1 is 100%, the NOE value reaches a maximum of 1.988 $(=\gamma_H/2\gamma_C)$. For ^{13}C nuclei where DD relaxation competes with other mechanisms, the contribution of the dipole−dipole mechanism can be calculated if the experimental NOE (NOE_{exp}) is determined:

$$\%\ DD\ relaxation = \frac{NOE_{exp}}{1.988} \times 100 \quad (5)$$

2.4. Computational Details. MD simulations were performed with the AMBER 11 package[23] (both CPU and GPU versions of PMEMD)[24] using a cubic box containing about 11000 atoms of the pure NMP or of the NMP+W mixtures at different x_w, covering the whole composition range. The adopted simulation protocol is described in our previous paper.[9] For each simulation, a conformational analysis was performed by analyzing the changes in the ring puckering of selected NMP residues. The quantitative description of puckering in five-membered rings involves two parameters: the pseudorotational angle and the amplitude. In the present paper, the calculations of these parameters were done using the *Altona and Sundarlingam* algorithm[25] as implemented in the *ptraj* analysis program of the AMBER package.[23]

The most populated NMP conformations in neat NMP or in its aqueous mixtures were studied also *in vacuo* by means of DFT calculations. In detail, selected starting geometries were taken from MD trajectories and optimized at the B3LYP/6-311++G(d,p) theory level using Gaussian 09 software.[26] The character of the stationary points was verified by carrying out the vibrational analysis at the same theory level.

3. RESULTS AND DISCUSSION

3.1. Calorimetric Measurements. In Figure 2, the experimental points and the smoothed curves of excess molar enthalpies, H^E, and partial molar enthalpies of constituents, $\bar{H}_j^E$, for the NMP−water mixtures are plotted as a function of the mole fraction of water, x_w. The direct experimental data concerning $\bar{H}_j^E$ are reported in Table S1 of the Supporting Information.

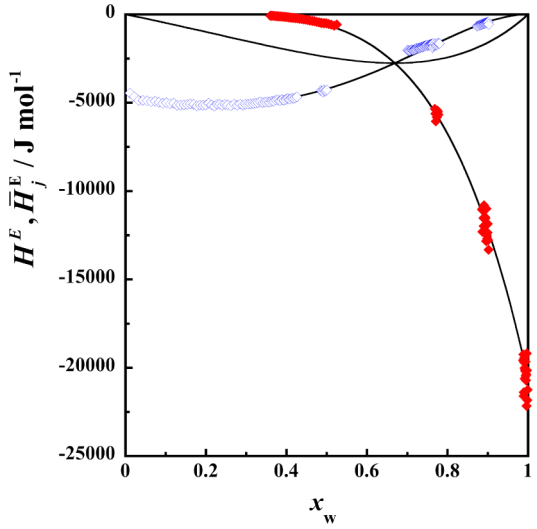

Figure 2. Excess molar enthalpies, H^E, and partial molar enthalpies, $\bar{H}_j^E$, of the NMP + water system as a function of the water mole fraction, x_w: ◆, $\bar{H}_N^E$; ◇, $\bar{H}_W^E$. Curves are calculated according to eq 1.

From a least-squares treatment by using eq 1, we obtained the following values of the dimensionless coefficients: $c_1 = -3.88358$; $c_2 = +2.91937$; $c_3 = -1.17099$; $c_4 = +0.32630$. From the standard deviations of the above c_k parameters, we calculated the uncertainty on the excess molar enthalpy at equimolar composition $(H^E_{x_w=0.5} = -2407 \pm 20\ J\ mol^{-1})$ and on the excess partial molar enthalpy of each component at infinite dilution $(\bar{H}_N^{E,\infty} = -20.6 \pm 0.3$ and $\bar{H}_W^{E,\infty} = -4.5 \pm 0.3\ kJ\ mol^{-1})$. Our H^E and $\bar{H}_i^{E,\infty}$ data agree with those of the literature: the H^E values at equimolar composition obtained by the RK coefficients from the work of Zaichikov et al.[27] and Macdonald et al.[5] are -2440 ± 25 and $-2476 \pm 75\ J\ mol^{-1}$, respectively; the $\bar{H}_N^{E,\infty}$ obtained by other authors[28,29] are -21.1 ± 0.4 and $-21.2 \pm 0.4\ kJ\ mol^{-1}$. As concerns the excess partial molar enthalpies, there are no data for this mixture available in the literature to compare directly with the present results. The high exothermic mixing effect of the NMP−water system is indicative of the presence of strong interactions between the components of the mixture. Indeed, generally mixtures between two different organic compounds are characterized by the endothermic effect, while the mixing is exothermic when two components give rise to attractive interactions among unlike molecules stronger that those present in like molecules.[30]

dx.doi.org/10.1021/jp505286z | J. Phys. Chem. B 2014, 118, 10493−10502

As can be seen in Figure 2, the shape of the H^E curve is highly asymmetric with a minimum value of −2754 J mol^{-1} at $x_w \approx 0.7$, calculated from the RK coefficients. The asymmetry of H^E is explained with the nonspecular peculiar shape of $\bar{H}_j^E$. At infinite dilution, excess partial molar enthalpies of water, $\bar{H}_W^E$, have absolute values much lower with respect to $\bar{H}_N^E$. In fact, the addition of 1 mol of NMP caused a thermal effect roughly 4 times higher than that associated with the dissolution of 1 mol of water. This behavior results in stronger attractive interactions played by the water solvent in the dissolution and solvation of the solute NMP, with respect to the same process in which the same components play exchanged roles. It is not common that the mixing of an organic compound with water originates such a high, in absolute value, heat of mixing,[30] but some exceptions are found such as the case of dimethyl sulfoxide,[5] which shows a heat of mixing value similar to that of the NMP−water system. Exothermic mixing effects of NMP have been observed in mixtures with chloro-alkanes and -alkenes, the highest exceptional value ($H^E_{x_W=0.5}$ = −4750 J mol^{-1}) being observed in NMP + 1,1,2,2-tetrachloroethane mixtures.[31] The higher exothermic mixing effect of this latter system, compared to those of the NMP−water mixtures, could be ascribed to the strong electron-withdrawing effect of chloro atoms on the hydrocarbon protons: the deshielded H atoms of halogenated hydrocarbon are able to establish a hydrogen bond (HB) with NMP stronger than that between NMP and water.

3.2. ^{1}H NMR Spectroscopy. Figure 3 shows a stack plot of the ^{1}H NMR spectra of dried NMP and its mixtures with H_2O.

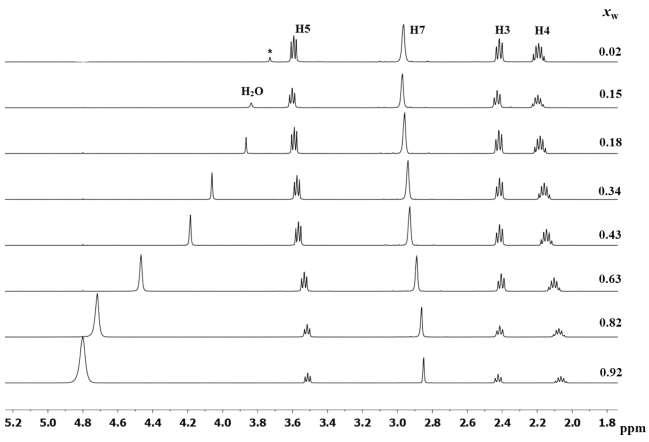

Figure 3. ^{1}H NMR spectra of dried NMP (top) and its aqueous mixtures at different water mole fractions, x_w. The asterisk denotes the residual water peak in dried NMP.

As can be seen, the proton chemical shifts (δ) of both NMP and water peaks were sensibly affected by the mixture composition. Since δ is a sensitive indicator of the degree of magnetic shielding of the nucleus, being influenced by surrounding electrons and neighboring atoms and groups in the molecule, chemical shift variations were indicative of the occurrence of changes in the local chemical environment experienced by protons in both molecules. In order to facilitate the comparison among the δ changes of individual hydrogen atoms in NMP, deviations expressed as the difference between the positions of the signals in the presence and absence of water ($\Delta\delta$) are depicted in Figure 4 as a function of the water mole fraction, x_w.

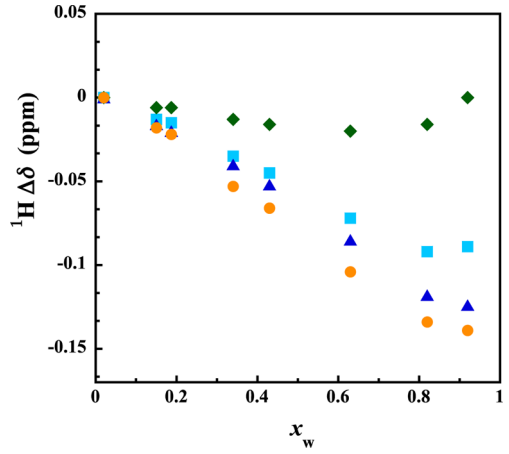

Figure 4. ^{1}H chemical shift deviations from dried NMP, $\Delta\delta$ (δ_{mix} − δ_{dried}), as a function of the water mole fraction, x_w. Symbols for the individual NMP protons are as follows: ◆, H3; ●, H4; ■, H5; ▲, H7.

It can be seen that, upon dilution, all NMP proton peaks moved upfield, with the weakest effect on the proton in the carbon adjacent to the C═O group (H3). Simultaneously, the water peak was monotonously downfield shifted on increasing the water content, approaching the pure water signal (δ_w = 4.78 ppm). The shift to higher fields (lower δ_H) for H4, H5, and H7 protons of NMP evidenced a significant increase in magnetic shielding of these nuclei upon hydration up to $x_w \approx 0.8$ (Figure 4). Above this value, δ_{H4}, δ_{H5}, and δ_{H7} were all scarcely affected by the mixture composition. These δ trends can be explained satisfactorily if we consider recent results of MD simulations, pointing out the occurrence of a preferential directionality in the assembling of NMP molecules.[9] In particular, spatial density functions (SDFs) analysis indicated a high probability for the C═O group of a molecule to be close to the methyl carbon and the methylenic carbon C4 of another one. It is, therefore, likely that protons lying near the plane of the carbonyl groups in spatially close molecules experience deshielding due to the C═O anisotropic effect. Accordingly, the further away the proton is from the carbonyl group, the weaker this effect becomes. In view of these considerations, the chemical shift trends of H4, H5, and H7 may refer to the change in the spatial arrangement of NMP. In the NMP-rich region, these protons are pushed away from the C═O group, and thus from its deshielding cone, as additional water enters into the NMP network and NMP molecules move away from each other. In the water-rich region, above $x_w \approx 0.8$, the spatial distance among NMP molecules would be such that H4, H5, and H7 are not subject to the deshielding contribution to their chemical shift by the magnetic anisotropy of the carbonyl groups of other molecules. Concerning the changes of δ_{H7}, although our NMR data did not provide direct evidence of a hydrogen bonding between the methyl and carbonyl groups,[7] we do not exclude a possible contribution also from the breaking of this binding to the increased shielding on the methyl protons upon dilution.

Differently from H4, H5, and H7, the H3 proton chemical shift exhibited a weak concentration dependence (Figure 4), evidencing changes in the magnetic environment of this nucleus of lower entity with respect to those occurring around the other protons. Likely, the H3 proton experiences only the magnetic anisotropy of the adjacent carbonyl group, thus δ_{H3} being almost independent of the mixture composition. This hypothesis is in good agreement with the low probability of the

dx.doi.org/10.1021/jp505286z | J. Phys. Chem. B 2014, 118, 10493−10502

C3 carbon of solvating NMP molecules to lie below and above the carbonyl group of another NMP molecule at any concentration, as seen from the SDFs.[9]

Concerning the ^{1}H chemical shift of water, being proportional to the electron density about the nucleus, δ_w can be taken as a measure of the polarization of water molecules, averaged over the protons of all molecules in solution,[32] and thus of the hydrogen-bonding strength of water hydrogen: the larger the δ_w, the stronger is the HB of water. Thus, the δ_w value measured at x_w = 0.02 (i.e., 3.8 ppm), being lower than that of pure water, evidenced a smaller polarization of water molecules in the presence of a large excess of NMP than in pure water. This observation is consistent with the reported lowering of the dielectric constant[33] and surface tension[2] of water with increasing concentrations of NMP. It was interesting to note that, during the course of titration, the ^{13}C peak of the carbonyl group downfield shifted (Figure S1 of the Supporting Information), evidencing a reduction of the shielding on the C2 carbon. According to the literature,[32] this increase in δ_{C2} may be ascribed to the involvement of the C═O oxygen atom in HB with water. Therefore, on the basis of this experimental evidence, the change in the water chemical shift occurring upon NMP dilution could be explained as follows. When a small amount of water is added to NMP, water molecules tend to HB interact with the oxygen atom of C═O, presumably replacing the intermolecular interactions between the carbonyl and methyl groups. With δ_w being upfield shifted compared to pure water, the OH···O═C HB is weaker than that between water molecules. On increasing the water content, water−water interactions also take place, with the number of water−water HBs increasing with the composition and becoming dominant when x_w approaches the neat water.

3.3. Puckering Analysis. To evaluate a possible correlation between the composition dependence of the ^{1}H chemical shifts of NMP and conformational changes of this molecule, a conformational analysis was done through MD simulations. The possible conformations of a nonplanar five-membered ring, such as that of NMP, can be grouped into two main classes of different symmetry: the envelope (E) and the twist (T) forms. In the E form, four atoms lay in the same plane with one atom out of the plane, while, in the T form, three adjacent atoms define a plane and the other two are found one below and one above that plane. The relationship between T and E conformations and the pseudorotational angles according to the *Altona and Sundarlingam* convention[25] is shown in Figure 5. Several T and E conformations are possible, depending on which atoms are found to be below or above the plane defined by the other atoms. For each form, the superscript and/or subscript indicate the atoms above and/or below the plane, respectively. Twist conformations are even multiples of 18° of the pseudorotational phase angles (P = 0°, 36°, ...), while envelope conformations are odd multiples (P = 18°, 54°, ...).

Figure 6 shows the relative populations of the possible conformational forms calculated for selected NMP residues (right) and the average values of the puckering amplitude (left) as a function of the pseudorotational phase angle in the NMP−water systems at different compositions. Previous puckering analysis performed on neat NMP[7] showed that the E and T forms are uniformly distributed in the neat NMP and the relative population was found to be 50.13:49.86. This finding is confirmed by our conformational analysis. Furthermore, our data showed that (i) the favorite puckerings at all compositions are the E form with C4 outside the plane formed by the other

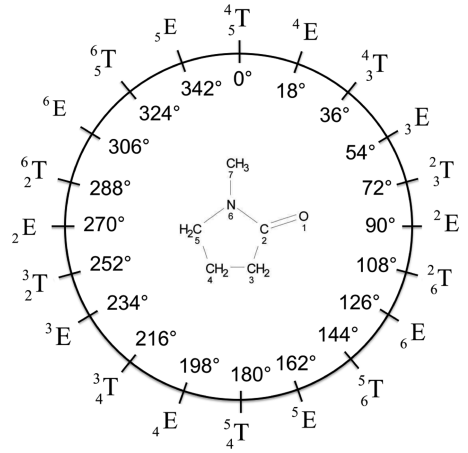

Figure 5. Pseudorotational circle of the NMP ring. Each point on the circle represents a specific value of the pseudorotation phase angles, P.

ring atoms (^{4}E and $_4$E) and the T form with C4 and C3 on the opposite side of the plane defined by the other three atoms ($^3_4$T and $^4_3$T) (Figure 6, right side); (ii) the favorite ring puckering forms are characterized by having the largest amplitude values (ca. 20°) (Figure 6, left side); (iii) the addition of water to NMP does not induce changes of its conformation equilibrium. In conclusion, the ring puckering of NMP molecules is not influenced by the presence of water over the whole concentration range, and hence, the NMR chemical shift trends shown in Figure 4 were excluded to be linked to conformational change effects.

It is known that NMP puckering preferences in the solid state are affected by the packing of the molecules in the crystals.[8] To verify whether in the liquid state the conformational preferences are affected by the interaction with solvating molecules, DFT calculations were performed on selected conformations. The calculations were done *in vacuo* to exclude the effect of the solvent. Representative configurations of the four most populated puckering states were selected from the MD trajectories and optimized at the B3LYP/6-311++G(d,p) level of theory. The optimization led to some minor pseudorotation angle variation with respect to the starting value, but it remained in all cases within the 18° range of the original puckering. As shown in Table 1, the energy differences among the puckering states were found to be negligible (3×10^{-3} kJ/mol). This result indicates that the distribution of the population among the highest populated puckering states in the liquid neat NMP, or in its water solutions, is not due to the solvation. The dihedral angle values of the ^{4}E form compare well with those of the minimum energy conformer calculated by Müller et al.[8] at the RHF/6-31G theory level (see Table 1).

3.4. 2D ROESY Spectra. Information on the location of water in the proximity of NMP was provided by homonuclear NOEs in the rotating frame (ROEs). ^{1}H,^{1}H ROESY is a 2D NMR experiment for correlating signals arising from protons close in space (interproton distance usually within about 5 Å). In fact, the correlation peaks observed in ROESY spectra are the result of cross-relaxation between neighboring protons, the main mechanism of which is a through-space dipole−dipole interaction.[34,35] The cross-peak intensity reflects the extent of magnetization transfer between interacting nuclei and is inversely proportional to the sixth power of their internuclear distance. Figure 7 shows the 2D ROESY spectrum of dried NMP. As can be seen, cross-peaks clearly establish spatial

dx.doi.org/10.1021/jp505286z | J. Phys. Chem. B 2014, 118, 10493−10502

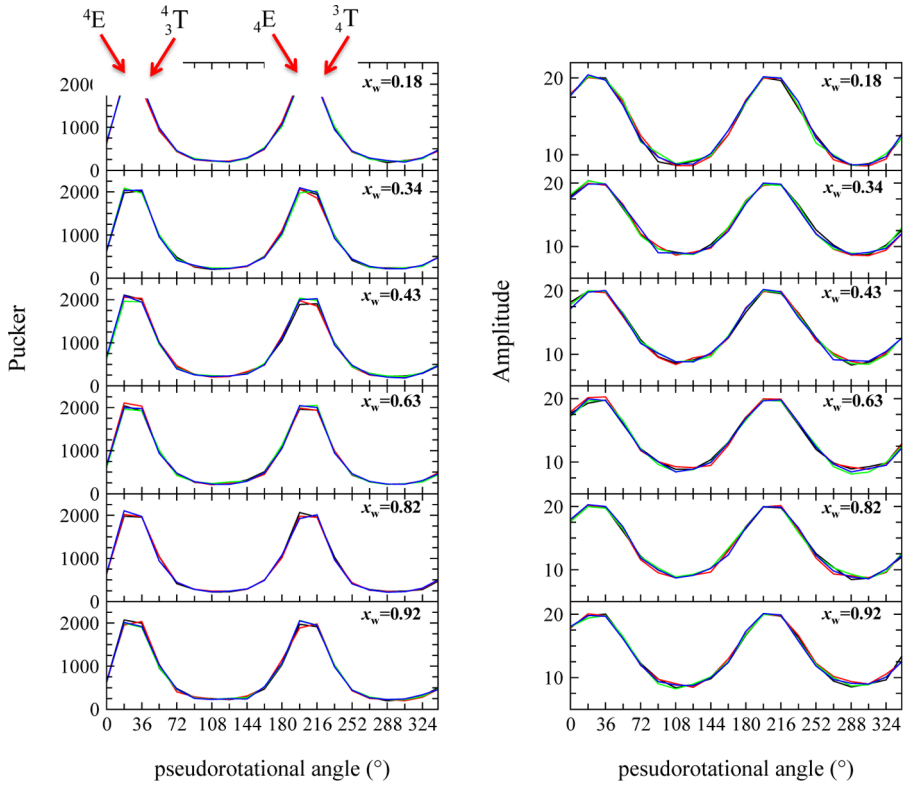

Figure 6. Populations of the possible conformational states (left) and average values of the amplitude of the puckering (right) calculated for selected NMP residues in NMP−water systems at different compositions as a function of the pseudorotation angle.

Table 1. Dihedral and Pseudorotation Angles and Relative Energies (Electronic + Thermal Free Energy) of B3LYP/6-311++G(d,p) Optimized NMP Conformations

	NMP conformations				
dihedral angles	$^3_4$T	$^4_3$T	^{4}E	$_4$E	Müller et al.[a]
C5−N6−C2−C3	18.0	−14.0	−4.4	1.5	−4.4
N6−C2−C3−C4	−33.3	31.8	−13.3	7.8	−13.3
C2−C3−C4−C5	36.4	−35.4	24.4	−13.2	24.4
C3−C4−C5−N6	−26.6	32.5	−26.5	13.9	−26.6
C4−C5−N6−C2	8.3	−14.0	20.1	−10.2	20.1
pseudorotation angles	218°	36°	190°	12°	
ΔE (kJ mol^{-1})	3×10^{-3}	0	3×10^{-3}	0	

[a]See ref 8.

interactions among all proton atoms. Unfortunately, the separation of the intra- and intermolecular dipolar contacts in this system was not feasible, both because it comprises molecules of the same kind and because the average intramolecular distances between the H atoms of interest calculated by MD simulations[9] are all lower than 5 Å (Figure S2 in the Supporting Information). It is worth reminding that this sample was characterized by the presence of a residual amount of adsorbed water (x_w = 0.02). No cross-peaks were observed between water and NMP protons (Figure 7), meaning that the spatial correlation between the two molecules was rather weak.

Figure 8 shows some sections of the 2D-ROESY spectra of selected NMP−water mixtures. The spectra evidenced the presence of NOE contacts between water and all NMP protons at all compositions. Comparing the volume of these cross-peaks, determined by integration and divided by the numbers of equivalent protons of NMP and water contributing on these, showed that water was within closer proximity to H7 with respect to other protons up to x_w = 0.43. Above this mole fraction, the spatial correlations with water were almost the same for all NMP protons. These observations suggest that, when low amounts of water are added, water preferentially interacts with NMP nearby the carbonyl domain, as hypothesized also by our ^{1}H and ^{13}C NMR chemical shift data, while at the highest water concentrations all sites are surrounded by water molecules. This picture is in good agreement with the NMP−water organization shown from SDFs calculated in our previous study.[9]

3.5. ^{13}C NMR Spin−Lattice Relaxation. Complementary information on the NMP−water interaction was finally assessed by ^{13}C NMR relaxation measurements. Figure 9a shows the values of the ^{13}C spin−lattice relaxation rate R_1 (=1/T_1) for the samples under investigation. The smallest R_1 values were recorded for the carbonyl carbon, while those of the protonated carbons followed the order C5 > C3 > C4 ≫ C7. It can be seen that the relaxation of all carbons speeded up upon dilution below $x_w \approx 0.8$ and, then, slowed down with further additions of water, this behavior being particularly pronounced for CH_2

dx.doi.org/10.1021/jp505286z | J. Phys. Chem. B 2014, 118, 10493−10502

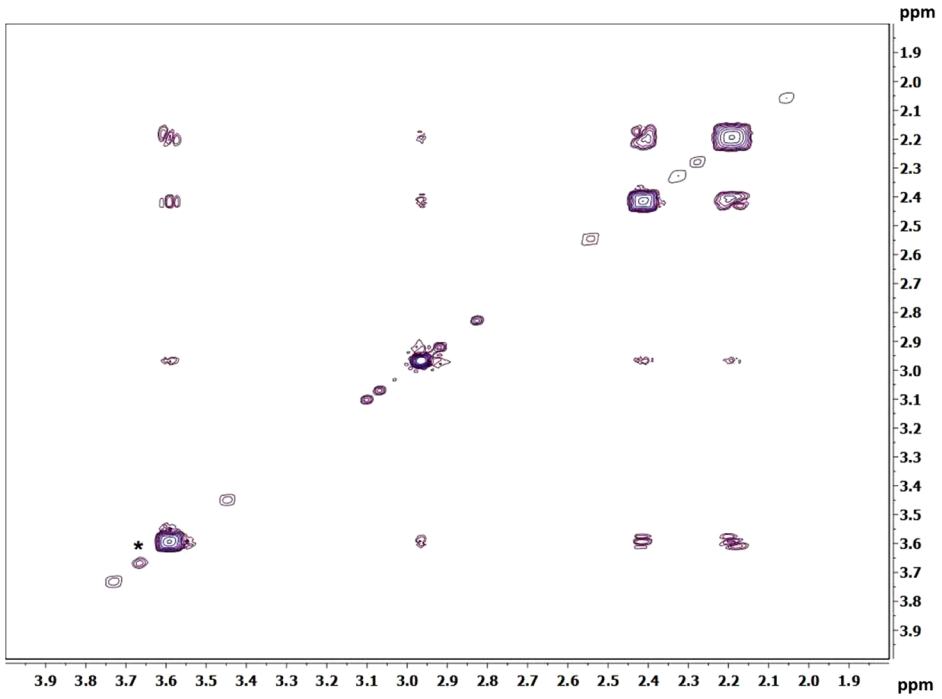

Figure 7. 2D-ROESY spectrum of dried NMP. The asterisk denotes the peak of residual absorbed water.

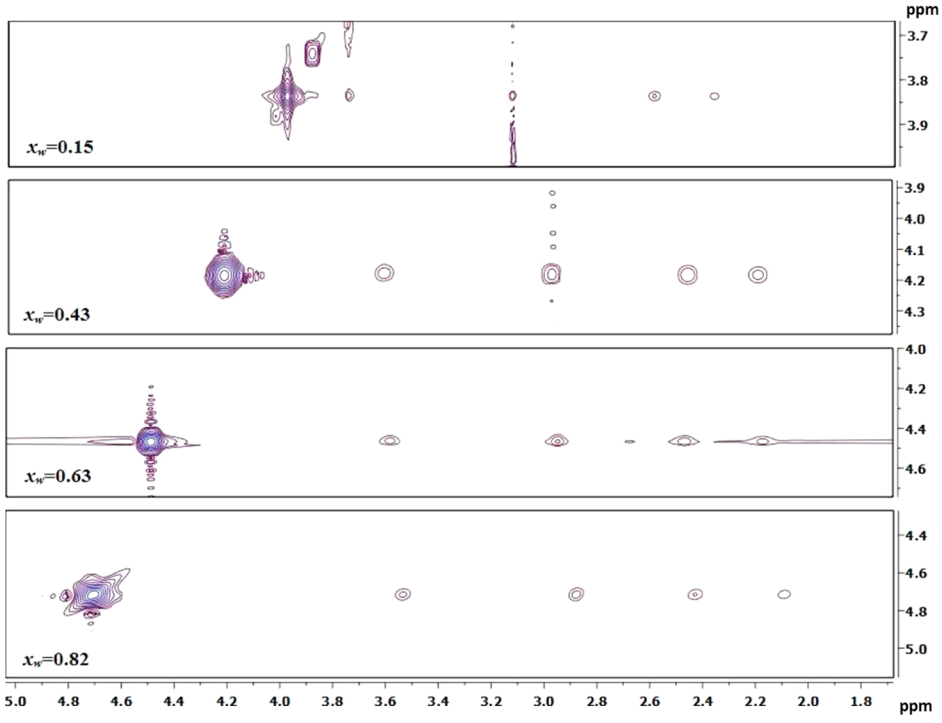

Figure 8. Expanded regions of the 2D-ROESY NMR spectra of NMP−water mixtures at different water mole fractions, x_w. The vertical axis shows the frequency region of the water H atoms.

carbons. By measuring the NOE factor, the dipolar contribution (T_1^{DD}) to the ^{13}C relaxation was calculated (eq 5). NOE values varied from 1.9 to 2.0 for the CH_2 carbons and 1.7 to 1.8 for the CH_3 carbon. Thus, the T_1^{DD} contribution was assumed to be dominant for protonated carbons. As for the carbonyl carbon, the values obtained for NOE ranged between 1.1 and 1.3; the T_1^{DD} contribution was estimated to be ≈60% of the total T_1 relaxation mechanism. Another possible contribution to the ^{13}C relaxation of C2 may arise from chemical shift anisotropy, known to be important in samples with double bonds, aromatic groups, and carbonyl carbons.[36]

Therefore, assuming the relaxation for the alkyl carbons to undergo only by the dipolar mechanism, the R_1's of proton-bearing carbons of NMP were used to compute the rotational correlation times of each resolved site (eqs 2−4), and thus to investigate the NMP local mobility as a function of water concentration. As expected, the correlation time, τ_c, values for the methyl group were shorter than those for CH_2 groups due

dx.doi.org/10.1021/jp505286z | J. Phys. Chem. B 2014, 118, 10493−10502

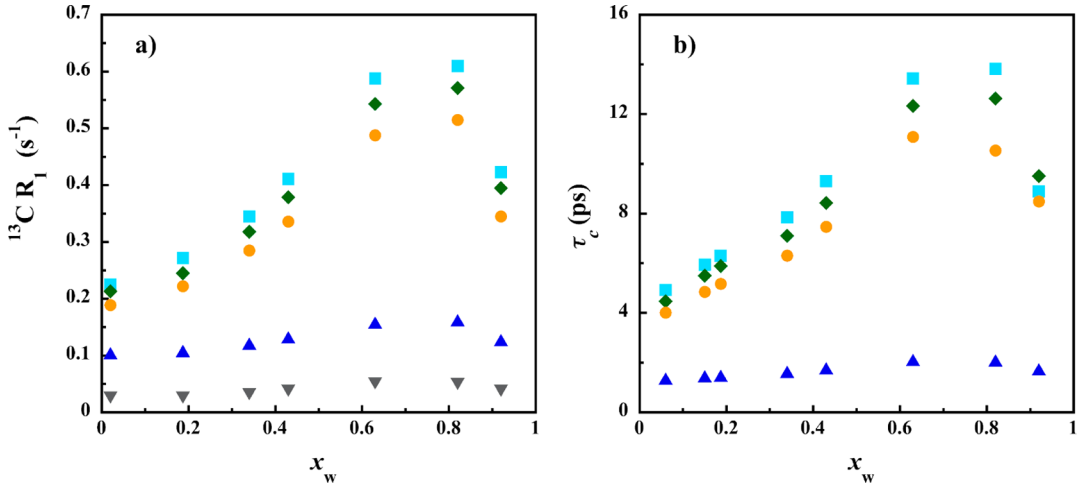

Figure 9. (a) ^{13}C spin−lattice relaxation rates and (b) rotational correlation times, τ_c, for NMP as a function of the water mole fraction, x_w. Symbols for the individual carbon atoms are as follows: ▼, C2; ◆, C3; ●, C4; ■, C5; ▲, C7.

to the rotation of the H_3C-N bond (Figure 9b). It can also be seen that the dynamics of all carbon sites were equally influenced by the mixture composition, showing a remarkably nonlinear behavior with a break point at x_w values within 0.6 and 0.8. In particular, in the NMP-rich region, a monotonic increase of τ_c's took place with increasing water content, indicating that NMP molecules experienced a reduction of overall molecular motion. Differently, the notable feature of the measured concentration dependence of τ_c's in the water-rich region was an overall decrease with the increase of added water, thus showing a dynamic state of NMP opposite to that observed below $x_w \approx 0.8$.

Similarly to the concentration dependence of τ_c, data in the literature report a maximum value of viscosity (η) for the NMP−water mixture at x_w near 0.7 within the temperature range 293.15−323.15 K. For the sake of comparison, the η values, measured at 298.15 and 300.15 K over the whole concentration range,[37] are included in Figure 10 together with the rotational correlation times for the C3 carbon atom as a function of x_w. It is apparent from this plot that the τ_c behavior

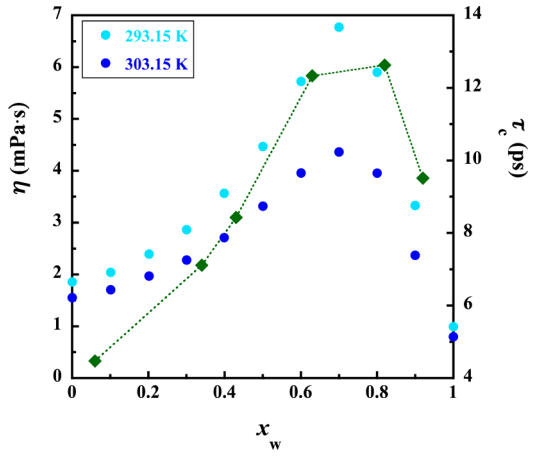

Figure 10. Concentration dependence of the rotational correlation time, τ_c, for the C3 atom and viscosity, η, values of aqueous solutions of NMP taken from the literature[37] at 293.15 and 303.15 K. Symbols are as follows: ◆, τ_c; ●, η. Lines were used as a visual aid. The experimental τ_c data are those shown in Figure 9b.

strongly correlated with the changes in viscosity. In classical mechanics, the relation between these two properties for isotropically reorienting spherical molecules approximately follows the Stokes−Einstein equation:

$$\tau_c = \frac{4\pi\eta a^3}{3\kappa_B T} \tag{6}$$

where a is the radius of the molecule, T is the absolute temperature, and k_B is the Boltzmann constant. It is however worth noting in Figure 9b that, despite the similar curve shape, the rate of τ_c changes for CH_2 carbons is much higher than that of the CH_3 carbon. This result may be indicative of a different microviscosity around carbons in NMP.[38] In particular, with the methyl group being involved in a HB interaction with the carbonyl one,[7] it is not ruled out that the breaking of this intermolecular bonding upon NMP dilution may provide an additional contribution to the mobility of the methyl group, thus differentiating its rate of τ_c change with respect to carbons in the ring.

4. CONCLUSIONS

In the present work, combined thermodynamic, NMR, and computational data have provided deep insights into the structural and dynamic behavior of the binary water/*N*-methyl-2-pyrrolidone (NMP) system. The main information from our study is the occurrence of changes in the NMP assembling upon dilution, corroborating our previous computed model.[9]

In our calorimetric experiments, the solvation of NMP by the water solvent was found to result in an interaction stronger with respect to the solvation of water by NMP solvent. The different behavior played by the components is the origin of the asymmetry of the H^E curve. Of note is that the ^1H chemical shifts and ^{13}C spin−lattice relaxation times were sensibly dependent on the mixture composition, both showing a trend below $x_w \approx 0.8$ different from that observed above this mole fraction. This behavior coincides with those reported for other physicochemical properties of NMP aqueous solutions such as viscosity, density, and self-diffusion coefficients. Overall, our NMR results are discussed in terms of hydrogen bonding interactions. Those established between water and NMP are responsible for the reduced water polarization in the presence of NMP than in pure water. By increasing the concentration of

dx.doi.org/10.1021/jp505286z | J. Phys. Chem. B 2014, 118, 10493−10502

water, more and more water−water HBs are formed, favoring the disruption of the NMP network. The NMP structural assembling is significantly altered up to $x_w \approx 0.8$. Above this value, all sites in pyrrolidone are surrounded by water molecules. In parallel, changes in τ_c, estimated from the ^{13}C spin−lattice relaxation rates, correlate well with variation in the system viscosity[37] in the whole concentration range. Differences in the rate of τ_c change among the carbon sites suggested a microviscosity around the methyl group different from those of carbons in the ring.

Analysis of MD simulations performed at different water contents allowed us to exclude that the singular trends observed for NMP properties were to be attributed to variations in NMP conformations. Indeed, the detailed analysis of the puckering preferences of NMP revealed that the conformational preferences are not influenced at all by the addition of water to neat liquid NMP or by the water concentration. Furthermore, the favored conformations (^4E, $_4E$, ^3_4T, and ^4_3T) do not differ in energy even in the absence of solvent, as shown by DFT calculations performed *in vacuo*. Overall, the findings of the present study are expected to be useful for the understanding of the behavior of NMP in aqueous solutions on the molecular level.

■ ASSOCIATED CONTENT

Supporting Information

Experimental calorimetric data (x_w and $\bar{H}_j^E$) (Table S1), ^{13}C chemical shift concentration dependence of the carbonyl group in NMP−water mixtures (Figure S1), and intramolecular distances between H atoms for a selected NMP molecule from MD trajectories (Figure S2). This material is available free of charge via the Internet at http://pubs.acs.org.

■ AUTHOR INFORMATION

Corresponding Author

*Phone: + 39 070 675 4389. Fax: +39 070 675 4388. E-mail: flaminia@unica.it.

Notes

The authors declare no competing financial interest.

■ ACKNOWLEDGMENTS

This research was financially supported by PRIN (2009 WHPHRH). M.U. gratefully acknowledges Sardinia Regional Government for the financial support of her Ph.D. scholarship (P.O.R. Sardegna F.S.E. 2007−2013). M.U. and F.C.M. wish to thank Prof. Adolfo Lai for insightful comments. M.U. and S.P. express their gratitude to Dr. Enrico Matteoli (Istituto per i Processi Chimico-Fisici, IPCF-CNR, Pisa), for helpful discussion and advice on data treatment and technical issues, and to the IPCF-CNR for allowing the use of calorimetric instrumentations and methods within the collaboration agreement between DSCG and IPCF. L.G. acknowledges support form FIRB RBFR086BOQ.

■ REFERENCES

(1) *N-Methyl-2-pyrrolidone Storage and Handling*; BASF Intermediates: New Jersey, 1998.

(2) Sanghvi, R.; Narazaki, R.; Machatha, S. G.; Yalkowsky, S. H. Solubility Improvement of Drugs Using *N*-Methyl Pyrrolidone. *AAPS PharmSciTech* **2008**, *9*, 366−376.

(3) Chen, G.; Hou, Y.; Knapp, H. Diffusion Coefficients, Kinematic Viscosities, and Refractive Indices for Heptane + ethylbenzene, sulfolane + 1-Methylnaphtalene, water + *N,N*-Dimethylformamide, Water + Methanol, water + *N*-Formylmorpholine, and water + *N*-Methylpyrrolidone. *J. Chem. Eng. Data* **1995**, *40*, 1005−1010.

(4) Ambrosone, L.; D'Errico, G.; Sartorio, R.; Vitagliano, V. Analysis of Velocity Cross-Correlation and Preferential Solvation for the System *N*-Methylpyrrolidone-Water at 20 °C. *J. Chem. Soc., Faraday Trans* **1995**, *91*, 1339−1344.

(5) Macdonald, D. D.; Dunay, D.; Hanlon, G.; Hyne, J. B. Propierties of the *N*-Methyl-2-Pyrrolidinone Water System. *Can. J. Chem. Eng.* **1971**, *49*, 420−423.

(6) Henni, A.; Hromek, J. J.; Tontiwachwuthikul, P.; Chakma, A. Volumetric Properties and Viscosities for Aqueous *N*-Methyl-2-Pyrrolidone Solutions from 25 to 70 °C. *J. Chem. Eng. Data* **2004**, *49*, 231−234.

(7) Gontrani, L.; Caminiti, R. The Structure of Liquid *N*-Methyl Pyrrolidone Probed by X-Ray Scattering and Molecular Simulations. *J. Chem. Phys.* **2012**, *136*, 074505.

(8) Muller, G.; Lutz, M.; Harder, S. Methyl Group Conformation-Determining Intermolecular C-H···O Hydrogen Bonds: Structure of *N*-Methyl-2-Pyrrolidone. *Acta Crystallogr., Sect. B* **1996**, *52*, 1014−1022.

(9) Usula, M.; Mocci, F.; Cesare Marincola, F.; Porcedda, S.; Gontrani, L.; Caminiti, R. The Structural Organization of *N*-Methyl-2-Pyrrolidone + Water Mixtures: A Densitometry, X-Ray Diffraction, and Molecular Dynamics Study. *J. Chem. Phys.* **2014**, *140*, 124503.

(10) Porcedda, S.; Usula, M.; Marongiu, B. Physical-Chemical Properties of Ionic Liquid-Containing Mixtures. In *The Structure of Ionic Liquids, Soft and Biological Matter*; Caminiti, R., Gontrani, L., Eds.; Springer International Publishing: Cham, Switzerland, 2014; pp 171−191.

(11) Matteoli, E.; Lepori, L.; Spanedda, A. Thermodynamic Study of Heptane + Amine Mixtures. *Fluid Phase Equilib.* **2003**, *212*, 41−52.

(12) Matteoli, E.; Lepori, L. Determination of the Excess Enthalpy of Binary Mixtures from the Measurements of the Heat of Solution of the Components: Application to the Perfluorohexane + Hexane Mixture. *Fluid Phase Equilib.* **2000**, *174*, 115−131.

(13) Marsh, K. N. Excess Enthalpies of Benzene + Cyclohexane Mixtures. *Int. DATA Ser., Sel. Data Mixtures, Ser. A* **1973**, 1−5.

(14) Hansen, D. F.; Kay, L. E. Improved Magnetization Alignment Schemes for Spin-Lock Relaxation Experiments. *J. Biomol. NMR* **2007**, *37*, 245−255.

(15) Bax, A. D.; Davis, D. G. Practical Aspects of Two-Dimensional Transverse NOE Spectroscopy. *J. Magn. Reson.* **1985**, *63*, 207−213.

(16) Antony, J. H.; Dölle, A.; Mertens, D.; Wasserscheid, P.; Carper, W. R.; Wahlbeck, P. G. ^{13}C NMR Relaxation Rates in the Ionic Liquid 1-Methyl-3-Nonylimidazolium Hexafluorophosphate. *J. Phys. Chem. A* **2005**, *109*, 6676−6682.

(17) Carper, W. R.; Wahlbeck, P. G.; Dolle, A. NMR Relaxation Rates: Separation of Dipolar and Chemical Shift Anisotropy Effects. *J. Phys. Chem. A* **2004**, *108*, 6096−6099.

(18) Heimer, N. E.; Wilkes, J. S.; Wahlbeck, P. G.; Carper, W. R. C NMR Relaxation Rates in the Ionic Liquid 1-Ethyl-3-Methylimidazolium Butanesulfonate. *J. Phys. Chem. A* **2006**, *110*, 868−874.

(19) Imanari, M.; Tsuchiya, H.; Seki, H.; Nishikawa, K.; Tashiro, M. Characterization of the Molecular Reorientational Dynamics of the Neat Ionic Liquid 1-Butyl-3-Methylimidazolium Bromide in the Super Cooled State Using ^1H and ^{13}C NMR Spectroscopy. *Magn. Reson. Chem.* **2009**, *47*, 67−70.

(20) Marincola, F. C.; Piras, C.; Russina, O.; Gontrani, L.; Saba, G.; Lai, A. NMR Investigation of Imidazolium-Based Ionic Liquids and Their Aqueous Mixtures. *ChemPhysChem* **2012**, *13*, 1339−1346.

(21) Mocci, F.; Laaksonen, A.; Wang, Y.-L.; Saba, G.; Lai, A.; Cersare Marincola, F. CompChem. and NMR Probing Ionic Liquids. In *The Structure of Ionic Liquids, Soft and Biological Matter*; Caminiti, R., Gontrani, L., Eds.; Springer International Publishing: Cham, Switzerland, 2014; pp 95−124.

(22) Abragam, A. *Principles of Nuclear Magnetism*; Oxford Science Pubblications: London, 1961.

(23) Case, D. A.; Darden, T. A.; Cheatham, T. E., III; Simmerling, C. L.; Wang, J.; Duke, R. E.; Luo, R.; Walker, R. C.; Zhang, W.; Merz, K.

M.; et al. *AMBER 11*; University of California: San Francisco, CA, 2010.
(24) Goetz, A. W.; Williamson, M. J.; Xu, D.; Poole, D.; Le Grand, S.; Walker, R. C. Routine Microsecond Molecular Dynamics Simulations with AMBER on GPUs. 1. Generalized Born. *J. Chem. Theory Comput.* **2012**, *8*, 1542−1555.
(25) Altona, C.; Sundaralingam, M. Conformational Analysis of the Sugar Ring in Nucleosides and Nucleotides. *J. Am. Chem. Soc.* **1972**, *94*, 8205−8212.
(26) Frisch, M. J.; Trucks, G. W.; Schlegel, H. B.; Scuseria, G. E.; Robb, M. A.; Cheeseman, J. R.; Scalmani, G.; Barone, V.; Mennucci, B.; Petersson, G. A.; et al. *Gaussian 09*, revision D.01; Gaussian, Inc.: Wallingford, CT, 2009.
(27) Zaichikov, A. M. Thermodynamic Characteristics of water + *N*-Methylpyrrolidone Mixtures and Intermolecular Interactions in Them. *Russ. J. Gen. Chem.* **2006**, *76*, 626−633.
(28) Kimura, F.; Sugiura, T.; Ogawa, H. Solvation of *N*-Methyl-2-Pyrrolidone and *N,N*-Dimethylpropanamide in Cyclohexane, Heptane, *N*-Alkan-1-ols(C_1−C_4) and Water at 298.15K. *Thermochim. Acta* **2013**, *573*, 206−212.
(29) Dohnal, V.; Roux, A. H.; Hynek, V. Limiting Partial Molar Excess Enthapies by Flow Calorimetry. *J. Solution Chem.* **1994**, *23*, 889−900.
(30) Groelier, J. P. E.; Wormald, C. J.; Fontaine, C. J.; Sosnokowska-Kehiaian, K.; Kehiaian, H. V. *Heats of Mixing and Solutions*; Springer-Verlag: Berlin, 2004.
(31) Gnanakumari, P.; Rao, M. V. P.; Prasad, D. H. L.; Kumar, Y. V. L. R. Vapor - Liquid Equilibria and Excess Molar Enthalpies for N -Methyl-2-Pyrrolidone with Chloroethanes and Chloroethenes. *J. Chem. Eng. Data* **2003**, *48*, 535−540.
(32) Mizuno, K.; Ochi, T.; Shindo, Y. Hydrophobic Hydration of Acetone Probed by Nuclear Magnetic Resonance and Infrared: Evidence for the Interaction C−H···OH_2. *J. Chem. Phys.* **1998**, *109*, 9502.
(33) Maloka, I. E.; Ibrahim, S. Y. Physical Properties of Aqueous *N*-Methyl Pyrrolidone at Different Temperatures. *Pet. Sci. Technol.* **2004**, *22*, 1571−1579.
(34) Abragam, A. *The Principles of Nuclear Magnetism*; Oxford University Press: London, 1961.
(35) Mele, A.; Tran, C. D.; De Paoli Lacerda, S. H. The Structure of a Room-Temperature Ionic Liquid with and without Trace Amounts of Water: The Role of C-H···O and C-H···F Interactions in 1-N-Butyl-3-Methylimidazolium Tetrafluoroborate. *Angew. Chem., Int. Ed. Engl.* **2003**, *42*, 4364−4366.
(36) Mandai, T.; Masu, H.; Imanari, M.; Nishikawa, K. Comparison between Cycloalkyl- and *N*-Alkyl-Substituted Imidazolium-Based Ionic Liquids in Physicochemical Properties and Reorientational Dynamics. *J. Phys. Chem. B* **2012**, *116*, 2059−2064.
(37) García-Abuín, A.; Gómez-Diaz, D.; La Rubia, M. D.; Navaza, J. M. Density, Speed of Sound, Viscosity, Refractive Index, and Excess Volume of *N*-Methyl-2-Pyrrolidone + Ethanol (or Water or Ethanolamine) from T = (293.15 to 323.15) K. *J. Chem. Eng. Data* **2011**, *56*, 646−651.
(38) Endo, T.; Imanari, M.; Seki, H.; Nishikawa, K. Effects of Methylation at Position 2 of Cation Ring on Rotational Dynamics of Imidazolium-Based Ionic Liquids Investigated by NMR Spectroscopy: [C_4mim]Br vs [C_4C_1mim]Br. *J. Phys. Chem. A* **2011**, *115*, 2999−3005.

Supporting Information for

NMR, calorimetry and computational studies of aqueous solutions of *N*-methyl-2-pyrrolidone

Marianna Usula,[†] *Silvia Porcedda,*[†] *Francesca Mocci,*[†,‡] *Lorenzo Gontrani,*[§,‖] *Ruggero Caminiti,*[‖] *Flaminia Cesare Marincola*[†,*]

[†] Dipartimento di Scienze Chimiche e Geologiche - Università degli Studi di Cagliari, S.S. 554 Bivio Sestu, 09042 Monserrato (Italy)

[‡] Department of Materials and Environmental Chemistry, Arrhenius Laboratory, Stockholm University, S-106 91, Stockholm (Sweden)

[§] CNR – Istituto di Struttura della Materia, Area della Ricerca di Roma Tor Vergata, Via del Fosso del Cavaliere 100, I-00133 Roma (Italy)

[‖] Dipartimento di Chimica - Università di Roma "La Sapienza", P.le Aldo Moro 5, I-00185 Roma (Italy)

Table S1. Experimental values of water mole fractions and of excess partial molar enthalpies of each component, $\bar{H}_j^{\mathrm{E}}$, expressed in J mol^{-1}, for the NMP + water system.

x_w	$\bar{H}_N^E$	x_w	$\bar{H}_N^E$	x_w	$\bar{H}_W^E$	x_w	$\bar{H}_W^E$	x_w	$\bar{H}_W^E$
0.3594	-73.4	0.7748	-5440.9	0.0112	-4446.7	0.3465	-4972.5	0.7411	-1796.6
0.3628	-75.1	0.7761	-5510.0	0.0221	-4649.2	0.3521	-4943.3	0.7429	-1798.2
0.3662	-75.5	0.7774	-5675.6	0.0328	-4870.9	0.3576	-4960.0	0.7447	-1763.9
0.3698	-83.5	0.8856	-11050.2	0.0433	-4865.8	0.3630	-4914.8	0.7465	-1759.3
0.3734	-95.2	0.8865	-12295.7	0.0536	-4887.3	0.3683	-4915.1	0.7482	-1739.2
0.3770	-98.2	0.8873	-10984.3	0.0636	-4941.6	0.3736	-4860.9	0.7499	-1781.0
0.3808	-112.2	0.8881	-10982.2	0.0734	-4904.8	0.3787	-4827.9	0.7516	-1744.2
0.3846	-108.3	0.8890	-11527.8	0.0830	-4974.8	0.3838	-4878.8	0.7533	-1754.0
0.3885	-118.9	0.8898	-11980.7	0.0925	-5033.8	0.3887	-4823.3	0.7550	-1715.5
0.3925	-130.8	0.8907	-10796.7	0.1017	-4995.4	0.3936	-4860.8	0.7566	-1712.7
0.3966	-137.5	0.8915	-11550.4	0.1107	-5046.8	0.3984	-4795.1	0.7582	-1681.7
0.4007	-148.3	0.8924	-12255.9	0.1196	-5014.6	0.4032	-4763.9	0.7598	-1675.0
0.4049	-161.4	0.8932	-11469.1	0.1283	-5147.6	0.4079	-4798.8	0.7614	-1671.5
0.4093	-174.1	0.8941	-11540.3	0.1368	-5120.4	0.4125	-4747.6	0.7629	-1675.6
0.4137	-186.0	0.8949	-11960.4	0.1452	-5111.4	0.4170	-4759.3	0.7631	-1869.3
0.4182	-193.2	0.8958	-12831.7	0.1534	-5098.8	0.4214	-4719.7	0.7644	-1630.6
0.4228	-212.5	0.8966	-10994.1	0.1614	-5066.4	0.4258	-4668.2	0.7654	-1797.3
0.4275	-216.7	0.8975	-12499.8	0.1693	-5088.9	0.4858	-4310.8	0.7676	-1718.8
0.4324	-235.4	0.8983	-12700.1	0.1771	-5183.2	0.4882	-4346.4	0.7697	-1657.9
0.4373	-251.3	0.8992	-12347.1	0.1847	-5129.9	0.4906	-4391.5	0.7719	-1744.8
0.4423	-273.2	0.9001	-11860.3	0.1921	-5135.7	0.4930	-4272.3	0.7740	-1704.2
0.4475	-294.3	0.9009	-12774.8	0.1994	-5131.3	0.4954	-4352.8	0.7760	-1618.0
0.4528	-319.9	0.9018	-13324.1	0.2066	-5022.7	0.4977	-4329.5	0.7780	-1639.9
0.4582	-341.2	0.9877	-19573.1	0.2137	-5114.1	0.5001	-4272.3	0.7800	-1646.6
0.4638	-362.4	0.9883	-19245.2	0.2206	-5187.0	0.7008	-2021.1	0.8734	-666.8
0.4694	-382.6	0.9889	-21597.4	0.2274	-5091.1	0.7032	-2040.4	0.8759	-642.7
0.4753	-420.0	0.9895	-21385.1	0.2341	-5084.5	0.7056	-2051.4	0.8783	-618.8
0.4808	-447.5	0.9901	-19688.3	0.2407	-5141.1	0.7080	-2034.6	0.8806	-599.9
0.4812	-447.2	0.9907	-19437.5	0.2472	-5091.8	0.7103	-1989.2	0.8828	-580.7
0.4867	-475.6	0.9913	-20013.9	0.2535	-5117.8	0.7126	-2020.1	0.8849	-559.5
0.4873	-482.6	0.9919	-20613.5	0.2619	-5176.6	0.7148	-2017.0	0.8870	-545.3
0.4927	-499.4	0.9926	-20112.0	0.2700	-5085.4	0.7170	-1992.6	0.8890	-528.6
0.4936	-498.2	0.9932	-20189.0	0.2780	-5138.9	0.7192	-1976.8	0.8909	-513.8
0.4988	-500.2	0.9938	-19649.0	0.2848	-5075.7	0.7213	-1945.9	0.8927	-497.2
0.5051	-541.1	0.9944	-20458.7	0.2915	-5134.4	0.7234	-1900.0	0.8945	-486.3
0.5116	-580.6	0.9950	-20709.2	0.2981	-5079.9	0.7255	-1929.2	0.8963	-470.4
0.5183	-632.4	0.9956	-20381.3	0.3045	-5086.6	0.7276	-1895.4	0.8979	-457.9
0.5251	-572.0	0.9963	-22155.1	0.3108	-5067.1	0.7296	-1913.3	0.8996	-444.7
0.7684	-5341.8	0.9969	-19189.5	0.3171	-5047.1	0.7316	-1884.8	0.9011	-433.2
0.7697	-5615.4	0.9975	-20149.5	0.3232	-5024.5	0.7335	-1864.0	0.9027	-556.7
0.7710	-6045.1	0.9981	-21826.9	0.3291	-4997.7	0.7355	-1842.1		
0.7722	-5643.8	0.9987	-21248.4	0.3350	-4944.7	0.7374	-1852.0		
0.7735	-5824.8			0.3408	-4996.0	0.7392	-1833.7		

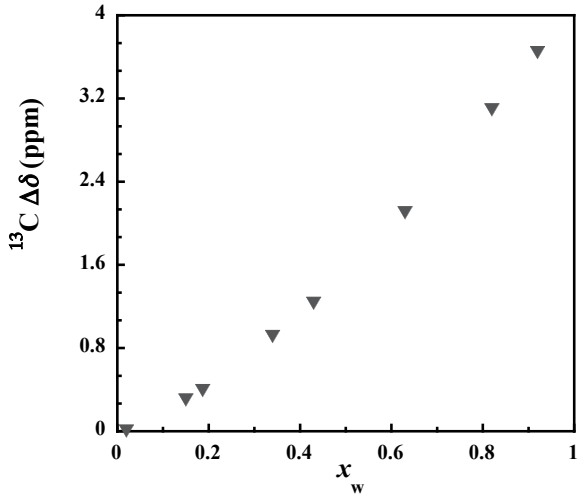

Figure S1. ^{13}C chemical shift deviations of NMP carbonyl group from dried NMP, $\Delta\delta=(\Delta\delta_{mix}-\Delta\delta_{neat})$, as a function of the water mole fraction, x_w.

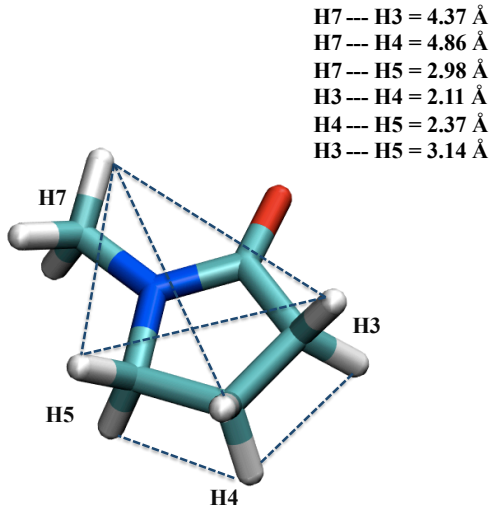

Figure S2. Intra-molecular distances between different H atoms for a selected NMP molecule from MD trajectories.

PAPER III

Reprinted with the permission:

Thermo-Physical Properties of Ammonium-Based Ionic Liquid + *N*-methyl-2-pyrrolidone Mixtures at 298.15 K.

M. Usula, E. Matteoli, F. Leonelli, F. Mocci, F. Cesare Marincola L. Gontrani, and S. Porcedda.

Citation: *Fluid Phase Equilibria* **383**, 49-54 (2014)

DOI: 10.1016/j.fluid.2014.09.031

Published by the **Elsevier B.V.**

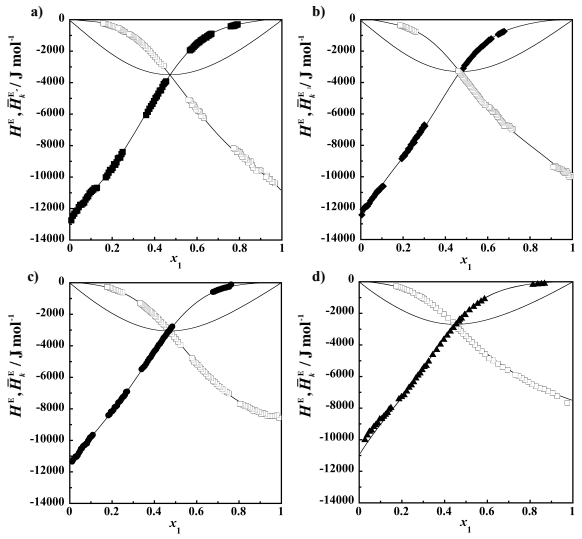

Fluid Phase Equilibria 383 (2014) 49–54

Contents lists available at ScienceDirect

Fluid Phase Equilibria

journal homepage: www.elsevier.com/locate/fluid

Thermo-physical properties of ammonium-based ionic liquid + *N*-methyl-2-pyrrolidone mixtures at 298.15 K

Marianna Usula [a], Enrico Matteoli [b], Francesca Leonelli [c], Francesca Mocci [a,d], Flaminia Cesare Marincola [a], Lorenzo Gontrani [c], Silvia Porcedda [a,*]

[a] Dipartimento di Scienze Chimiche e Geologiche – Università degli Studi di Cagliari, Cittadella Universitaria di Monserrato, S.P. 8, Monserrato, I-09042, Italy
[b] IPCF-CNR Istituto per I Processi Chimico Fisici del Consiglio Nazionale delle Ricerche, Via Moruzzi 1, Pisa I-56124, Italy
[c] Dipartimento di Chimica - Università di Roma "La Sapienza", P. le Aldo Moro 5, Roma I-00185, Italy
[d] Department of Materials and Environmental Chemistry, Arrhenius Laboratory, Stockholm University, Stockholm S-106 91, Sweden

ARTICLE INFO

Article history:
Received 21 July 2014
Received in revised form 25 September 2014
Accepted 26 September 2014
Available online 28 September 2014

Keywords:
Ionic liquid
N-methyl-2-pyrrolidone
Density
Molar excess volume
Molar excess enthalpy

ABSTRACT

A systematic study of a series of room-temperature ionic liquids, belonging to the alkylammonium nitrate family (XAN), was carried out at 298.15 K and 0.1 MPa with the aim of investigating the effect of the cationic chain length on some thermo-physical properties and their behavior in the organic solvent *N*-methyl-2-pyrrolidone (NMP), over the whole concentration range. Experimental densities were used to calculate molar volumes, V_m, and excess molar volumes, V^E. Complementary information was obtained by isothermal titration calorimetry that provided the values of the heat of mixing, H^E, and the excess partial molar enthalpies of each component, $\overline{H}_1^E$ and $\overline{H}_2^E$. The density values of neat XAN samples decreased as the alkyl chain length of the cation increases, whereas, the addition of the methoxy group to the considered smaller alkyl chain resulted in an increase of density. Negative V^E and H^E values were found for each XAN + NMP system, indicating the presence of strong attracting interactions between the constituents.

1. Introduction

Room-temperature ionic liquids (RTILs) belong to the class of organic salts, liquid at room temperature in their neat state. The rapid growth in ionic liquid literature indicates that, thanks to their characteristics especially their non-volatile nature and good solvation properties, RTILs attract much attention as a valid alternative way to traditional volatile organic solvents [1–3]. An interesting aspect is that a slight variation in the constituent ions of ionic liquids can lead significant differences in their physicochemical properties.

RTILs consist of two groups: protic (PILs) and aprotic (AILs) ionic liquids. The acid proton, which is responsible for hydrogen bonding, makes PILs different from other ionic liquids and suitable for different potential applications, such as self-assembly media [4,5], catalysts in chemical reactions [6,7], biological applications [8]. Despite their interest and potentiality, a deep knowledge of thermophysical properties of liquid mixtures containing PILs, which is important for the design of any technological processes, has not been fully accomplished yet by the scientific community.

Over the last years, the main goal of numerous research groups and industries was to investigate a great number of different ionic liquids for a range of novel applications [9–13]. Experimental and/or theoretical thermodynamic studies on pure RTILs and their mixtures with organic solvents [14–20] or water [21–24] were reported. Heintz [14] reviewed the developments of thermodynamic and thermophysical studies of RTILs + non-aqueous solvent mixtures including an overview on the experimental data available. The review is limited to systems having the most promising chance to be used successfully in the different fields of chemistry and chemical engineering.

In this work, a series of PILs, belonging to the alkylammonium nitrate family (XAN), were selected with the aim of investigating their behavior in the organic solvent *N*-methyl-2-pyrrolidone (NMP), over the whole concentration range. In particular, the study is focused on ethylammonium nitrate (EAN), *n*-propylammonium nitrate (PAN), *n*-butylammonium nitrate (BAN), and 2-methoxyethylammonium nitrate (MEOEAN) ionic liquids (Table 1), with the purpose to understand the effect of XAN alkyl chain length on their mixing properties with NMP. NMP, known for its low toxicity, low volatility and high solvent power, is one of the most popular

* Corresponding author. Tel.: +39 0706754415; fax: +39 0706754388.
E-mail address: porcedda@unica.it (S. Porcedda).

0378-3812/$ – see front matter © 2014 Elsevier B.V. All rights reserved.
http://dx.doi.org/10.1016/j.fluid.2014.09.031

Table 1
Investigated compounds: name with abbreviation, source, purity, final water content, purification and analysis methods.

Chemical name (abbreviation)	Source	Purity/mole fraction	Purification method	Final water content/mole fraction	Analysis method
Ethylammonium nitrate (EAN)	Iolitec	>0.97	Dehydration *in vacuo*	<0.02	^{1}H NMR
N-propylammonium nitrate (PAN)	Iolitec	>0.97	Dehydration *in vacuo*	<0.02	^{1}H NMR
N-butylammonium nitrate (BAN)	Synthesis	–	Dehydration *in vacuo*	<0.01	^{1}H NMR
2-methoxyethylammonium nitrate (MEOEAN)	Synthesis	–	Dehydration *in vacuo*	<0.01	^{1}H NMR
N-methyl-2-pyrrolidone (NMP)	Sigma–Aldrich	>0.995	Dehydration *in vacuo*	<0.02	^{1}H NMR

and widely used solvent in the industries and academics and it is becoming the product of choice for paint strippers, agricultural chemicals, and process solvent applications [25]. Recently, different studies have pointed out the interesting properties of NMP with some RTILs [18–20] or simply with water [26].

EAN and PAN are the most known PILs and their properties make them suitable for electrochemical, organic, or biochemical applications. To cite a few, they are used as solvent/catalyst in organic reactions leading high yields [27]; EAN is a useful polar stationary phase for gas-liquid chromatography [28] and it was used to enhance the recovery of denatured-reduced hen egg white lysozyme showing the ability to prevent aggregation of the denatured protein [29]. Concerning the thermodynamics properties of BAN and MEOEAN with molecular solvents, to the best of our knowledge, no studies were published in the open literature. A series of ammonium based ionic liquids, similar to those selected in this work, with *N*-methyl-2-pyrrolidone mixtures were studied by Kavitha et al. [18–20]; RTILs + NMP showed structure-based and temperature dependent properties.

Characterization of mixtures containing ionic liquids and organic solvents is needed to test their applicability in substitution of neat compounds which could have inappropriate properties for a selected application, i.e. limited solvent power range, high viscosity etc [30]. To the best of our knowledge, results of V_m, V^E, H^E, $\overline{H}_1^E$, and $\overline{H}_2^E$ have not been reported in the literature for the selected XAN with NMP binary mixtures.

2. Experimental

2.1. Materials

Names with abbreviations, sources, purities, water content, purification and analysis methods of the investigated compounds are reported in Table 1.

2-Methoxy-ethylammonium nitrate and *n*-butylammonium nitrate were prepared following a previously reported procedure [31,32]. Solvents (LC–MS grade), 2-methoxyethylamine (99%) and *n*-butylamine were purchased from Aldrich. Nitric acid (65%) was purchased from Carlo Erba.

Before using, all materials were dried *in vacuo* ($p = 7 \times 10^{-1}$ mbar) for 48 h at room temperature. The XAN (1) + NMP (2) mixtures were prepared by mass as follow: the proper amounts of XAN and NMP were weighted with an analytical balance (Sartorius A210P, Data Weighing Systems Inc. IL-USA; precision and accuracy of $\pm 1 \times 10^{-7}$ kg and $\pm 5 \times 10^{-7}$ kg, respectively) in screw-cap glass vials in a glove-bag under nitrogen atmosphere. For density determinations, XAN and NMP were degassed for about 2 h by means of an ultrasonic device (WVR model USC100T −45 kHz, 30 W). The residual water content of NMP and XAN, estimated by ^{1}H-NMR spectroscopy by using Varian Unity INOVA 500 spectrometer operating at the proton resonance frequency of 499.84 MHz, was reported in Table 1.

2.2. Volumetric measurements and data treatment

The densities of the liquid mixtures and the pure compounds were measured at 298.15 K and 0.1 MPa, by means of a vibrating tube densitometer (model DMA 58-Anton Paar – Gratz, Austria). Accuracy in the temperature was better than ±0.01 K. Density precision and accuracy were $\pm 1 \times 10^2$ kg m^{-3} and $\pm 5 \times 10^2$ kg m^{-3}, respectively. The instrument was calibrated before each experimental run using dry air and distilled water as references. Solutions were prepared by weight in septum-capped vials of approximately 2 cm^3 using needles and syringes to transfer liquids. The molar volumes, V_m, were obtained from:

$$V_m = \frac{(x_1 M_1 + x_2 M_2)}{\rho_{mix}} \quad (1)$$

and the excess molar volumes, V^E, were calculated by the following equation:

$$V^E = V_m - \frac{(x_1 M_1)}{\rho_1} - \frac{(x_2 M_2)}{\rho_2} \quad (2)$$

where ρ_{mix} is the density of the mixture and x_k, M_k, and ρ_k are the mole fraction, the molar mass, and the density of the component k ($k = 1$ or 2), respectively. V^E data were fitted by means of the Redlich–Kister (RK) equation having the form:

$$V^E = x_1 x_2 \sum_{i=0}^{n-1} a_i (x_1 - x_2)^i \quad (3)$$

The absolute standard deviation of the fit, $\sigma(V^E)$, was calculated by the following equation:

$$\sigma(V^E) = \sqrt{\frac{\sum (V^E_{j,\,calc} - V^E_{j,\,exp})^2}{N - n}} \quad (4)$$

where N is the number of experimental points and n is the number of coefficients. By un-weighted least squares treatment a smoothed curve was obtained for each XAN (1) + NMP (2) system. The RK coefficients values obtained for XAN (1) + NMP (2) mixtures are reported in Table 2.

Excess molar volumes at infinite dilution, $\overline{V}_k^{E,\infty}$, of each component k, is defined as the difference between the molar volumes at infinite dilution and in the neat state: $\overline{V}_k^{E,\infty} = \overline{V}_k^{E,\infty} - V_k^*$. Their values were calculated from the RK parameters by means of:

$$\overline{V}_k^{E,\infty} = \sum_{i=0}^{n} (-1)^k a_i \quad (5)$$

Furthermore, from the standard deviations of the above RK parameters we calculated the SD, and the uncertainties, u ($u = 2 \times$ SD), of the excess molar volumes at equimolar composition, $V^E_{x=0.5}$, and of the partial molar volumes of each component at infinite dilution, $\overline{V}_k^{E,\infty}$, which are reported in Table 2.

The procedure was checked by comparison of our experimental V^E data of the water + ethanol system with reliable literature data

Table 2
Values of the coefficients, a_i, obtained from the Redlich–Kister Eq. (3) with the standard deviations, $\sigma(V^E)$. Values of molar excess volumes at equimolar composition, $V^E_{x=0.5}$, of partial molar volumes at infinite dilution for each component, $\overline{V}^{\infty}_k$, and of associated uncertainties, u.

System	a_0 $10^{-6}\times m^3\,mol^{-1}$	a_1	a_2	a_3	$\sigma\,(V^E)$	$V^E_{x=0.5}\pm\mu$	$\overline{V}^{\infty}_1\pm\mu$	$\overline{V}^{\infty}_2\pm\mu$
EAN + NMP	−2.3258	4.2359	−2.6674	−1.4055	0.02	−0.58 ± 0.02	−7.8 ± 0.4	−2.2 ± 0.4
PAN + NMP	−3.0289	3.4931	−1.6539	0	0.02	−0.76 ± 0.02	−8.18 ± 0.06	−1.19 ± 0.06
BAN + NMP	−2.8169	3.3232	−1.5604	0	0.01	−0.70 ± 0.01	−7.70 ± 0.05	−1.05 ± 0.05
MEOEAN + NMP	−2.3009	2.9592	−1.2011	0	0.01	−0.56 ± 0.02	−6.46 ± 0.04	−0.54 ± 0.05

[33]. We found a difference lower than 0.8% in the whole composition range.

2.3. Calorimetric measurements and data treatment

Heats of solution were collected through a heat flow calorimeter by Thermometric (model 2277, Thermal Activity Monitor – Järfälla, Sweden) at (298.15 ± 0.01) K and 0.1 MPa. Experiments were conducted by adding a pure component, via Hamilton gas-tight syringes of capacity in the range of (250.0 ÷ 1000) μL driven by Cole-Parmer (model 74900 – Vernon Hills, Illinois, USA) pumps, to an ampoule of 4 cm^3 capacity initially charged with the other component or with a stock mixture of them. With this system, we were able to make accurate injections starting from a minimum of 1 μL, with precision 0.5 %, and to measure accurate heat effects as small as 0.01 J, with sensitivity 0.5 μW. We chose this technique instead of mixing-flow calorimetry to avoid errors due to incomplete mixing and to obtain more precise values of the partial molar enthalpy at infinite dilution [34].

The experimental solution heats, Q_{exp}, released by the additions of very small quantities of the titrant, n_k, practically represent partial molar enthalpies, $\overline{H}_k, \overline{H}_k \cong Q/n_k$. From this equation, calculated values of the solution heats, Q_{calc}, can be obtained, being $\overline{H}_{k,calc}$ accounted for by proper differentiation of the equation $H^E = f(x)$, such as the modified Margules one [35].

$$\frac{H^E}{RT} = x_1x_2\left(A_{12}x_2 + A_{21}x_1 - \frac{\alpha_{12}\alpha_{21}x_1x_2}{\alpha_{12}x_1 + \alpha_{21}x_2 + \eta x_1x_2}\right) \quad (6)$$

A standard least squares procedure identifies the best values of dimensionless parameters: A_{21}, A_{12}, α_{21}, α_{12} and η, at the minimum of the objective function $OF = \Sigma(Q_{exp} - Q_{calc})^2$. Proper allowance was made for the heat involved in the phase composition changes brought about by the vapour–liquid equilibration after each addition. An exhaustive description of the apparatus, the experimental procedure, and the data treatment, can be found in literature [36,37].

The coefficients values obtained for XAN (1) + NMP (2) mixtures are reported in Table 3. From the standard deviations of the Margules equation we calculated the uncertainties, u, on H^E at equimolar mixtures and on partial molar enthalpies of each component at infinite dilution, $\overline{H}^{E,\infty}_k$, also reported in Table 3.

As explained in previous papers [36,37], the calorimetric experimental procedure generates a large amount of experimental data (*c.a.* 200 experimental points for each binary mixture investigated, each composed of 4 numbers), which are not worth an extensive tabulation herein. These data can be retrieved as supplementary electronic material (xls-file) from the Authors.

The reliability of the whole procedure was checked by measuring the H^E, in the whole range of concentration, of the system benzene (1) + cyclohexane (2). Comparison with reliable literature [38] data revealed a discrepancy lower than 2 %. The uncertainty in the observed heat, Q, as determined by the reproducibility of the experiments and by integration of the peak area, can be evaluated as 0.5 %.

3. Results and discussion

3.1. Volumetric properties

In Table 4, the mixture composition expressed as XAN mole fraction, x_1, experimental densities, molar volumes, and excess molar volumes for each investigated XAN (1) + NMP (2) mixture were reported. Each density value represents the mean of two determinations. Virtually, the physico-chemical properties of RTILs mainly depend on the nature and structure of ions and on the alkyl chain length of the cation. As it can be seen in Table 4, the density value of the neat XAN decreases as the alkyl chain length of the cation increases, whereas, the addition of the methoxy group to the smaller alkyl chain considered, results in an increase of density. This behaviour is probably due to the difference in molecular weight and to the enhanced capability to give polar–polar attractive interactions. This indicates that a long alkyl chain inhibits the compaction of neat XAN, while the addition of a polar group in a short chain has opposite effect, i.e. promotes a greater compaction of the neat ionic liquids. In Fig. 1, the density values of the XAN (1) + NMP (2) mixtures are plotted with respect to x_1. In general, the density trend of each XAN + NMP system is monotonic with a downward concavity. RTILs are miscible with molecular solvents with medium- to high- dielectric constants i.e. solvents containing polar groups and immiscible with low dielectric liquids [39–41]. In the present study, we found that all XAN are completely miscible in NMP over the whole mole fraction range, since NMP is a very polar solvent with a moderately high relative dielectric constant (ε = 32.2 at T = 298.15 K) [42]. Molar volumes, V_m, and excess molar volumes, V^E, values were calculated by processing density data using Eqs. (1) and (2). The V_m trend is falsely linear, in fact, each curve is fitted by a polynomial equation of 2nd degree having an upward concavity (Figure S1 of the supplementary material). This concavity is more easily visible and magnified in the V^E curves representation, Fig. 2. Negative V^E values were found for

Table 3
Values of the coefficients obtained from the Margules Eq. (5), of molar excess enthalpies at equimolar composition, $H^E_{x=0.5}$, of partial molar enthalpies at infinite dilution for each component, $\overline{H}^{\infty}_k$, and of associated uncertainties, u.

System	A_{12}	A_{21}	α_{21}	α_{12}	η	$H^E_{x=0.5}\pm\mu$ J mol^{-1}	$\overline{H}^{\infty}_1\pm\mu$ kJ mol^{-1}	$\overline{H}^{\infty}_2\pm\mu$
EAN + NMP	−5.142	−4.351	2.353	1.426	−3.799	−3494 ± 25	−12.74 ± 0.07	−10.79 ± 0.09
PAN + NMP	−5.112	−4.073	1.403	−0.920	−2.887	−3300 ± 24	-12.67 ± 0.06	-10.10 ± 0.08
BAN + NMP	−4.623	−3.445	2.315	1.772	−3.529	−3046 ± 14	−11.46 ± 0.06	−8.55 ± 0.06
MEOEAN + NMP	−4.426	−3.031	1.467	0.718	−2.493	−2658 ± 36	−11.0 ± 0.2	−7.5 ± 0.1

Table 4
Mixture composition expressed as the mole fraction of XAN, x_1, experimental density, ρ, molar volumes, V_m, and excess molar volumes, V^E, values at 298.15 K and 0.1 MPa of XAN (1) + NMP (2) mixtures.[a]

System	x_1	$10^{-3}\times\rho$/kg m^{-3}	$10^6\times V_m$/m^3 mol^{-1}	$10^6\times V^E$/m^3 mol^{-1}	x_1	$10^{-3}\times\rho$/kg m^{-3}	$10^6\times V_m$/m^3 mol^{-1}	$10^6\times V^E$/m^3 mol^{-1}
EAN (1)	0.000	1.02825	96.41	0.00	0.480	1.11962	92.38	−0.61
+	0.049	1.04083	95.67	−0.39	0.540	1.12936	92.06	−0.50
NMP (2)	0.138	1.05994	94.69	−0.74	0.592	1.13795	91.78	−0.41
	0.166	1.06580	94.41	−0.81	0.630	1.14372	91.61	−0.30
	0.223	1.07659	93.93	−0.88	0.684	1.15322	91.28	−0.25
	0.242	1.08027	93.77	−0.91	0.763	1.16768	90.76	−0.21
	0.292	1.08923	93.41	−0.92	0.830	1.17962	90.34	−0.15
	0.347	1.09875	93.05	−0.88	0.915	1.19554	89.78	−0.11
	0.457	1.11643	92.46	−0.69	0.981	1.20767	89.36	−0.06
	0.413	1.10961	92.68	−0.78	1.000	1.21076	89.28	0.00
–								
PAN (1)	0.000	1.02825	96.41	0.00	0.551	1.10572	101.12	−0.67
+	0.046	1.03838	96.49	−0.37	0.582	1.10868	101.48	−0.60
NMP (2)	0.167	1.05942	97.19	−0.84	0.628	1.11318	102.03	−0.51
	0.202	1.06453	97.48	−0.89	0.661	1.11642	102.41	−0.45
	0.263	1.07330	98.00	−0.98	0.721	1.12267	103.07	−0.37
	0.329	1.08153	98.64	−0.97	0.781	1.12874	103.73	−0.30
	0.367	1.08639	99.02	−0.97	0.808	1.13096	104.08	−0.21
	0.406	1.09060	99.45	−0.91	0.862	1.13673	104.64	−0.17
	0.461	1.09652	100.07	−0.83	1.000	1.15035	106.16	0.00
–								
BAN(1)	0.000	1.02825	96.41	0.00	0.439	1.07493	107.34	−0.81
+	0.048	1.03644	97.36	−0.33	0.538	1.08043	110.19	−0.61
NMP (2)	0.108	1.04494	98.68	−0.60	0.670	1.08806	113.91	−0.42
	0.163	1.05172	99.98	−0.78	0.843	1.09720	118.79	−0.17
	0.267	1.06231	102.62	−0.93	1.000	1.10549	123.16	0.00
	0.365	1.06991	105.27	−0.89				
–								
MEOEAN (1)	0.000	1.02825	96.41	0.00	0.564	1.16698	102.85	−0.46
+	0.053	1.04490	96.75	−0.31	0.670	1.18850	104.27	−0.33
NMP (2)	0.109	1.06124	97.21	−0.53	0.694	1.19351	104.60	−0.30
	0.173	1.07865	97.85	−0.67	0.873	1.22836	107.02	−0.07
	0.208	1.08771	98.22	−0.73	0.963	1.24595	108.19	−0.002
	0.367	1.12526	100.16	−0.73	1.000	1.25324	108.64	0.00
	0.448	1.14299	101.24	−0.65				

[a] Standard uncertainties u are $\mu(T) = 0.01$ K, $\mu(x_1) = 0.001$, $\mu(V^E) = 0.02\times10^{-6}$ m^3 mol^{-1}, $\mu(V_m) = 0.02\times10^{-6}$ m^3 mol^{-1}.

each XAN + NMP system. The moderately negative V^E values (maximum lost in volume around 1×10^{-6} m^3 mol^{-1}) found for EAN/PAN/BAN + NMP systems, indicates the presence of strong attractive interactions between the constituents, greater than in neat compounds. The V^E curves of each XAN + NMP system show a comparable trend and they overlap in the NMP-rich region. Being the compaction under mixing of EAN/PAN/BAN + NMP systems almost the same, V^E curves are not affected by the alkyl chain length. As far as the MEOEAN + NMP system, the reduction of volume is smaller than those obtained for the other XAN + NMP systems (maximum lost in volume around 0.76×10^{-6} m^3 mol^{-1}), indicating that the addition of a polar group, such as the methoxy one, prevents the compaction of the mixture.

4. Calorimetric properties

Complementary information was obtained by the calorimetric determination of the heat of mixing. In Fig. 3, the experimental points and the smoothed curves of partial molar enthalpies of constituents, $\overline{H}_k^E$, and the excess molar enthalpies, H^E, for the

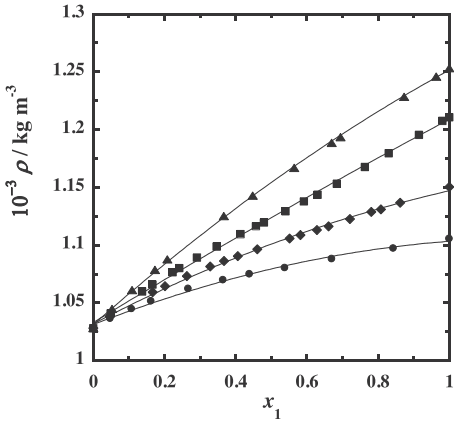

Fig. 1. Experimental densities, ρ, at 298.15 K and 0.1 MPa, of XAN (1) + NMP (2) mixtures as a function of x_1, the mole fraction of component (1). Symbols: ■, EAN + NMP; ◆, PAN + NMP; ●, BAN + NMP; ▲, MEOEAN + NMP.

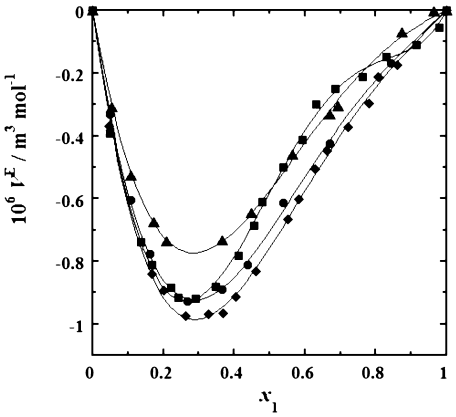

Fig. 2. Excess molar volumes, V^E, of XAN (1) + NMP (2) mixtures at 298.15 K and 0.1 MPa as a function of x_1, the mole fraction of component (1). The V^E curve is calculated with the a_i-parameters Redlich–Kister Eq. (3) reported in Table 2. Symbols: ■, EAN + NMP; ◆, PAN + NMP; ●, BAN + NMP; ▲, MEOEAN + NMP.

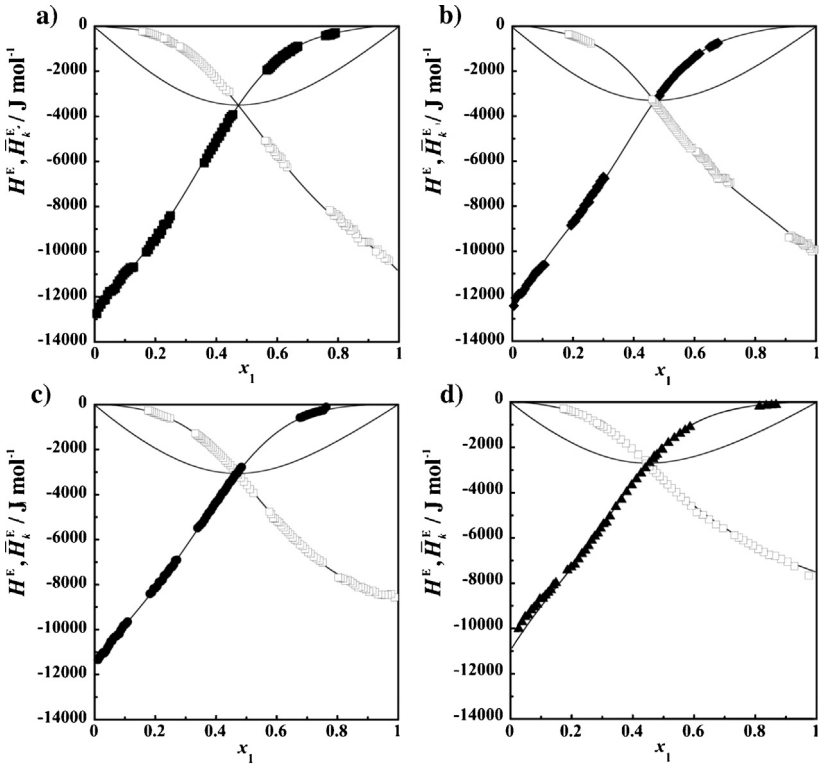

Fig. 3. Molar excess enthalpies, H^E, and excess partial molar enthalpies, $\overline{H}_k^E$, for the binary mixtures XAN (1) + NMP (2) as function of x_1, the mole fraction of component (1), at 298.15 K and 0.1 MPa. (a) EAN + NMP system; (b) PAN + NMP system; (c) BAN + NMP system; (d) MEOEAN + NMP system. $\overline{H}_1^E$, full symbols: ■, EAN; ◆, PAN; ●, BAN; ▲, MEOEAN; and, □, NMP. Curves fitting are calculated with the parameters of the Margules Eq. (6) reported in Table 3.

XAN + NMP mixtures are plotted as a function of the mole fraction of XAN, x_1. As can be seen, the shape of the H^E curves are moderately asymmetric, the values of the minimum at $x_1 = 0.47$ for each system, calculated from the Margules coefficients, are: $-3509\,J\,mol^{-1}$ for EAN + NMP system, $-3319\,J\,mol^{-1}$ for PAN + NMP system, $-3062\,J\,mol^{-1}$ for BAN + NMP system, and $-2689\,J\,mol^{-1}$ for MEOEAN + NMP system. The very high negative excess enthalpies found for each system suggested the presence of strong attractive interactions between the mixture constituents. Indeed, generally mixtures between two different organic compounds are characterized by endothermic effect, while the mixing is exothermic when two components give rise to attractive interactions among unlike molecules stronger than those present in like molecules. Exothermic mixing effects of NMP were observed in mixtures with water ($H^E_{x=0.5} = -2407 \pm 20\,J\,mol^{-1}$) [43] and with chloro-alkanes and -alkenes. The highest exceptionally value ($H^E_{x=0.5} = -4750\,J\,mol^{-1}$) was observed in NMP + 1,1,2,2-tetrachloroethane mixtures [44]. The slight asymmetry of H^E curve is explained with the non-specular peculiar shape of $\overline{H}_k^E$. At infinite dilution, excess partial molar enthalpies of XAN, $\overline{H}_1^{E,\infty}$, have absolute values higher than $\overline{H}_2^{E,\infty}$: the dissolution of XAN by NMP solvent was found to result in an interaction stronger with respect to the dissolution of NMP by the ionic liquids, indicating stronger attractive interactions played by NMP in the dissolution of the solute XAN, with respect to the same process in which the same components play exchanged roles. It could be highlighted that, as the alkyl chain length of the cation increases, $\overline{H}_k^{E,\infty}$ and $H^E_{x=0.5}$ decrease and the difference between $\overline{H}_k^{E,\infty}$ values increases. This indicates that the mixing process is more exothermic when the alkyl chain of the cation is smaller. Indeed, considering the absolute values at equimolar composition, the $H^E_{x=0.5}$ decreases in the following order: $H^E_{x=0.5}$ EAN > $H^E_{x=0.5}$ PAN > $H^E_{x=0.5}$ BAN. MEOEAN + NMP system showed the lowest $H^E_{x=0.5}$ absolute value, indicating that the addition of the polar methoxy group inhibits the interaction between XAN and NMP or more likely that the endothermic contribution necessary to separate the ions constituting MEOEAN is greater than the corresponding values associated with the other considered XAN.

5. Conclusions

In the present work, selected thermodynamic properties of some alkylammonium nitrate ionic liquids were studied with the aim of investigating their behavior in the organic solvent *N*-methyl-2-pyrrolidone (NMP) over the whole concentration range. Density measurements and calorimetric titrations were employed to characterize the mixing properties of these compounds.

The main information from the density measurements is that the increase of the alkyl chain length of the XAN cation inhibits the compaction of neat XAN. Negative and similar V^E values for each XAN + NMP system were found indicating that the alkyl chain length does not significantly influence the mixture compaction.

Negative H^E values were obtained for all of the investigated systems indicating the presence of strong attractive interaction between the components; in addition, it can be highlighted that the mixing process is more exothermic for short alkyl chain length ammonium nitrate ionic liquids. In general, the dissolution of XAN by the NMP solvent was found to result in stronger interactions with respect to those accompanying the NMP dissolution by the ionic liquids. MEOEAN showed a different behaviour compared to the other selected alkylammonium nitrate ionic liquids: (i) the addition of the polar group to the shorter alkyl chain considered promotes a greater compaction of the neat ionic liquids than EAN,

PAN and BAN, (ii) when MEOEAN is mixed with the organic solvent NMP, the methoxy group inhibits the interaction between the ions of XAN and NMP.

The present results provide valuable new information on these alkylammonium nitrate ionic liquids and their mixture with the useful solvent NMP, and allow us to dispose, in a direct and reliable way, quantities that are necessary for the chemical plants design.

Acknowledgments

This research was financially supported by PRIN-ITALY (2009 WHPHRH). M.U. gratefully acknowledges Sardinia Regional Government (Italy) for the financial support of her PhD scholarship (P.O.R. Sardegna F.S.E. 2007–2013). M.U. and S.P. express their gratitude to the Istituto per i Processi Chimico–Fisici, IPCF-CNR, Pisa, for allowing the use of calorimetric instrumentation and methods within the collaboration agreement between DSCG and IPCF. M.U. and S.P. wish to thank Ruggero Caminiti for insightful comment and for helpful discussion.

Appendix A. Supplementary data

Supplementary data associated with this article can be found, in the online version, at http://dx.doi.org/10.1016/j.fluid.2014.09.031.

References

[1] K.R. Seddon, Review ionic liquids for clean technology, J. Chem. Tech. Biotechnol. 68 (1997) 351–356.
[2] T.L. Greaves, C. Drummond, Protic ionic liquids: properties and applications, Chem. Rev. 108 (2008) 206–237.
[3] R.D. Rogers, K. Seddon, Ionic liquids – solvents of the future? Science 302 (2003) 792–793.
[4] M.U. Araos, G.G. Warr, Self-assembly of nonionic surfactants into lyotropic liquid crystals in ethylammonium nitrate, a room-temperature ionic liquid, J. Phys. Chem. B 109 (2005) 14275–14277.
[5] J.C. Gálvez-Ruiz, G. Holl, K. Karaghiosoff, T.M. Klapötke, K. Löhnwitz, P. Mayer, H. Nöth, K. Polborn, C.J. Rohbogner, M. Suter, et al., Derivatives of 1,5-diamino-1H-tetrazole: a new family of energetic heterocyclic-based salts, Inorg. Chem. 44 (2005) 4237–4253.
[6] C. Yue, A. Mao, Y. Wei, M. Lü, Knoevenagel condensation reaction catalyzed by task-specific ionic liquid under solvent-free conditions, Catal. Commun. 9 (2008) 1571–1574.
[7] Y.O. Sharma, M.S. Degani, CO_2 absorbing cost-effective ionic liquid for synthesis of commercially important alpha cyanoacrylic acids: a safe process for activation of cyanoacetic acid, Green Chem. 11 (2009) 526.
[8] J. Pernak, I. Goc, I. Mirska, Anti-microbial activities of protic ionic liquids with lactate anion, Green Chem. 6 (2004) 323.
[9] N.V. Plechkova, K.R. Seddon, Applications of ionic liquids in the chemical industry, Chem. Soc. Rev. 37 (2008) 123–150.
[10] P. Attri, P. Venkatesu, A. Kumar, N. Byrne, A protic ionic liquid attenuates the deleterious actions of urea on α-chymotrypsin, Phys. Chem. Chem. Phys. 13 (2011) 17023–17026.
[11] Y. Yue, X.-Y. Jiang, J.-G. Yu, K.-W. Tang, Enantioseparation of mandelic acid enantiomers in ionic liquid aqueous two-phase extraction systems, Chem. Pap. 68 (2013) 465–471.
[12] A. Hernoux-Villière, J.-M. Lévêque, J. Kärkkäinen, N. Papaiconomou, M. Lajunen, U. Lassi, Task-specific ionic liquid for the depolymerisation of starch-based industrial waste into high reducing sugars, Catal. Today 223 (2014) 11–17.
[13] T. Suzuki, K. Kono, K. Shimomura, H. Minami, Preparation of cellulose particles using an ionic liquid, J. Colloid Interface Sci. 418 (2014) 126–131.
[14] A. Heintz, Recent developments in thermodynamics and thermophysics of non-aqueous mixtures containing ionic liquids. A review, J. Chem. Thermodyn. 37 (2005) 525–535.
[15] A. Diedrichs, J. Gmehling, Measurement of heat capacities of ionic liquids by differential scanning calorimetry, Fluid Phase Equilib. 244 (2006) 68–77.
[16] E.J. Gonzàlez, B. Gonzàlez, N. Calvar, A. Domìnguez, Physical properties of binary mixtures of the ionic liquid 1-ethyl-3-methylimidazolium ethyl sulfate with several alcohols at T = 298.15, 313.15, and 328.15) K and atmospheric pressure, J. Chem. Eng. Data 52 (2007) 1641–1648.
[17] M.E. Kandil, K.N. Marsh, A.R.H. Goodwin, Measurement of the viscosity, density, and electrical conductivity of 1-hexyl-3-methylimidazolium bis (trifluorosulfonyl) imide at temperatures between (288 and 433) K and pressures below 50 MPa, J. Chem. Eng. Data 52 (2007) 2382–2387.
[18] T. Kavitha, P. Attri, P. Venkatesu, R.S. Rama Devi, T. Hofman, Influence of temperature on thermophysical properties of ammonium ionic liquids with *N*-methyl-2-pyrrolidone, Thermochim. Acta 545 (2012) 131–140.
[19] T. Kavitha, P. Attri, P. Venkatesu, R.S. Rama Devi, T. Hofman, Temperature dependence measurements and molecular interactions for ammonium ionic liquid with *N*-methyl-2-pyrrolidone, J. Chem. Thermodyn. 54 (2012) 223–237.
[20] T. Kavitha, P. Attri, P. Venkatesu, R.S. Devi, T. Hofman, Influence of alkyl chain length and temperature on thermophysical properties of ammonium-based ionic liquids with molecular solvent, J. Phys. Chem. B 116 (2012) 4561–4574.
[21] S. Porcedda, B. Marongiu, M. Schirru, D. Falconieri, A. Piras, Excess enthalpy and excess volume for binary systems of two ionic liquids + water, J. Therm. Anal. Calorim. 103 (2010) 29–33.
[22] H. Rodrìguez, J.F. Brennecke, Temperature and composition dependence of the density and viscosity of binary mixtures of water + ionic liquid, J. Chem. Eng. Data 51 (2006) 2145–2155.
[23] G. García-Miaja, J. Troncoso, L. Romaní, Excess enthalpy, density, and heat capacity for binary systems of alkylimidazolium-based ionic liquids + water, J. Chem. Thermodyn. 41 (2009) 161–166.
[24] W. Guan, L. Li, H. Wang, J. Tong, J. Yang, Studies on thermochemical properties of ionic liquids based on transition metal, J. Therm. Anal. Calorim. 94 (2008) 507–510.
[25] BASF Intermediates Chemicals Division. *N*-methyl-2-pyrrolidone Storage and Handling. New Jersey, 1998, http://compchemmpi.wikispaces.com/file/view/nmp_brochure_bio.pdf.
[26] M. Usula, F. Mocci, F. Cesare Marincola, S. Porcedda, L. Gontrani, R. Caminiti, The structural organization of *N*-methyl-2-pyrrolidone+water mixtures: a densitometry, X-ray diffraction, and molecular dynamics study, J. Chem. Phys. 140 (2014) 124503.
[27] Y. Hu, P. Wei, H. Huang, Z. Le, Z. Chen, Organic reactions in ionic liquids: ionic liquid ethylammonium nitrate–promoted knoevenagel condensation of Meldrum's acid with aromatic aldehydes, Synth. Commun. 35 (2005) 2955–2960.
[28] F. Pacholec, H.T. Butler, F. Poole, Molten organic salt phase for gas–liquid chromatography, Anal. Chem. 54 (1982) 1938–1941.
[29] C.A. Summer, R.A. Flowers, Protein renaturation by the liquid organic salt ethylammonium nitrate, Protein Sci. 9 (2000) 2001–2008.
[30] B. Clare, R. Giernoth, M.F. Costa Gomes, B. Kirchner, J.N. Canongia Lopes, D.R. MacFarlane, A.-V. Mudring, A.A.H. Padua, M. Pucheault, A. Stark, A. Sirwardana, S.S. Yin Tan, A. Taubert, M. Vaultier, in: B. Kirchner (Ed.), Ionic Liquids, Vol. 9, Springer, Leipzig, Germany, 2010.
[31] L. Gontrani, E. Bodo, A. Triolo, F. Leonelli, P.D. Angelo, V. Migliorati, R. Caminiti, The interpretation of diffraction patterns of two prototypical protic ionic liquids: a challenging task for classical molecular dynamics simulations, J. Phys. Chem. B 116 (2012) 13024–13032.
[32] M. Campetella, L. Gontrani, E. Bodo, F. Ceccacci, F. Cesare Marincola, R. Caminiti, Conformational isomerisms and nano-aggregation in substituted alkylammonium nitrates ionic liquids: an X-ray and computational study of 2-methoxyethylammonium nitrate, J. Chem. Phys. 138 (2013) 184506.
[33] K.N. Marsh, A.E. Richards, Aust. J. Chem. 33 (1980) 2121–2132.
[34] S. Porcedda, M. Usula, B. Marongiu, Physical-chemical properties of ionic liquid-containing mixtures, in: R. Caminiti, L. Gontrani (Eds.), The Structure of Ionic Liquids, Soft and Biological Matter, Springer International Publishing, Switzerland, 2014, pp. 171–191.
[35] M.M. Abbott, H.C. Van Ness, Vapor–liquid equilibrium Part III. Data reduction with precise expressions for GE, AIChE J. 21 (1975) 62–71.
[36] E. Matteoli, L. Lepori, A. Spanedda, Thermodynamic study of heptane + amine mixtures, Fluid Phase Equilib. 212 (2003) 41–52.
[37] E. Matteoli, P. Gianni, L. Lepori, Thermodynamic study of heptane + secondary, tertiary and cyclic amines mixtures. Part IV. Excess and solvation enthalpies at 298.15 K, Fluid Phase Equilib. 306 (2011) 234–241.
[38] K.N. Marsh, Excess enthalpies of benzene + cyclohexane mixtures, Int. Data Ser. Sel. Data Mix. Ser. A (1973) 1–5.
[39] M. Freemantle, An Introduction to Ionic Liquid, in: M. Freemantle (Ed.), RSC Publishing, Cambridge, UK, 2010.
[40] P. Bonhôte, A.-P. Dias, M. Armand, N. Papageorgiou, K. Kalyanasundaram, M. Grätzel, Hydrophobic, highly conductive ambient-temperature molten salts, Inorg. Chem. 37 (1998) 166.
[41] P. Wasserscheid, W. Keim, Ionic liquids-new "solutions" for transition metal catalysis, Angew Chem. Int. Ed. 39 (2000) 3772–3789.
[42] J.A. Riddick, W.B. Bunger, T.K. Sakano, Organic Solvents, fourth ed., Wiley-Interscience, New York, 1986, pp. 1986.
[43] M. Usula, S. Porcedda, F. Mocci, L. Gontrani, R. Caminiti, F. Cesare Marincola, NMR, calorimetry, and computational studies of aqueous solutions of *N*-methyl-2-pyrrolidone, J. Phys. Chem. B 118 (2014) 10493–10502.
[44] P. Gnanakumari, M.V.P. Rao, D.H.L. Prasad, Y.V.L.R. Kumar, Vapor–liquid equilibria and excess molar enthalpies for *N*-methyl-2-pyrrolidone with chloroethanes and chloroethenes, J. Chem. Eng. Data 48 (2003) 535–540.

Supporting Information of

Thermo-physical Properties of Ammonium-based Ionic Liquid + *N*-methyl-2-pyrrolidone Mixtures at 298.15 K

Marianna Usula[a], Enrico Matteoli[b], Francesca Leonelli[c], Francesca Mocci[a,d], Flaminia Cesare Marincola[a], Lorenzo Gontrani[c], Silvia Porcedda[a,*]

[a] *Dipartimento di Scienze Chimiche e Geologiche - Università degli Studi di Cagliari, Cittadella Universitaria di Monserrato, S.P. 8, I-09042 Monserrato (Italy)*

[b] *IPCF-CNR Istituto per I Processi Chimico Fisici del Consiglio Nazionale delle Ricerche, Via Moruzzi 1, I-56124 Pisa (Italy)*

[c] *Dipartimento di Chimica - Università di Roma "La Sapienza", P.le Aldo Moro 5, I-00185 Roma (Italy)*

[d] *Department of Materials and Environmental Chemistry, Arrhenius Laboratory, Stockholm University, S-106 91 Stockholm (Sweden)*

***Corresponding author.** Phone: +390706754415; fax: +390706754388. E-mail address: porcedda@unica.it

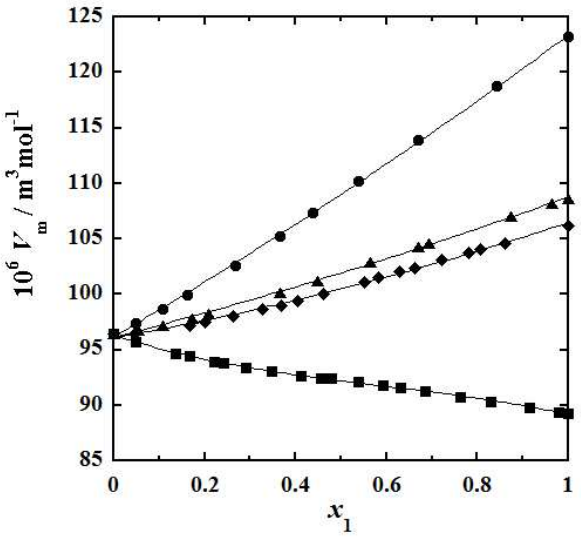

Fig. S1. Molar volumes, V_m, of XAN (1) + NMP (2) mixtures at 298 K and 0.1 MPa as a function of x_1, the mole fraction of component (1). The V_m curves are calculated with a 2nd degree polynomial equation. Symbols: ■, EAN+NMP; ♦, PAN+NMP; ●, BAN+NMP; ▲, MEOEAN+NMP.

III.1. Supplementary Data

III.1.1. NMR experiments of XAN (1) + NMP (2) systems

Figure III.1 shows a stack plot of the ^{1}H NMR spectra of dried ionic liquids, NMP and their mixtures at different composition. In order to simplify the comparison among the proton chemical shifts (δ) changes occurring upon NMP dilution, deviations expressed as difference between the positions of peaks in the neat compounds and in their mixtures, are represented in Figures III.2-III.4 as a function of the NMP mole fraction, x_2. As can be seen, the proton δ of NMP and XAN peaks were sensibly affected by the mixture composition: the alkyl proton signals in both XAN (Figure III.2) and NMP (Figure III.3) compounds moved upfield upon NMP dilution, while those of the $[NH_3]^+$ group of XAN (Figure III.4) moved downfield. In addition, the ^{13}C chemical shift of the carbonyl carbon (Figure III.4) moved upfield upon NMP dilution, suggesting the presence of hydrogen bond between XAN and NMP.[1] Since δ is a sensitive indicator of the degree of magnetic shielding of the nucleus, being influenced by surrounding electrons and neighbouring atoms and groups in the molecule, chemical shift variations were indicative of the occurrence of changes in the local chemical environment experienced by protons in both molecules. It is worth mentioning that recently *Alvarez et al*.[2] proposed a model for the interaction between EAN and water according to which the $[NO_3]^-$ anion is replaced by the water solvent. Therefore, in the light of these considerations, a possible contribution also by the XAN anion on the observed chemical shift variations is not excluded.

Complementary information on the XAN-NMP interaction was assessed by ^{13}C NMR relaxation measurements. Figures III.5-III.7 show the values of the ^{13}C spin-lattice relaxation rate R_1 (= $1/T_1$) for the samples under investigation. In Figure III.5-III.6 the spin-lattice relaxation rates of NMP carbons of each XAN mixture were reported. As can be seen in Figure III.5, the R_1 trends for the three XAN + NMP systems were very similar: the smallest R_1 values were recorded for the carbonyl carbon, while those of the protonated carbons followed the order C5 > C3 > C4 > C7 > C2.

By comparing the R_1 values of each NMP protonated carbon (Figure III.6), and those of the XAN alkyl chains (Figure III.7), it can be noticed that the ring carbons in NMP and those of the methylenic groups in XAN speeded up upon dilution below $x_2 \approx 0.3$ and, then, slowed down with further additions of NMP, this behaviour being more pronounced for BAN ionic liquid. This inversion point is not observed for CH_3 carbons both in XAN and in NMP, probably due to the rotational contribution.

The analysis of the present NMR data is currently still in progress, coupled with MD simulations to a more detailed investigation of the structural and dynamical properties of these mixtures.

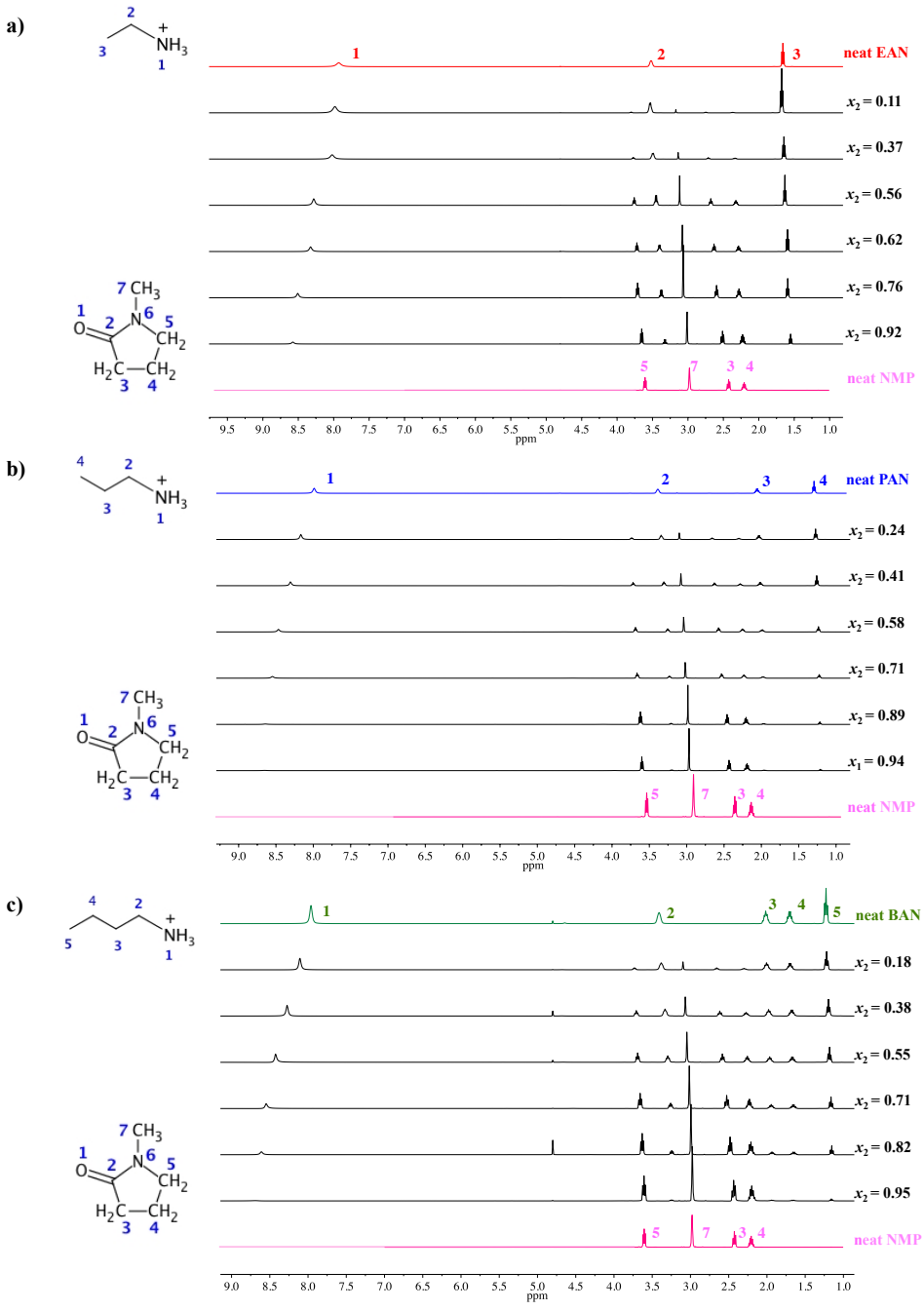

Figure III.1. ^{1}H NMR spectra of neat compounds, XAN and NMP, and their mixtures at different NMP mole fractions, x_2. a) EAN + NMP system; b) PAN + NMP system; c) BAN + NMP system.

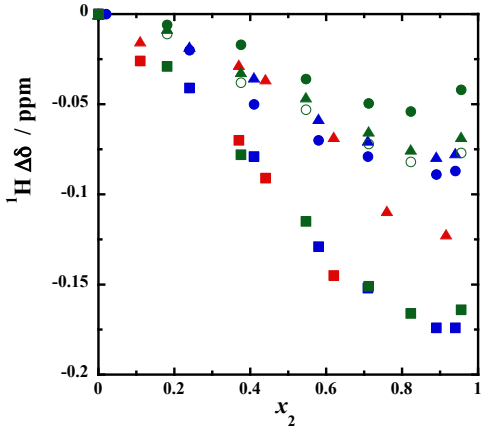

Figure III.2. ^{1}H chemical shift deviations of alkyl chain protons in XAN from neat ionic liquids, $\Delta\delta$ (δ_{mix}-δ_{neat}), as a function of the NMP mole fraction, x_2. Symbols: EAN (red), PAN (blue), BAN (green): ■, N-CH_2; ●, CH_2-CH_3 of PAN and BAN; ❍, CH_2-CH_2-CH_3 of BAN; ▲, CH_3.

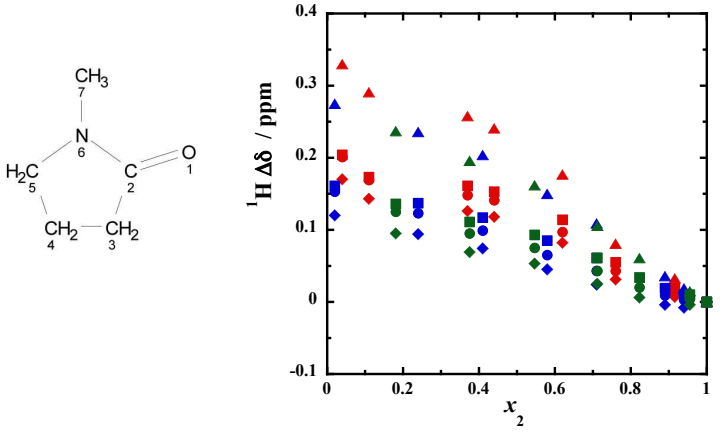

Figure III.3. ^{1}H chemical shift deviations of NMP protons from neat NMP, $\Delta\delta$ (δ_{mix}-δ_{neat}), as a function of the NMP mole fraction, x_2. Symbols: EAN (red), PAN (blue), BAN (green); ■, 5; ▲, 3; ◆, 4; ●, 7.

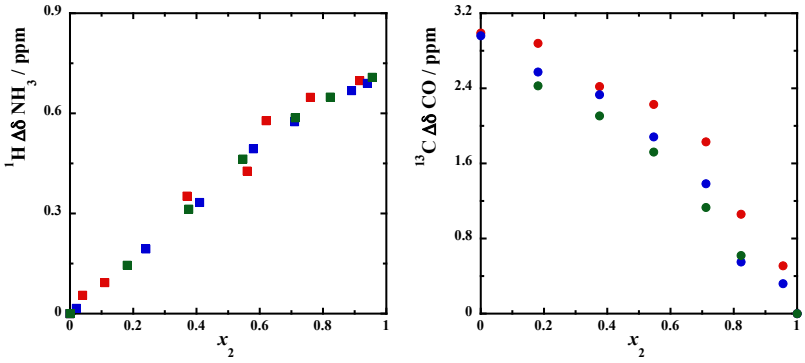

Figure III.4. ^{1}H chemical shift deviations of NH_3 protons in XAN (left) and ^{13}C chemical shift deviations of CO carbon in NMP (right), as a function of the NMP mole fraction, x_2. $\Delta\delta = (\delta_{mix}-\delta_{neat})$, where δ_{mix} is the chemical shift in the mixture and δ_{neat} the chemical shift of the neat compounds. Symbols: EAN (red), PAN (blue), BAN (green).

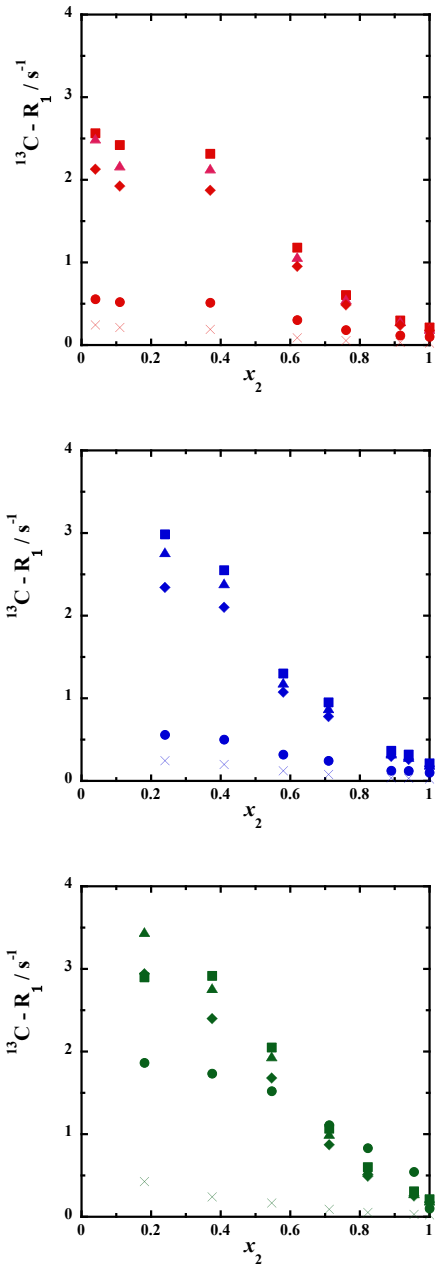

Figure III.5. ^{13}C spin-lattice relaxation rates for NMP in the presence of a) EAN (red); b) PAN (blue); c) BAN (green) as a function of the NMP mole fraction, x_2. Symbols: ■, C5; ▲, C3; ◆, C4; ●, C7; ×, C2.

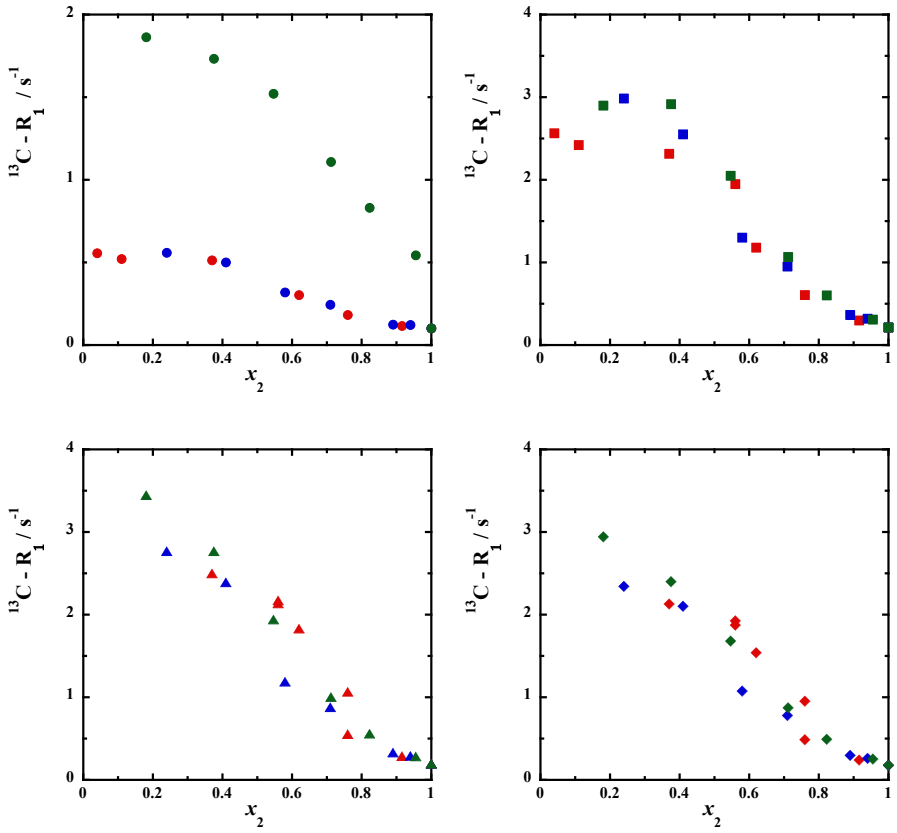

Figure III.6. ^{13}C spin-lattice relaxation rates of NMP as a function of the NMP mole fraction, x_2. Symbols: EAN (red), PAN (blue), BAN (green); ■, C5; ▲, C3; ◆, C4; ●, C7.

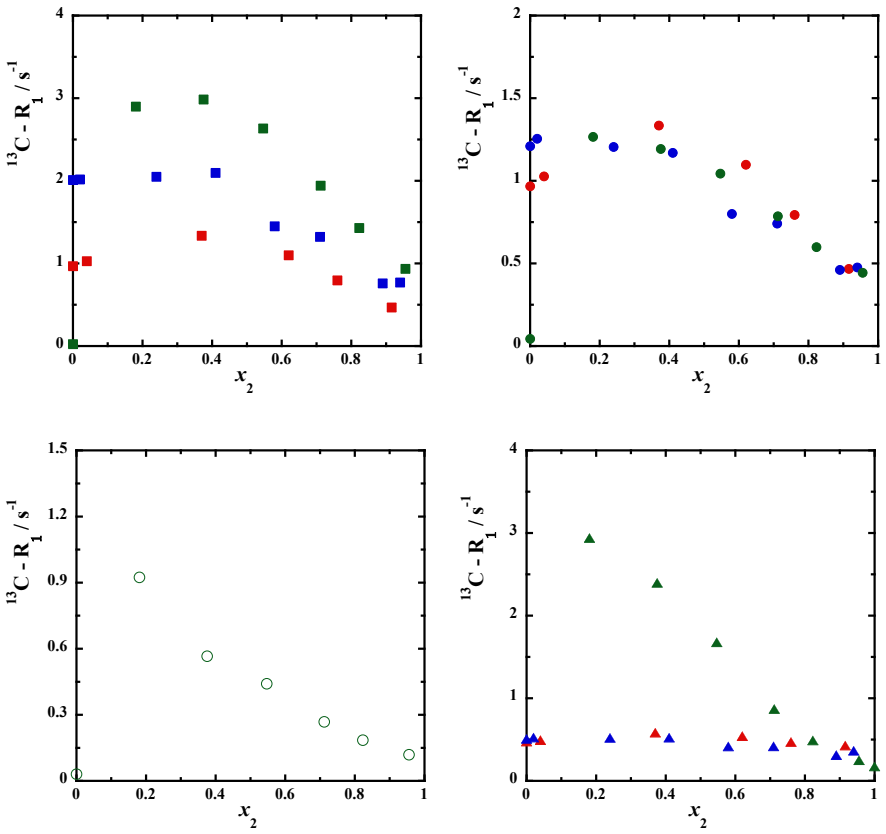

Figure III.7. ^{13}C spin-lattice relaxation rates of XAN as a function of the NMP mole fraction, x_2. Symbols, EAN (red), PAN (blue), BAN (green): ■, N-CH_2; ●, $\underline{C}H_2$-CH_3 of PAN and BAN; ○, $\underline{C}H_2$-CH_2-CH_3 of BAN; ▲, CH_3.

III.2 Volumetric data of XAN (1) + Water (2) systems

In Table III.1, the mixture composition expressed as XAN mole fraction, x_1, experimental densities, molar volumes, and excess molar volumes for each investigated XAN (1) + Water (2) mixture were reported. Each density value represents the mean of two determinations. Virtually, the physico-chemical properties of RTILs mainly depend on the nature and structure of ions and on the alkyl chain length of the cation. As it can be seen in Table III.2, the density value of the neat XAN decreases as the alkyl chain length

of the cation increase, whereas the addition of the methoxy group to the smaller alkyl chain considered, results in an increase of density. This behaviour is probably due to the difference in molecular weight and to the enhanced capability to give polar-polar attractive interactions. This indicates that a long alkyl chain inhibits the compaction of neat XAN, while the addition of a polar group in a short chain has opposite effect, *i.e.* promotes a greater compaction of the neat ionic liquids. In Figure III.8, the density values of the XAN (1) + Water (2) mixtures are plotted with respect to x_1. In general, the density trend of each XAN + Water system is monotonic with a downward concavity. RTILs are miscible with molecular solvents with medium- to high- dielectric constants *i.e.* solvents containing polar groups and immiscible with low dielectric liquids.[3–5] In the present study, we found that all XAN are completely miscible in water over the whole mole fraction range, since water is a polar solvent with a very high relative dielectric constant (ε_r= 78.5 at T = 298.15 K).[6]

Negative V^E values were found for each XAN + Water system. The moderately negative V^E values (maximum lost in volume around 0.6×10^{-6} m^3 mol^{-1}) found for EAN/PAN/BAN + Water systems, indicates the presence of strong attractive interactions between the constituents, greater than in neat compounds. The V^E curves of each XAN + Water system showed a comparable trend and they overlap in the water-rich region. Being the compaction under mixing of EAN/PAN/BAN + Water systems almost the same, V^E curves are not affected by the alkyl chain length. As far as the MEOEAN + Water system, the reduction of volume is smaller than those obtained for the other XAN + Water systems (maximum lost in

volume around 0.5×10^{-6} m^3 mol^{-1}), indicating that the addition of a polar group, such as the methoxy one, limits the compaction of the mixture.

Excess partial molar volumes at infinite dilution of each XAN we considered, $\overline{V}_1^{E,\infty}$, vary in the range [-6.18 to -5.10] cm^3 mol^{-1}. Such values indicate that the molar volume of each XAN in an infinitely diluted solution is reduced, with respect to the neat state, $\left(\overline{V}_1^{E,\infty}/V_1^*\right)$ by a quite important amount, in the range [-5.8 % to -4.1 %].

The related quantities of water are in general lower, amounting to -4.3 %, -2.6 % and -2.6 % for solutions in PAN, BAN and MEOAN, respectively, with the exception of EAN-containing mixtures where the $\left(\overline{V}_2^{E,\infty}/V_2^*\right)$ ratio amount to -8.5 %.

Table III.1

Mixture composition expressed as the mole fraction of XAN, x_1, experimental density, ρ, molar volumes, V_m, and excess molar volumes, V^E, values at 298.15 K and 0.1 MPa of XAN (1) + Water (2) mixtures.[a]

System	x_1	$10^{-3}\times\rho$ /kg m^{-3}	$10^{6}\times V_m$ /m^3 mol^{-1}	$10^{6}\times V^E$ /m^3 mol^{-1}	x_1	$10^{-3}\times\rho$ /kg m^{-3}	$10^{6}\times V_m$ /m^3 mol^{-1}	$10^{6}\times V^E$ /m^3 mol^{-1}
	0.000	0.99704	18.07	0.00	0.374	1.17091	44.12	-0.57
	0.006	1.00558	18.49	-0.04	0.443	1.17984	49.06	-0.55
	0.024	1.02679	19.68	-0.12	0.456	1.18111	50.01	-0.54
EAN (1)	0.050	1.05191	21.41	-0.22	0.497	1.18544	52.94	-0.53
+	0.073	1.07055	22.97	-0.30	0.618	1.19473	61.67	-0.44
Water (2)	0.087	1.08035	23.93	-0.34	0.747	1.20199	71.00	-0.34
	0.125	1.10247	26.55	-0.42	0.819	1.20480	76.17	-0.25
	0.160	1.11859	29.01	-0.48	0.908	1.20740	82.63	-0.12
	0.214	1.13748	32.77	-0.54	0.911	1.20774	82.88	-0.13
	0.297	1.15774	38.64	-0.57	0.955	1.20942	86.06	-0.11
	0.298	1.15798	38.73	-0.57	1.000	1.20991	89.34	0.00
	0.000	0.99704	18.07	0.00	0.424	1.13374	54.79	-0.58
	0.013	1.01180	19.09	-0.08	0.464	1.13616	58.39	-0.55
	0.018	1.01812	19.59	-0.11	0.498	1.13794	61.35	-0.52
PAN (1)	0.052	1.04740	22.40	-0.27	0.600	1.14242	70.43	-0.45
+	0.074	1.06168	24.24	-0.36	0.699	1.14543	79.26	-0.35
Water (2)	0.115	1.08155	27.76	-0.46	0.799	1.14777	88.13	-0.25
	0.186	1.10309	33.86	-0.56	0.838	1.14853	91.65	-0.20
	0.204	1.10719	35.49	-0.57	0.967	1.15040	103.15	-0.04
	0.275	1.11906	41.66	-0.60	1.000	1.15090	106.11	0.00
	0.313	1.12392	45.03	-0.60				
	0.000	0.99705	18.07	0.00	0.464	1.09807	66.34	-0.50
BAN (1)	0.045	1.03613	22.48	-0.28	0.562	1.10065	76.72	-0.44
+	0.093	1.05733	27.45	-0.41	0.580	1.10084	78.57	-0.41
Water (2)	0.143	1.07120	32.56	-0.51	0.667	1.10247	87.80	-0.35
	0.193	1.07965	37.84	-0.54	0.745	1.10339	96.07	-0.27
	0.330	1.09218	52.20	-0.56	0.877	1.10460	110.10	-0.12
	0.401	1.09542	59.72	-0.51	1.000	1.10554	123.15	0.00
	0.000	0.99705	18.07	0.00	0.495	1.22497	63.20	-0.42
	0.039	1.05734	21.48	-0.19	0.573	1.23224	70.51	-0.37
MEOEAN	0.113	1.12422	28.09	-0.38	0.646	1.23749	77.22	-0.31
(1)	0.161	1.15110	32.47	-0.44	0.738	1.24288	85.77	-0.22
+	0.229	1.17686	38.66	-0.48	0.693	1.24051	81.58	-0.27
Water (2)	0.318	1.19933	46.88	-0.49	0.926	1.25123	103.27	-0.06
	0.428	1.21718	57.00	-0.45	1.000	1.25380	110.16	0.00

[a] Standard uncertainties u are $u(T)$=0.01 K, $u(x_1)$=0.001, $u(V^E)$=0.02×10^{-6} m^3 mol^{-1}, $u(V_m)$=0.02×10^{-6} m^3 mol^{-1}

Table III.2

Values of the coefficients, a_i, and standard deviations, $\sigma(V^E)$ obtained from the RK equation. Values of molar excess volumes at equimolar composition, $V^E_{x=0.5}$, excess partial molar volumes at infinite dilution for each component k, $\overline{V}_k^{E,\infty}$, and associated uncertainties, u.

System	a_0	a_1	a_2	a_3	$\sigma\,(V^E)$	$V^E_{x=0.5} \pm u$	$\overline{V}_1^{E,\infty} \pm u$	$\overline{V}_2^{E,\infty} \pm u$
	$10^{-6} \times m^3\ mol^{-1}$							
EAN + Water	-2.07	1.01	-1.28	0.80	0.002	-0.519±0.005	-5.17±0.04	-1.54±0.04
PAN + Water	-2.07	1.21	-1.40	1.49	0.001	-0.520±0.004	-6.18±0.03	-0.78±0.03
BAN + Water	-1.86	1.11	-1.54	2.01	0.002	-0.466±0.004	-5.1±0.1	-0.46±0.1
MEOEAN + Water	-1.63	1.17	-1.15	1.15	0.001	-0.407±0.004	-5.10±0.04	-0.46±0.05

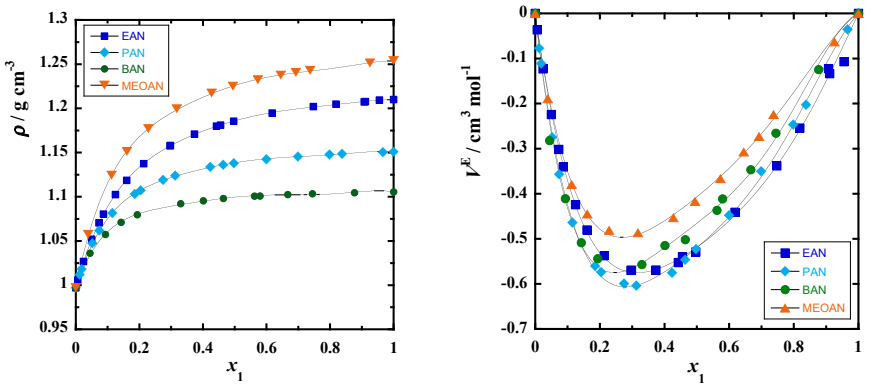

Figure III.8. Experimental densities, ρ, (left) and excess molar volumes, V^E, (right) of XAN (1) + Water (2) mixtures as a function of x_1, the mole fraction of component (1). The V^E curve is calculated with the a_i-parameters of RK equation reported in Table III.2.

REFERENCES

(1) Usula, M.; Porcedda, S.; Mocci, F.; Gontrani, L.; Caminiti, R.; Cesare Marincola, F. NMR, Calorimetry, and Computational Studies of Aqueous Solutions of *N*-Methyl-2-Pyrrolidone. *J. Phys. Chem. B* **2014**, *118*, 10493–10502.

(2) Docampo-Álvarez, B.; Gómez-González, V.; Méndez-Morales, T.; Carrete, J.; Rodríguez, J. R.; Cabeza, Ó.; Gallego, L. J.; Varela, L. M. Mixtures of Protic Ionic Liquids and Molecular Cosolvents: A Molecular Dynamics Simulation. *J. Chem. Phys.* **2014**, *140*, 214502.

(3) Freemantle, M. *An Introduction to Ionic Liquid*; Freemantle, M., Ed.; RSC Publishing: Cambridge, UK, **2010**.

(4) Bonhôte, P.; Dias, A.-P.; Armand, M.; Papageorgiou, N.; Kalyanasundaram, K.; Grätzel, M. Hydrophobic, Highly Conductive Ambient-Temperature Molten Salts. *Inorg. Chem.* **1998**, *37*, 166.

(5) Wasserсheid, P.; Keim, W. . *Angew. Chem. Int. Ed.* **2000**, *39*, 3772–3789.

(6) Riddick, J. A.; Bunger, W. B.; Sakano, T. K. *Organic Solvents*; fourth edi.; Wiley-Interscience: New York, **1986**; p. 1986.

PAPER IV

Ethylammonium Alkanoate-based Ionic Liquid + Water Mixtures: a Calorimetric and Volumetric Study at 298.15 K.

M. Usula, N. V. Plechkova, A. Piras, and S. Porcedda.

Submitted (November 2014) to *The Journal of Thermal Analysis and Calorimetry*

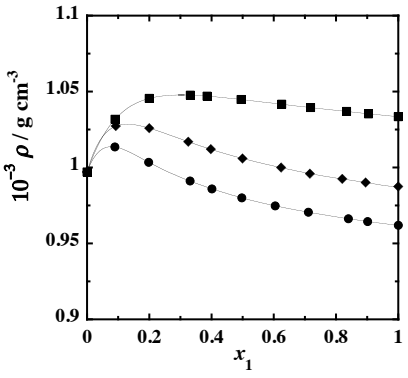

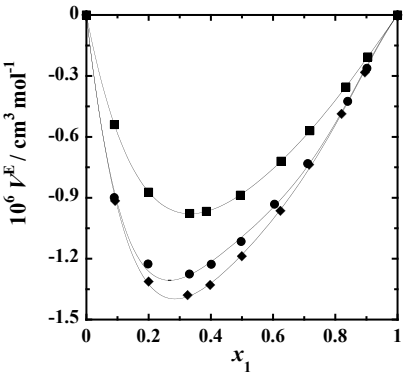

Journal of Thermal Analysis and Calorimetry

Ethylammonium Alkanoate-based Ionic Liquid + Water Mixtures: a Calorimetric and Volumetric Study at 298.15 K

--Manuscript Draft--

Manuscript Number:	JTAC-D-14-01239
Full Title:	Ethylammonium Alkanoate-based Ionic Liquid + Water Mixtures: a Calorimetric and Volumetric Study at 298.15 K
Article Type:	S.I. : AICAT2014
Corresponding Author:	Silvia Porcedda ITALY
Corresponding Author Secondary Information:	
Corresponding Author's Institution:	
Corresponding Author's Secondary Institution:	
First Author:	Marianna Usula, Master degree
First Author Secondary Information:	
Order of Authors:	Marianna Usula, Master degree
	Natalia V. Plechkova, Doctor
	Alessandra Piras, Doctor
	Silvia Porcedda
Order of Authors Secondary Information:	
Abstract:	A systematic study of a series of room-temperature ionic liquids, belonging to the ethylammonium alkanoate family (EAX), was carried out at 298.15 K and 0.1 MPa with the aim of investigating the effect of the anionic chain length on some thermophysical properties and their behaviour in water (W), over the whole mole fraction range. The determination of Gutmann acceptor numbers (AN) for the neat EAX by using 31P NMR spectroscopy, allowed us to obtain a quantitative measure of Lewis acidity. Experimental densities, , were used to calculate molar volumes, Vm, and excess molar volumes, VE. Complementary information was obtained by isothermal titration calorimetry that provided the values of the heat of mixing, HE, and the excess partial molar enthalpies of each component, H1 and H2. The density values of neat EAX samples decrease as the alkyl chain length of the anion increases. Moderate negative VE and HE values were found for each EAX + W system, indicating the presence of attracting interactions between the constituents.
Suggested Reviewers:	

Ethylammonium Alkanoate-based Ionic Liquid + Water Mixtures: a Calorimetric and Volumetric Study at 298.15 K

Marianna Usula[a], Natalia V. Plechkova[b], Alessandra Piras[a], Silvia Porcedda[a,*]

[a] *Dipartimento di Scienze Chimiche e Geologiche - Università degli Studi di Cagliari, Cittadella Universitaria di Monserrato, S.P. 8, I-09042 Monserrato (Italy)*

[b] *QUILL, The Queen's University of Belfast, Stranmillis Road, Belfast, Northern Ireland, UK BT9 5AG.*

KEYWORDS: ethylammonium, methanoate, propanoate, butanoate, excess molar volume and enthalpy.

***Corresponding author.** Phone: +390706754415; fax: +390706754388. E-mail address: porcedda@unica.it

ABSTRACT

A systematic study of a series of room-temperature ionic liquids, belonging to the ethylammonium alkanoate family (EAX), was carried out at 298.15 K and 0.1 MPa with the aim of investigating the effect of the anionic chain length on some thermophysical properties and their behaviour in water (W), over the whole mole fraction range. The determination of Gutmann acceptor numbers (AN) for the neat EAX by using ^{31}P NMR spectroscopy, allowed us to obtain a quantitative measure of Lewis acidity. Experimental densities, ρ, were used to calculate molar volumes, V_m, and excess molar volumes, V^E. Complementary information was obtained by isothermal titration calorimetry that provided the values of the heat of mixing, H^E, and the excess partial molar enthalpies of each component, $\bar{H}_1^E$ and $\bar{H}_2^E$. The density values of neat EAX samples decrease as the alkyl chain length of the anion increases. Moderate negative V^E and H^E values were found for each EAX + W system, indicating the presence of attracting interactions between the constituents.

1. Introduction

Ionic liquids (ILs) and, in particular, room-temperature ionic liquids (RTILs) have been generating increasing interest over the last two decades [1] and many research groups and industries have been engaged to investigate a great number of different ionic liquids for a range of novel applications [2-6]. As witnessed by the rapid growth of scientific papers concerning this class of compounds, RTILs attract large attention as an alternative to traditional volatile organic solvents, thanks to some of their characteristics such as low volatility under ambient conditions, and good solvation properties towards polar and apolar compounds [7-9].

Nitrogen-containing cations, such as ammonium, imidazolium, pyridinium, with weak nucleophilic anions such as $[BF_4]^-$, $[PF_6]^-$, $[CF_3SO_3]^-$, $[(CF_3SO_2)_2N]^-$ are typical ILs constituents. An interesting aspect is that, being composed of two parts (a cation and an anion, with different alkyl chain lengths on either of them, or both), it is possible to synthesise an huge number of different ILs characterised by a unique set of physicochemical properties [10]. However, the employment of ILs in scientific research and technical applications requires exact knowledge on their physical properties, which are connected with the IL-IL and/or IL-solute interactions. These interactions and their strength, influenced by intermolecular van der Waals forces, intermolecular Coulomb interactions, and ability of a solvent to form hydrogen bonds, can be quantified by using the so-called "donor–acceptor concept" approach developed by Victor Gutmann [11, 12]. He defined the acceptor number (AN), which is a method for quantifying the electrophilic or electron accepting properties of a solvent. The Gutmann AN [12] is a well-established quantitative measure of Lewis acidity and it could help to predict the intermolecular interactions of nucleophiles and other electron-rich substrates with the IL cations.

Over the last years, experimental and/or theoretical thermodynamic studies on pure RTILs and their mixtures with water [13-16], which is important for the design of any technological processes, were reported. In the majority of published studies, the effect of the alkyl chain length of the cation has been investigated. More recently, alkanoate anions have been considered in the synthesis of new ILs [10, 17-23]. Greaves *et al*. [23, 24] synthesised different alkanoate ionic liquids and studied their nanostructure and some physicochemical properties. Ethyl-, *n*-propyl-, and *n*-butylammonium methanoate (EAM, PAM, and BAM, respectively) were synthesised and tested as mobile-phase for reversed phase liquid chromatography. EAM, which has a polarity similar to that of methanol or acetonitrile, has been indicated as suitable for use as mobile phase in

Liquid Cromathography 18, 19, 25]. Chhotaray *et al*. [20], reported the values of density, viscosity and speed of sound at atmospheric pressure and different temperatures for five ILs: propylammonium methanoate or ethanoate and 3-hydroxy-propylammonium methanoate, ethanoate or trifluoroethanoate. Diisopropylethylammonium methanoate + water mixtures have been investigated by Anouti *et al*. [21], to obtain the values of density, heat capacity, refractive index and excess quantities. Another promising alkanoate-based IL for practical applications, because of its low toxicity, is 2-hydroxyethylammonium methanoate, which has been synthesised for the first time by Bicak in 2005 [17]. Density and ultrasonic speed of their mixtures with water or methanol or ethanol have been measured by Iglesias *et al*. [22].

In this work we report the experimental measurements of Gutmann AN of different ethylammonium alkanoate, EAX (ethylammonium methanoate, EAM; etylammonium propanoate, EAP; and etylammonium butanoate, EAB), and H^{E} and V^{E} values of their aqueous mixtures over the whole mole fraction range with the aim to evaluate the effect of alkyl chain length on some thermodynamic properties of these mixtures. Ethylammonium ethanoate being solid in the neat state [18] has not been considered.

To the best of our knowledge, experimental measurements of V_{m}, V^{E}, H^{E}, $\bar{H}_1^E$, and $\bar{H}_2^E$ have not been reported in the literature for the selected EAX + water binary mixtures.

2. Experimental Section

2.1. Synthesis. Alkylcarboxylic acid (methanoic, > 98 % puriss. Glacial, Riedel-de Haën; propanoic, ≥ 99.5 %, Sigma Aldrich; butanoic, ≥ 99 %, Sigma Aldrich) was added dropwise to an equimolar amount of an aqueous ethylamine solution (70 % in water, Fluka Chemika) in a one-neck one-litre round-bottom flask, cooled with liquid N_2 (as the reaction is exothermic). The flask was kept closed after each acid addition, and cooled by adding more liquid N_2 when necessary. The reaction is fairly exothermic and maintaining the temperature low is important. After all the acid had been added, the reaction was left to warm up to room temperature for approximately two hours, and then stirred at room temperature for one hour. Water was removed by freeze-drying technique at 0.03 mbar pressure. After a 12 h cycle, the water content was checked by Karl-Fischer titration. The result showed over 3 w/w % water content, so the freeze-drying cycle was repeated twice more, until no decrease in the water content was observed. The resulting ethylammonium methanoate, EAM (97 % yield); ethylammonium propanoate, EAP (97 % yield); and

ethylammonium butanoate, EAB (98 % yield) are extremely hygroscopic light yellow liquids, therefore they were kept under N_2 atmosphere, in a glove box until use. Abbreviated names, % yield synthesis, final water content, purification and analysis methods of the investigated ionic liquids are reported in Table 1.

Aqueous solutions of EAX were prepared in a glove box by weighing samples of EAX in screw-cap glass vials with an analytical balance (Sartorius A210P, Data Weighing Systems Inc., IL-USA; precision and accuracy mass of $\pm 1\times10^{-7}$ kg and $\pm 5\times10^{-7}$ kg, respectively). The proper amount of water to obtain different solutions of various compositions was added after removing the samples from the glove box.

2.2. Gutmann Acceptor Numbers and data treatment. Gutmann acceptor numbers (AN) [12], which quantify the electrophilicity or electron accepting properties of an ionic liquid, was determined from the ^{31}P-NMR chemical shift of a triethylphosphine oxide (TEPO) probe molecule, dissolved in the respective pure solvent [12]. RTIL-TEPO complexes induce a change in the chemical shift in the ^{31}P-NMR spectrum, which is directly proportional to the AN. To obtain precise data, the ^{31}P NMR chemical shifts are measured at several concentrations of TEPO as recommended by Gutmann, because the chemical shifts are affected by the concentration of TEPO and the magnetic permeability of the solvent. These data are then extrapolated to infinite dilution, δ_{inf} (^{31}P chemical shift at infinite dilution of TEPO). The AN value is calculated by using the following equation:

$$AN = 2.348\ \delta_{inf} \qquad 1)$$

The proportionality constant in eqn. 1 has been empirically determined from the endpoints of hexane (AN = 0) and 10^{-3} M solution in 1,2-dichloroethane of antimony(V) chloride (AN = 100) [11, 12].

Sample preparation was done in a glove box. Three samples (≈ 1 g) of EAX were weighed into a sample vial (10 cm^3) equipped with a magnetic stirring bar. The vial was left on the balance, and TEPO was added (approximately 3, 5 or 7 mol % per mol of ionic liquid cation; see Table 2 for the accurate masses). After a 5 hours-long stirring of the sample to ensure the complete dissolution, the liquids were loaded into NMR tubes (5 mm, borosilicate glass), each containing a capillary with benzene-d_6. Then the tubes were closed and taken out of the glove box immediately prior to measurement. ^{31}P-NMR spectra were acquired at 121.452 MHz using a Bruker 300

spectrometer. All samples were measured at 300.15 K.

2.3. Volumetric measurements and data treatment. The densities of the liquid mixtures and the pure compounds were measured, at 298.15 K and 0.1 MPa, by means of a vibrating tube densitometer (model DMA 4500 ME-Anton Paar - Gratz, Austria). Accuracy in the temperature was better than ±0.01 K. Density precision and accuracy were $\pm 1\times10^{2}$ kg m^{-3} and $\pm 5\times10^{2}$ kg m^{-3}, respectively. The instrument was calibrated before each experimental run using dry air and distilled water as references. Solutions were prepared by weight in septum-capped vials of approximately 2 cm^{3} using needles and syringes to transfer liquids. The molar volumes of mixture, V_{m}, were obtained from:

$$V_{\mathrm{m}} = \frac{\left(x_1 M_1 + x_2 M_2\right)}{\rho_{mix}} \qquad 2)$$

and the excess molar volumes, V^{E}, were calculated by the following equation:

$$V^{\mathrm{E}} = V_{\mathrm{m}} - \frac{\left(x_1 M_1\right)}{\rho_1} - \frac{\left(x_2 M_2\right)}{\rho_2} \qquad 3)$$

where ρ_{mix} is the density of the mixture and x_k, M_k, and ρ_k are the mole fraction, the molar mass, and the density of the component k (k = 1 or 2), respectively. V^{E} data were fitted by means of the Redlich-Kister (RK) equation having the form:

$$V^{\mathrm{E}} = x_1 x_2 \sum_{i=0}^{n-1} \mathrm{a}_i (x_1 - x_2)^i \qquad 4)$$

The absolute standard deviation of the fit, $\sigma(V^{\mathrm{E}})$, was calculated using the following equation:

$$\sigma(V^{\mathrm{E}}) = \sqrt{\frac{\Sigma(V^{\mathrm{E}}_{j,\,\mathrm{calc}} - V^{\mathrm{E}}_{j,\,\mathrm{exp}})^2}{N-n}} \qquad 5)$$

where N is the number of experimental points and n is the number of coefficients. By un-weighted least squares treatment a smoothed curve was obtained for each EAX (1) + W (2) system. The obtained RK coefficients are reported in Table 3.

Excess molar volumes at infinite dilution, $\bar{V}_k^{\mathrm{E},\infty}$, of each component *k*, is defined as the difference between the molar volumes at infinite dilution and in the neat state: $\bar{V}_k^{\mathrm{E},\infty} = \bar{V}_k^{\infty} - V_k^*$. Their values were calculated from the RK parameters by means of:

$$\bar{V}_k^{\mathrm{E},\infty} = \sum_{i=0}^{n} (-1)^k a_i \qquad 6)$$

Furthermore, from the standard deviations of the above RK parameters we calculated the SD, and the uncertainties, *u* (*u* = 2×SD), of the excess molar volumes at equimolar composition, $V_{x=0.5}^{E}$, and of the partial molar volumes of each component at infinite dilution, $\bar{V}_k^{\mathrm{E},\infty}$, which are reported in Table 3.

The procedure was checked by comparison of our experimental V^{E} data of the water + ethanol system with reliable literature data [26]. We found a difference lower than 0.8 % in the whole composition range.

2.4. Calorimetric measurements and data treatment. Heats of solution were collected through a heat flow calorimeter by Thermometric (model 2277, Thermal Activity Monitor - Järfälla, Sweden) at (298.15±0.01) K and 0.1 MPa. Experiments were conducted by adding a pure component, via Hamilton gas-tight syringes of capacity in the range of (250 to 500) μL driven by Cole-Parmer (model 74900 - Vernon Hills, Illinois, USA) pumps, to an ampoule of 1 cm^3 capacity initially charged with the other component or with a stock mixture of them. With this system, we were able to make accurate injections starting from a minimum of 1 μL, with precision 0.5 %, and to measure accurate heat effects as small as 0.01 J, with sensitivity 0.5 μW. We chose this technique instead of mixing-flow calorimetry to avoid errors due to incomplete mixing and to obtain more precise values of the partial molar enthalpy at infinite dilution [27].

The experimental solution heats, Q_{exp}, released by the additions of very small quantities of the titrant, n_k, practically represent partial molar enthalpies, $\bar{H}_k$, $\bar{H}_k \cong Q / n_k$. From this equation, calculated values of the solution heats, Q_{calc}, can be obtained, being $\bar{H}_{k,\mathrm{calc}}$ accounted for by proper differentiation of the equation $H^{\mathrm{E}} = f(x)$, such as the modified Redlich-Kister one [28]:

$$\frac{H^{\mathrm{E}}}{RT} = \frac{x_1 x_2 \sum_{k=1}^{n} c_k \left(x_1 - x_2\right)^{k-1}}{\left(1 + c_0 \left(x_1 - x_2\right)\right)} \qquad 7)$$

A standard least squares procedure identifies the best values of c_k parameters at the minimum of the objective function $OF = \Sigma \left(Q_{\mathrm{exp}} - Q_{\mathrm{calc}}\right)^2$. Proper allowance was made for the heat involved in the phase composition changes brought about by the vapour-liquid equilibration after each addition. An exhaustive description of the apparatus, the experimental procedure, and the data treatment, can be found in literature [29-31]. The coefficients values obtained for EAX (1) + W (2) mixtures are reported in Table 4. From the standard deviations of the RK equation we calculated the uncertainties, u, on H^{E} at equimolar mixtures and on excess partial molar enthalpies of each component at infinite dilution, $\bar{H}_k^{\mathrm{E},\infty}$, also reported in Table 4.

As explained in previous papers [29-31], the calorimetric experimental procedure generates a large amount of experimental data (*c.a.* 200 experimental points for each binary mixture investigated, each composed of 4 numbers), which are not worth an extensive tabulation herein. These data can be retrieved as supplementary electronic material (xls-file) from the Authors.

The reliability of the whole procedure was checked by measuring the H^{E}, in the whole range of concentration, of the system benzene (1) + cyclohexane (2). Comparison with reliable literature [32] data revealed a discrepancy lower than 2 %. The uncertainty in the observed heat, Q, as determined by the reproducibility of the experiments and by integration of the peak area, can be evaluated as 0.5 %.

3. Results

3.1. Gutmann Acceptor Numbers. ^{31}P-NMR chemical shifts for an infinite dilution of TEPO in ionic liquids, δ_{inf}, were determined by extrapolation of ^{31}P-NMR chemical shifts obtained for the three TEPO concentrations and the AN values of EAX were calculated (see Table 2). As an example, ^{31}P-NMR chemical shifts of TEPO in selected EAX compositions, along with the fitted straight lines, are shown in Figure 1. The P–O bond lengths in the complexes with the phosphine oxide may be related to the phosphorus deshielding in ^{31}P-NMR experiments, where TEPO is used as a ^{31}P-NMR probe.

3.2. Volumetric properties. Mixture composition, experimental densities, molar volumes, and excess molar volumes for each investigated EAX (1) + W (2) mixtures are reported in Table 5. Each density value represents the mean of two determinations. As it can be seen in Table 5, the density value of the neat EAX decreases as the alkyl chain length of the anion increase. In Figure 2, the density values of the EAX (1) + W (2) mixtures are plotted with respect to x_1. Each curve exhibits a maximum for $x_1 < 0.3$ which becomes more pronounced and shifted towards lower x_1 values as the alkyl chain of the anion increases. Molar volumes, V_m, and excess molar volumes, V^E, values were calculated by using equations 2 and 3. The V_m trend is falsely linear; in fact, each curve is fitted by a polynomial equation of 2nd degree having an upward concavity as can be seen in Figure S1 of the supplementary material. This concavity is more clearly observable in the V^E curves representation, Figure 3. All V^E values are negative and show a minimum at x_1 in the range (0.30 to 0.35) in the region of lower values of the more polar component, the IL. The V^E curves do not follow the order suggested by the alkyl chain length of the EAX, indeed the higher volume contraction (-1.4×10^{-6} m^3 mol^{-1}) is showed by EAP. The V^E curves of each EAX + W system show a comparable trend and they perfectly overlap only in the mole fraction range of $0.9 \le x_1 \le 1.0$.

By observing the $\overline{V}_k^{E,\infty}$ values reported in Table 3, it can be noticed that $\overline{V}_2^{E,\infty}$, the excess partial molar volume at infinite dilution of the common component of each mixture, have very close values as well as $\overline{V}_2^{\infty}$; the solvent molecules at infinite dilution occupy the same volume 16.0 cm^3 mol^{-1}. The first component, EAX, behaves in a different manner: $\overline{V}_1^{E,\infty}$ doubles its value passing from EAM to EAP, furthermore EAP and EAB have the same $\overline{V}_1^{E,\infty}$ value but different $\overline{V}_1^{\infty}$ amounting to (107.2 and 124.9) cm^3 mol^{-1}, respectively.

3.3. Calorimetric properties. By means of the ITC technique we obtained, in a direct manner, the excess partial molar enthalpy of each component, $\overline{H}_k^E$, and the value of the heat of mixing coinciding with H^E for the mixtures under investigation. In Figure 4, the experimental points and the smoothed curves of $\overline{H}_k^E$ and H^E for the EAX + W mixtures are plotted as a function of the mole fraction of EAX, x_1. As can be seen, the non-specular peculiar shape of $\overline{H}_k^E$ generate H^E curves quite asymmetric with the following coordinates of the minima, calculated from the RK coefficients: (0.33, -1020 J mol^{-1}) for EAM + W; (0.34, -1217 J mol^{-1}) for EAP + W; and (0.40, -1004 J mol^{-1}) for EAB + W system. By comparing excess partial molar enthalpies at infinite

dilution of EAX and W reported in Table 4, it can be noticed that $\bar{H}_2^{E,\infty}$ showed a similar value for each system indicating that the dissolution of water played by the ionic liquid is not influenced by the alkyl chain length of the anion; on the other hand $\bar{H}_1^{E,\infty}$ increase notably from EAM to EAB. $\bar{H}_1^{E,\infty}$ have absolute values much more higher than those of water, indicating that the dissolution of EAX by water solvent results in an interaction much stronger with respect to the dissolution of water by the ionic liquids. $\bar{H}_1^{E,\infty}$ of EAP and EAB have coinciding values and they are seven time higher than the value of $\bar{H}_2^{E,\infty}$.

4. Discussion and Conclusions

In the present work, combined calorimetric, volumetric, and Gutmann AN provided deep insights into some thermophysical properties of different ethylammonium alkanoate ionic liquids (EAX) with water (W) binary systems, which are also important for the design of technological processes.

As stated in literature [33-35], ILs are miscible with molecular solvents with medium- to high-dielectric constants *i.e*. solvents containing polar groups and immiscible with low dielectric liquids. Consequently, all ionic liquids investigated in the present study are completely miscible in the water solvent over the whole mole fraction range, since water is a very polar solvent with a high relative dielectric constant (ε_r = 78.3 at T = 298.15 K) [36].

The determination of AN by using the Gutmann method, allowed us to obtain a quantitative measure of electrophilicity of the investigated ionic liquids. It can be noticed from the AN values reported in Table 2, as the alkyl chain length of the anion increase the AN value decreases, indicating a greater acidity for EAM ionic liquid than the EAP and EAB. This could be due to the increase in steric hindrance of the cation–anion interactions on increasing the chain length, and to the aggregation of the long chain alkanoate anions, thus impeding the solvent–solute interactions. Similar results were obtained for some imidazolium cations [37]. By comparing our results with common organic solvent reported by Estager *et al*. [38], we can say that EAX ionic liquids are more acidic than the water as a solvent (AN = 54.8).

By observing density results of the neat EAX, coherent with those reported by Graves *et al*. [24], it is possible to note that the density value decreases as the alkyl chain length of the anion increases, which can be attributed to an increase in steric hindrance as the chains become more

voluminous. As can be seen in Figure 3, EAX + W mixtures can be classified as "contractive" binary mixtures. Therefore, the negative V^E values of each EAX + W system may be attributed to the interaction between unlike molecular interactions through hydrogen bonding, hence more efficient packing and/or attractive interaction occurred when the investigated ionic liquid and water were mixed. By comparing V^E trends, it is evident that the addition of the first -CH_2 group to the alkyl chain of the methanoate anion causes a relevant increase in compaction of the mixture, while a further extension of the alkyl chain has an opposite effect even if it is quite moderate.

In regards to calorimetric results, the negative excess enthalpies found for each system suggest the presence of attractive interactions between the mixture constituents stronger than the interactions acting in pure liquids. Indeed, generally mixtures between two different organic compounds are characterised by endothermic effect, while the mixing is exothermic only when attractive interactions among unlike molecules are stronger than those present in like molecules. $H^E_{x=0.5}$ values for each investigated system are quite close indicating that the alkyl chain length of the anion does not significantly influence the mixing process. Despite that, EAP + W system showed the highest $H^E_{x=0.5}$ absolute value. In agreement with V^E results, the addition of the first -CH_2 group to the alkyl chain of the methanoate anion favourites a greater interaction between the components, while a further extension of the alkyl chain inhibits this interaction.

Since thermodynamics properties of EAX with water mixtures, to the best of our knowledge, were not published in the open literature, it is possible to compare our thermodynamics results with an ionic liquid, which has the same cation (ethylammonium) but a different anion, as for example the ethylammonium nitrate (EAN). In our previous study [13], H^E and V^E of EAN + water mixtures showed a different behaviour: positive H^E ($H^E_{x=0.5}$ = 700 J mol^{-1}) and negative V^E (-0.52 cm^3 mol^{-1}) were found. When EAN is mixed with water, it exhibits a volume contraction as well as EAX, even if at a lesser extent than EAX; while H^E values have opposite sign in the whole range of composition. Positive excess enthalpies implicate weaker interaction between the components; the forces between the same kind of ions or molecules (IL–IL and water–water interactions) are stronger than those of IL-water. Indeed, ionic liquids containing the carboxylate anion, compared to those containing the nitrate one, show a greater affinity for water molecules.

SUPPLEMENTARY MATERIAL

The online version of this article (doi: ...) contains supplementary material, which is available to authorized users.

ACKNOWLEDGMENT

This research was financially supported by PRIN (2009 WHPHRH). M. U. gratefully acknowledges Sardinia Regional Government for the financial support of her PhD scholarship (P.O.R. Sardegna F.S.E. 2007-2013). M. U. and S. P. express their gratitude to the Istituto per i Processi Chimico-Fisici, IPCF-CNR, Pisa, for allowing the use of calorimetric instrumentations and methods within the collaboration agreement between DSCG and IPCF. M.U and S. P. wish to thank Enrico Matteoli, Francesca Mocci and Flaminia Cesare Marincola for insightful comments. M. U. wishes to thank Kenneth R. Seddon for the acceptance in Queen's University Ionic Liquid Laboratories (QUILL) for the Erasmus PlaceDoc and for helpful discussion. N. P. was supported by the industrial advisory board of QUILL. M. U. thanks Fergal Coleman from QUILL for his assistance with the Gutmann Acceptor Number studies.

REFERENCES

1. Wasserscheid P, Welton T. Ionic Liquids in Synthesis. Weinheim: VCH Wiley; 2002.
2. Plechkova NV, Seddon KR. Applications of ionic liquids in the chemical industry. Chem. Soc. Rev. 2008;37:123–50.
3. Attri P, Venkatesu P, Kumar A, Byrne N. A protic ionic liquid attenuates the deleterious actions of urea on α-chymotrypsin. Phys. Chem. Chem. Phys. 2011;13:17023–6.
4. Yue Y, Jiang X-Y, Yu J-G, Tang K-W. Enantioseparation of mandelic acid enantiomers in ionic liquid aqueous two-phase extraction systems. Chem. Pap. 2013;68:465–71.
5. Hernoux-Villière A, Lévêque J-M, Kärkkäinen J, Papaiconomou N, Lajunen M, Lassi U. Task-specific ionic liquid for the depolymerisation of starch-based industrial waste into high reducing sugars. Catal. Today. Elsevier B.V.; 2014;223:11–7.
6. Suzuki T, Kono K, Shimomura K, Minami H. Preparation of cellulose particles using an ionic liquid. J. Colloid Interface Sci. Elsevier Inc.; 2014;418:126–31.
7. Seddon KR. Review Ionic Liquids for Clean Technology. J. Chem. Tech. Biotechnol. 1997;68:351–6.
8. Greaves TL, Drummond CJ. Protic ionic liquids: properties and applications. Chem. Rev. 2008;108:206–37.
9. Rogers RD, Seddon KR. Ionic liquids-Solvents of the future? Science. 2003;302:792–3.
10. Welton T. Ionic liquids in catalysis. Coord. Chem. Rev. 2004;248:2459–77.
11. Gutmann V. Empirical parameters for donor and acceptor properties of solvents. Electrochim. Acta. 1976;21:661–70.
12. Gutmann V. The Donor Acceptor Approach to Molecular Interaction. New York: Plenum; 1978. p. 1978.
13. Porcedda S, Marongiu B, Schirru M, Falconieri D, Piras A. Excess enthalpy and excess volume for binary systems of two ionic liquids + water. J. Therm. Anal. Calorim. 2010;103:29–33.
14. Rodrìguez H; Brennecke JF. Temperature and Composition Dependence of the Density and Viscosity of Binary Mixtures of Water + Ionic Liquid. J. Chem. Eng. Data. 2006;51:2145–55.
15. García-Miaja G, Troncoso J, Romaní L. Excess enthalpy, density, and heat capacity for binary systems of alkylimidazolium-based ionic liquids + water. J. Chem. Thermodyn. Elsevier Ltd; 2009;41:161–6.
16. Guan W, Li L, Wang H, Tong J, Yang J. Studies on thermochemical properties of ionic liquids based on transition metal. J. Therm. Anal. Calorim. 2008;94:507–10.
17. Bicak N. A new ionic liquid: 2-hydroxy ethylammonium formate. J. Mol. Liq. 2005;116:15–8.
18. Waichigo MM, Riechel TL, Danielson ND. Ethylammonium Acetate as a Mobile Phase Modifier for Reversed Phase Liquid Chromatography. Chromatographia. 2004;61:17–23.
19. Waichigo MM, Danielson ND. Ethylammonium formate as an organic solvent replacement for ion-pair reversed-phase liquid chromatography. J. Chromatogr. Sci. 2006;44:607–14.
20. Chhotaray PK, Gardas RL. Thermophysical properties of ammonium and hydroxylammonium protic ionic liquids. J. Chem. Thermodyn. Elsevier Ltd; 2014;72:117–24.
21. Anouti M, Caillon-Caravanier M, Dridi Y, Jacquemin J, Hardacre C, Lemordant D. Liquid densities, heat capacities, refractive index and excess quantities for {protic ionic liquids+water} binary system. J. Chem. Thermodyn. Elsevier Ltd; 2009;41:799–808.
22. Iglesias M, Torres A, Gonzalez-Olmos R, Salvatierra D. Effect of temperature on mixing thermodynamics of a new ionic liquid: {2-Hydroxy ethylammonium formate (2-HEAF)+short hydroxylic solvents}. J. Chem. Thermodyn. 2008;40:119–33.

23. Greaves TL, Ha K, Muir BW, Howard SC, Weerawardena A, Kirby N, et al. Protic Ionic Liquids (PILs) Nanostructure and Physicochemical Properties: Development of High- Throughput Methodology for PIL Creation and Property Screens Tamar. Phys. Chem. Chem. Phys. 2014;
24. Greaves TL, Weerawardena A, Fong C, Krodkiewska I, Drummond CJ. Protic ionic liquids: solvents with tunable phase behavior and physicochemical properties. J. Phys. Chem. B. 2006;110:22479–87.
25. Waichigo MM, Danielson ND. Comparison of ethylammonium formate to methanol as a mobile-phase modifier for reversed-phase liquid chromatography. J. Sep. Sci. 2006;29:599–606.
26. Marsh, KN, Richards AE. Excess volumes for ethanol + ethanol mixtures at 10-K intervals from 278.15 to 338.15 K. Aust. J. Chem. 1980;33:2121–32.
27. Porcedda S, Usula M, Marongiu B. Physical-Chemical Properties of Ionic Liquid-Containing Mixtures. In: The Structure of Ionic Liquids, Soft and Biological Matter. Caminiti R, Gontrani L, editors. Springer International Publishing Switzerland; 2014. p. 171–91.
28. Abbott MM, Van Ness HC. Vapor-liquid equilibrium: Part III. Data reduction with precise expressions for GE. AIChE J. American Institute of Chemical Engineers; 1975;21:62–71.
29. Matteoli E, Lepori L, Spanedda A. Thermodynamic study of heptane + amine mixtures. Fluid Phase Equilib. 2003;212:41–52.
30. Matteoli E, Gianni P, Lepori L. Thermodynamic study of heptane + secondary, tertiary and cyclic amines mixtures. Part IV. Excess and solvation enthalpies at 298.15K. Fluid Phase Equilib. Elsevier B.V.; 2011;306:234–41.
31. Usula M, Matteoli E, Leonelli F, Mocci F, Cesare Marincola F, Gontrani L, et al. Thermo-physical properties of ammonium-based ionic liquid + N-methyl-2-pyrrolidone mixtures at 298.15K. Fluid Phase Equilib. Elsevier B.V.; 2014;383:49–54.
32. Marsh KN. Excess enthalpies of Benzene+cyclohexane mixtures. Int. Data Ser. Sel. Data Mix. Ser. A. 1973;1–5.
33. Freemantle M. An Introduction to Ionic Liquid. Freemantle M, editor. Cambridge, UK: RSC Publishing; 2010.
34. Bonhôte P, Dias A-P, Armand M, Papageorgiou N, Kalyanasundaram K, Grätzel M. Hydrophobic, Highly Conductive Ambient-Temperature Molten Salts. Inorg. Chem. 1998;37:166.
35. Wassercheid P, Keim W. Angew. Chem. Int. Ed. 2000;39:3772–89.
36. Riddick JA, Bunger WB, Sakano TK. Organic Solvents. fourth edi. New York: Wiley-Interscience; 1986. p. 1986.
37. Schmeisser M, Illner P, Puchta R, Zahl A, van Eldik R. Gutmann donor and acceptor numbers for ionic liquids. Chemistry. 2012;18:10969–82.
38. Estager J, Oliferenko A, Seddon KR, Swadźba-Kwaśny M. Chlorometallate(III) ionic liquids as Lewis acidic catalysts - a quantitative study of acceptor properties. Dalton Trans. 2010;39:11375–82.

Table 1
Investigated EAX ionic liquids: name with abbreviation, % yield of the synthesis, final water content, and purification and analysis methods.

Chemical name (abbreviation)	% yield	Purification method	Final water content /mole fraction	Analysis method
ethylammonium metanoate (EAM)	97	dehydration *in vacuo*	< 0.006	Karl-Fisher titration
ethylammonium propanoate (EAP)	97	dehydration *in vacuo*	< 0.006	Karl-Fisher titration
ethylammonium butanoate (EAB)	98	dehydration *in vacuo*	< 0.006	Karl-Fisher titration

Table 2
Quantities of components for the EAX ionic liquids systems used to prepare solutions for ^{31}P NMR spectroscopy; ^{31}P chemical shift of TEPO, and Gutmann Acceptor Numbers of reference solvent and each selected ionic liquid.

Solvent	Mass /g		mol % TEPO	^{31}P δ_{TEPO}	AN
	EAX	TEPO			
EAM	1.0188	0.0442	3	72.333	**69.3**
	1.0223	0.0734	5	72.225	
	1.0138	0.1023	7	72.095	
EAP	1.0018	0.0342	3	70.848	**65.7**
	1.0295	0.0504	5	70.797	
	1.0075	0.0804	7	70.711	
EAB	1.0159	0.0307	3	70.764	**65.4**
	1.0090	0.0509	5	70.742	
	1.0093	0.0716	7	70.681	

Table 3
Values of the coefficients, a_i, obtained from the Redlich-Kister equation (4) with the standard deviations, $\sigma(V^E)$. Values of excess molar volumes at equimolar composition, $V^E_{x=0.5}$, of excess partial molar volumes at infinite dilution for each component, $\bar{V}_k^{E,\infty}$, and of associated uncertainties, u.

System	a_0	a_1	a_2	a_3	$\sigma(V^E)$	$V^E_{x=0.5} \pm u$	$\bar{V}_1^{E,\infty} \pm u$	$\bar{V}_2^{E,\infty} \pm u$
	$10^{-6} \times m^3\ mol^{-1}$							
EAM + W	-3.52	2.09	-1.43	0.71	0.0006	-0.88±0.01	-7.76±0.02	-2.15±0.02
EAP + W	-4.72	3.19	-3.10	2.46	0.007	-1.18±0.01	-13.5±0.2	-2.2±0.2
EAB + W	-4.37	2.66	-3.43	3.17	0.001	-1.09±0.02	-13.6±0.6	-2.0±0.6

Table 4

Values of the coefficients obtained from the Redlich-Kister equation (6), of excess molar enthalpies at equimolar composition, $H^{E}_{x=0.5}$, of excess partial molar enthalpies at infinite dilution for each component, $\bar{H}^{E,\infty}_{k}$, and of associated uncertainties, u.

System	c_0	c_1	c_2	c_3	c_4	c_5	$H^{E}_{x=0.5} \pm u$ /J mol^{-1}	$\bar{H}^{E,\infty}_{1} \pm u$ /kJ mol^{-1}	$\bar{H}^{E,\infty}_{2} \pm u$ /kJ mol^{-1}
EAM + W	0.69	-1.500	-2.198	0	0	0	-929±3	-10.2±0.2	-2.53±0.03
EAP + W	7.26	-1.81	-4.41	1.19	4.77	-5.73	-1120±15	-20±3	-3.2±0.3
EAB + W	-8.45	-1.55	-6.71	3.89	2.01	-6.98	-960±19	-22±5	-3.1±0.3

Table 5

Mixture composition expressed as the mole fraction of EAX, x_1, experimental density, ρ, molar volumes, V_m, and excess molar volumes, V^E, values at 298.15 K and 0.1 MPa of EAX (1) + W (2) mixtures.[a]

System	x_1	$10^{-3} \times \rho$ /kg m^{-3}	$10^{6} \times V_m$ /m^3 mol^{-1}	$10^{6} \times V^E$ /m^3 mol^{-1}	x_1	$10^{-3} \times \rho$ /kg m^{-3}	$10^{6} \times V_m$ /m^3 mol^{-1}	$10^{6} \times V^E$ /m^3 mol^{-1}
EAM (1) + W (2)	0.000	0.99704	18.07	0.00	0.625	1.04167	61.18	-0.72
	0.090	1.03176	23.84	-0.54	0.718	1.03948	67.84	-0.57
	0.200	1.04552	31.20	-0.87	0.834	1.03691	76.15	-0.35
	0.332	1.04766	40.34	-0.98	0.905	1.03539	81.26	-0.21
	0.386	1.04701	44.13	-0.97	1.000	1.03354	88.15	0.00
	0.495	1.04480	51.86	-0.89				
EAP (1) + W (2)	0.000	0.99704	18.07	0.00	0.624	0.99997	81.12	-0.97
	0.093	1.02726	26.66	-0.92	0.716	0.99597	90.84	-0.74
	0.200	1.02592	37.28	-1.31	0.821	0.99245	101.78	-0.49
	0.325	1.01697	50.06	-1.38	0.895	0.99013	109.66	-0.28
	0.398	1.01204	57.57	-1.33	1.000	0.98742	120.68	0.00
	0.500	1.00591	68.17	-1.19				
EAB (1) + W (2)	0.000	0.99704	18.07	0.00	0.605	0.97475	89.91	-0.93
	0.089	1.01358	27.94	-0.90	0.711	0.97061	102.97	-0.73
	0.198	1.00347	40.69	-1.23	0.839	0.96630	118.70	-0.43
	0.331	0.99113	56.64	-1.28	0.901	0.96449	126.33	-0.26
	0.401	0.98595	65.12	-1.23	1.000	0.96200	138.45	0.00
	0.497	0.98010	76.83	-1.12				

[a]Standard uncertainties u are $u(T)$=0.01 K, $u(x_1)$=0.001, $u(V^E)$=0.01×10^{-6} m^3 mol^{-1}, $u(V_m)$=0.01 ×10^{-6} m^3 mol^{-1}

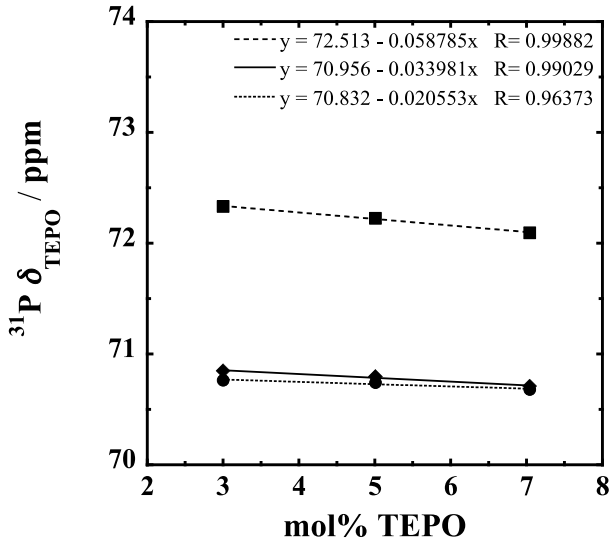

Fig. 1 Experimental ^{31}P-NMR chemical shifts for TEPO as a function of TEPO concentration in selected EAX compositions (see Table 2). Linear regression was used to extrapolate these data to infinite dilution, δ_{inf} /ppm. Symbols: ■, EAM; ♦, EAP; ●, EAB.

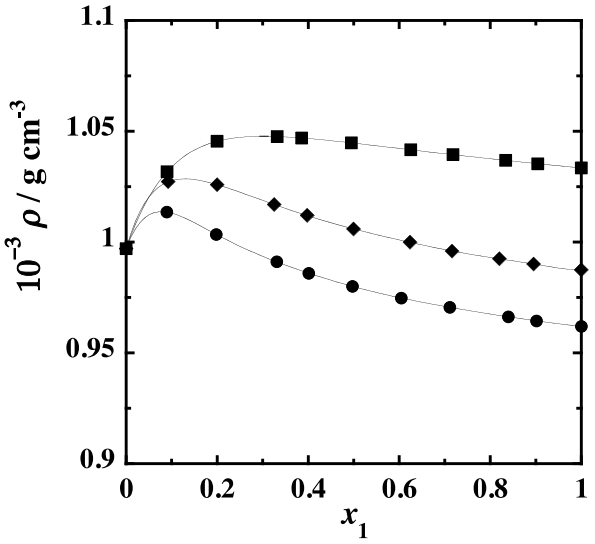

Fig. 2 Experimental densities, ρ, at 298.15 K and 0.1 MPa, of EAX (1) + W (2) mixtures as a function of x_1, the mole fraction of component (1). Symbols: ■, EAM + W; ♦, EAP + W; ●, EAB + W.

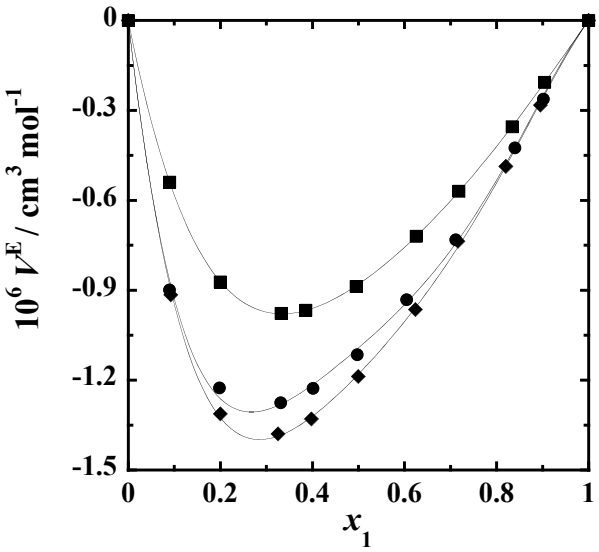

Fig. 3 Excess molar volumes, V^E, of EAX (1) + W (2) mixtures at 298.15 K and 0.1 MPa as a function of x_1, the mole fraction of component (1). The V^E curve is calculated with the a_i-parameters Redlich–Kister equation (3) reported in Table 3. Symbols: ■, EAM + W; ♦, EAP + W; ●, EAB + W.

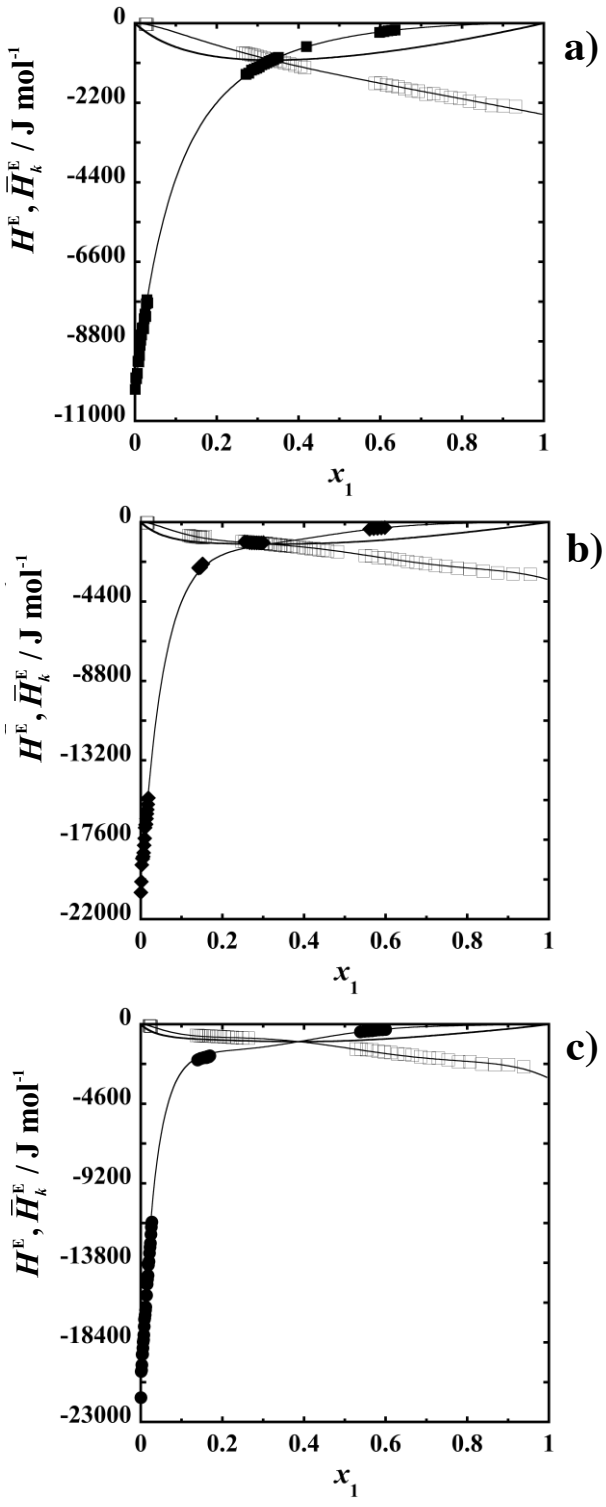

Fig. 4 Molar excess enthalpies, H^E, and excess partial molar enthalpies, $\bar{H}_k^E$, for the binary mixtures EAX (1) + W (2) as function of x_1, the mole fraction of component (1), at 298.15 K and 0.1 MPa. a) EAM + W system; b) EAP + W system; c) EAB + W system. $\bar{H}_1^E$, full symbols: ■, EAM; ♦, EAP; ●, EAB; and $\bar{H}_2^E$, □, W. Curves fitting are calculated with the parameters of the Redlich-Kister equation (6) reported in Table 4.

Supporting Material of

Ethylammonium Alkanoate-based Ionic Liquid + Water Mixtures: A Calorimetric and Volumetric Study at 298.15 K

Marianna Usula[a], Natalia V. Plechkova[b], Alessandra Piras[a], Silvia Porcedda[a,*]

[a] *Dipartimento di Scienze Chimiche e Geologiche - Università degli Studi di Cagliari, Cittadella Universitaria di Monserrato, S.P. 8, I-09042 Monserrato (Italy)*

[b] *QUILL, The Queen's University of Belfast, Stranmillis Road, Belfast, Northern Ireland, UK BT9 5AG.*

KEYWORDS: ethylammonium, methanoate, propanoate, butanoate, molar excess volume and enthalpy.

***Corresponding author.** Phone: +390706754415; fax: +390706754388. E-mail address: porcedda@unica.it

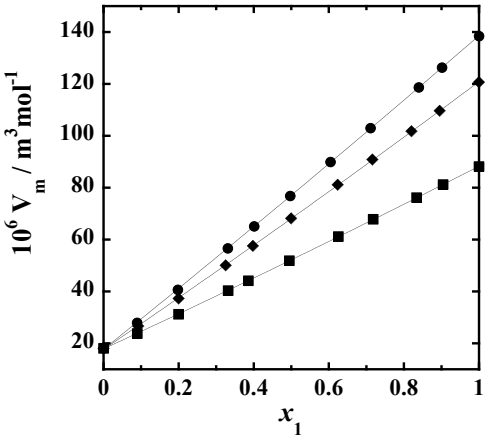

Fig. S1. Molar volumes, V_m, of EAX (1) + W (2) mixtures at 298 K and 0.1 MPa as a function of x_1, the mole fraction of component (1). The V_m curves are calculated with a 2nd degree polynomial equation. Symbols: ■, EAM + W; ♦, EAP + W; ●, EAB + W.

IV.1 Supplementary Data

IV.1.1. FT-IR experiments of EAX (1) + Water (2) systems

A comprehension at molecular level of the state of water dissolved in ILs is needed for further understanding of ILs as media for different kind of applications. Infrared spectroscopy is one of the most powerful techniques to probe the molecular state of water present in solvents. The vibrational modes of water that result in bands in the IR spectrum are very sensitive to the environment and to the state of water association via H-bonding.[1,2] Stretching modes of water have been used to understand the type of bonding between water molecules and many chemical substances. The water molecule has C_{2v} symmetry with three IR active vibrations: the bending IR band (ν_2) of water (either pure or dissolved in solvents), which usually absorbs in the region [1650-1595] cm^{-1}, and the antisymmetric (ν_3) and symmetric (ν_1) stretching bands of water, which usually lie in the region [3800-3000] cm^{-1}.[3,4] It should be remarked that is quite difficult to deduce information on the molecular state of water dissolved in various solvents based on the shifts of the stretching bands of water because there is a strong correlation between the ν_3 and ν_1 bands.

FT-IR spectra were recorded using a Perkin Elmer Spectrum100 in the range of [3800-600] cm^{-1}. As can be seen in Figure IV.1, two distinct bands corresponding to the ν_3 and ν_1 modes of water dissolved in EAX are in the range [3600-3200] cm^{-1}. Taking into account that the ν_3 and ν_1 bands in water vapor absorb at [3756 and 3657] cm^{-1} respectively,[3,4] and that these bands shift to lower wavenumber when water interacts with a solvent, the position of these two bands indicates that the water molecules can be

assigned as “free" water molecules interacting via H-bonding with the ionic liquids. This assignment is consistent with the literature data on the spectroscopic manifestation of the formation of symmetrical complexes of water molecules with bases such as: COO^----H-O-H--- ^-OOC.[3,4]

Further structural information from IR spectra can be achieved with computational simulations.

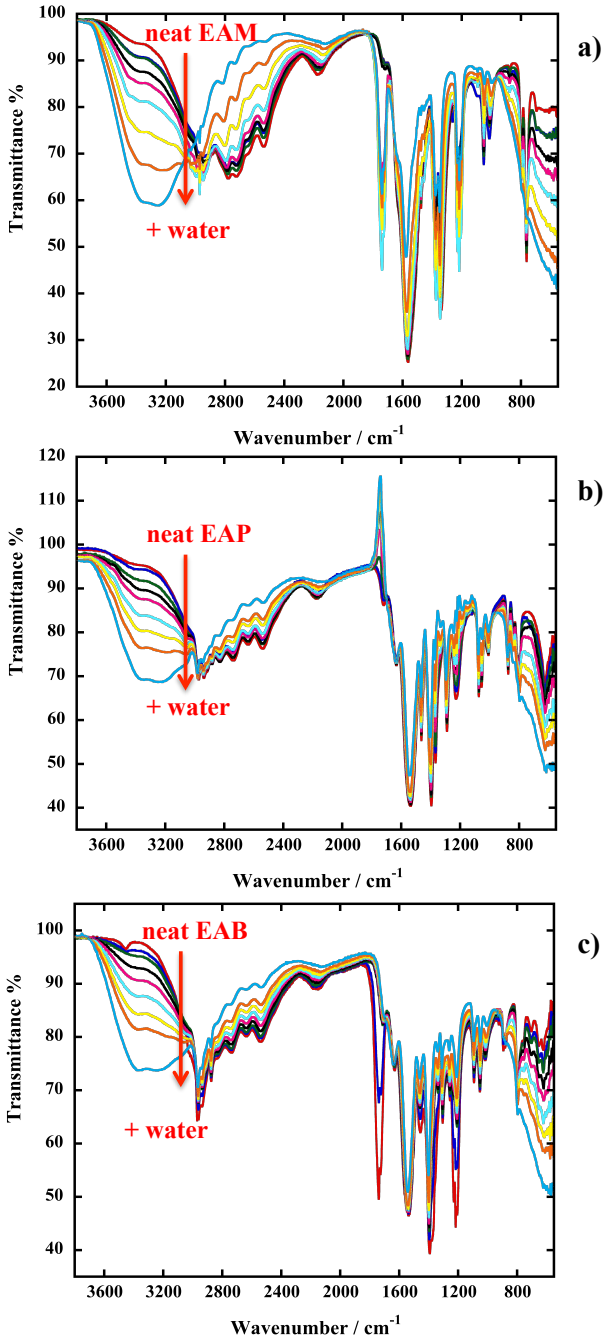

Figure IV.1. FT-IR spectra of EAX (1) + Water (2) mixtures. a) EAM; b) EAP; c) EAB.

IV.1.2. Volumetric and calorimetric data of EAX (1) + NMP (2) systems

Mixture composition, experimental densities, molar volumes, and excess molar volumes for each investigated EAX (1) + NMP (2) mixtures are reported in Table IV.1. Each density value represents the mean of two determinations. In Figure IV.2, the density values of the EAX (1) + NMP (2) mixtures are plotted with respect to x_1. The densities of the ILs containing the same cation, and similar anions, increase with increasing molecular weight of the associated anion.[5]

For EAP-containing mixtures the density trend is almost perfectly linear whereas the curves representing EAB-containing mixtures shows a moderate upwards concavity and that representing EAM + NMP exhibits a downward concavity.

Excess molar volumes, V^E, (Figure IV.1) are negative and quite small in absolute value, especially if compared to the volume contraction that these ILs exhibited in water (PAPER IV). V^E curves show a minimum at different x_1: EAM in the region of lower values of the more polar component, the IL; EAP approximately at equimolar composition; EAB in the IL-rich region. The V^E curves do not follow the order suggested by the alkyl chain length of the EAX and the higher volume contraction (-0.5×10^{-6} m^3 mol^{-1}) is showed by EAB. These results demonstrate that the anion affected significantly the IL-NMP interactions.

By observing the $\overline{V}_k^{E,\infty}$ values reported in Table IV.2, it can be noticed that all values are negative. In EAP + NMP system, $\overline{V}_k^{E,\infty}$ of both components have small similar values, [-0.562 and -0.530] cm^3 mol^{-1}, while

in EAM + NMP system, $\overline{V}_1^{E,\infty}$ is around 8 times greater (in absolute value) than $\overline{V}_2^{E,\infty}$ and in EAB + NMP system $\overline{V}_2^{E,\infty}$ is 2.5 times greater than $\overline{V}_1^{E,\infty}$. The largest volume contraction of a component at infinite dilution with respect to the neat state, expressed by $\left(\overline{V}_K^{E,\infty} / V_K^*\right) \cdot 100$, is showed by EAM (-2.5 %) and by NMP (-2.4 %) in the EAB-containing mixture.

Complementary information was obtained by the calorimetric determination of the heat of mixing by means of the ITC technique. We obtained, in a direct manner, the excess partial molar enthalpy of each component, $\overline{H}_k^E$, and the value of the heat of mixing coinciding with H^E for the mixtures under investigation. In Figure IV.3, the experimental points and the smoothed curves of $\overline{H}_k^E$ and H^E for the EAX + NMP mixtures are plotted as a function of the mole fraction of EAX, x_1. By comparing H^E curves, better visible in Figure IV.4, EAP and EAB when are mixed with NMP generate a weak endothermic effect in the NMP-rich region, while in the IL-rich region mixing is exothermic for the formation of mixtures containing EAP and, to a lesser extent, EAM. In the case of the EAM + NMP system, we found a moderate exothermic mixing effect in the whole concentration range. H^E curve of EAM + NMP is quite symmetric as suggested also by the coordinates of the minima, calculated from the RK coefficients of 0.55, -867.5 J mol^{-1}. EAP and EAB systems showed H^E curves quite asymmetric, due to the non-specular peculiar shape of $\overline{H}_k^E$, with the following coordinates of the minima, calculated from the RK coefficients: (0.15, 223.2 J mol^{-1}) for EAP + W; and (0.24, 325.9 J mol^{-1}) for EAB + W system. If we compare the H^E values of the three systems, we can observe

that a longer alkyl chain in the carboxylic anion prevent the IL-solvent interaction, while a shorter alkyl chain favoured it. By comparing excess partial molar enthalpies at infinite dilution of EAX and NMP reported in Table IV.3, it can be noticed that the absolute value of $\bar{H}_2^{E,\infty}$ values are negative and they decrease, in absolute value, as the alkyl chain length of the anion increase. On the other hand $\bar{H}_1^{E,\infty}$ increases notably from EAM to EAB passing from -1.6 kJ mol^{-1} to the positive values, (25 and 22) kJ mol^{-1} for EAP and EAB, respectively. For EAP or EAB + NMP mixtures the dissolution of the solvent at infinite dilution is exothermic while the solubilisation of the IL at infinite dilution in NMP is associated to a quite strong endothermic effect.

NMP reveals itself unable to exert strong attractive interactions towards EAX as, for example water does (PAPER IV), probably because of the well-known different capability to interact via hydrogen bond. EAM + NMP system shows a very particular behaviour; moreover it is not fully coherent with the other similar systems. A search in the literature revealed that mehanoate ionic liquids are very prone to amide formation, c.a. 25 % of amide after 4 years.[6] Since these calorimetric measurements were done one year later the synthesis, the not negligible amount of decomposition compounds that have contaminate our samples, could have influenced the global thermal effect measured also. The calorimetric data concerning EAM + NMP need to be validate before they can be submitted for publication.

Table IV.1

Mixture composition expressed as the mole fraction of EAX, x_1, experimental density, ρ, molar volumes, V_m, and excess molar volumes, V^E, values at 298.15 K and 0.1 MPa of EAX (1) + NMP (2) mixtures.[a]

System	x_1	$10^{-3}\times\rho$ /kg m^{-3}	$10^{6}\times V_m$ /m^3 mol^{-1}	$10^{6}\times V^E$ /m^3 mol^{-1}	x_1	$10^{-3}\times\rho$ /kg m^{-3}	$10^{6}\times V_m$ /m^3 mol^{-1}	$10^{6}\times V^E$ /m^{3}mol^{-1}
EAM (1) + NMP (2)	0.000	1.02793	96.44	0.00	0.624	1.03479	90.96	-0.29
	0.091	1.03019	95.52	-0.16	0.715	1.03458	90.27	-0.22
	0.199	1.03209	94.51	-0.28	0.834	1.03415	89.39	-0.11
	0.336	1.03368	93.29	-0.35	0.902	1.03392	88.88	-0.05
	0.396	1.03419	92.78	-0.36	1.000	1.03393	88.12	0.00
	0.499	1.03460	91.94	-0.34				
EAP (1) + NMP (2)	0.000	1.02802	96.43	0.00	0.606	1.00456	110.76	-0.17
	0.089	1.02432	98.52	-0.04	0.714	1.00041	113.39	-0.14
	0.199	1.02012	101.09	-0.11	0.831	0.99611	116.22	-0.10
	0.333	1.01505	104.23	-0.17	0.914	0.99380	118.16	-0.14
	0.393	1.01264	105.66	-0.17	1.000	0.98994	120.37	0.00
	0.501	1.00854	108.25	-0.18				
EAB (1) + NMP (2)	0.000	1.02802	96.43	0.00	0.090	1.02042	100.14	-0.07
	0.090	1.02042	100.14	-0.07	0.625	0.98464	122.31	-0.40
	0.200	1.01234	104.66	-0.19	0.716	0.97851	126.23	-0.29
	0.327	1.00373	109.84	-0.32	0.829	0.9726	130.95	-0.31
	0.401	0.99873	112.92	-0.35	0.910	0.96741	134.52	-0.16
	0.493	0.99241	116.80	-0.34	1.000	0.962	138.45	0.00

[a]Standard uncertainties, u, are $u(T)$=0.01 K, $u(x_1)$=0.001, $u(V^E)$=0.01×10^{-6} m^3 mol^{-1}, $u(V_m)$=0.01×10^{-6} m^3 m

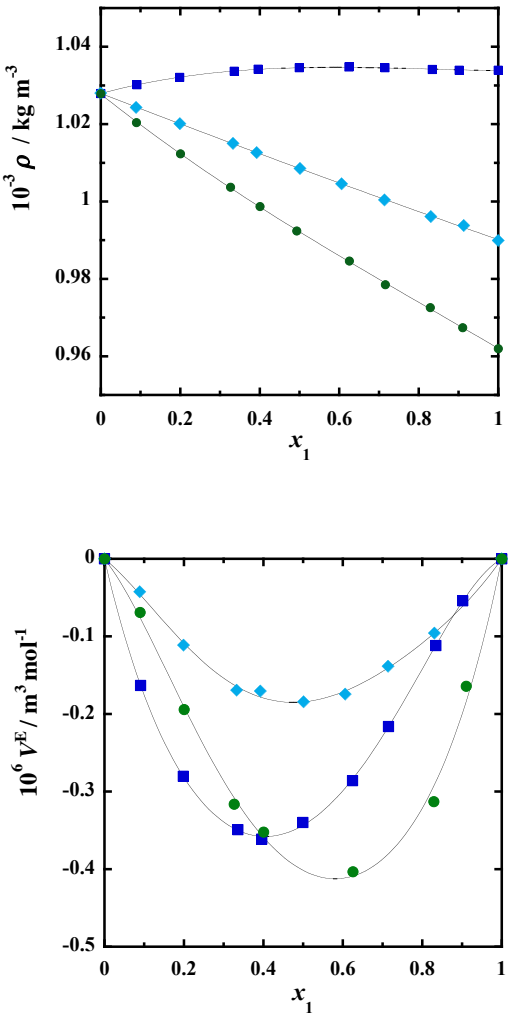

Figure IV.2. Experimental densities, ρ, and excess molar volumes, V^E, of EAX (1) + NMP (2) mixtures as a function of x_1, the mole fraction of component (1). The V^E curve is calculated with the a_i-parameters of the RK equation reported in Table IV.2. Symbols: ■, EAM; ♦, EAP; ●, EAB.

Table IV.2

Values of the coefficients, a_i, and standard deviations, $\sigma(V^E)$ obtained from the RK equation. Values of excess molar volumes at equimolar composition, $V^E_{x=0.5}$, excess partial molar volumes at infinite dilution for each component, $\overline{V}_k^{E,\infty}$, and associated uncertainties, u.

System	a_0	a_1	a_2	a_3	$\sigma(V^E)$	$V^E_{x=0.5} \pm u$	$\overline{V}_1^{E,\infty} \pm u$	$\overline{V}_2^{E,\infty} \pm u$
						$10^{-6} \times m^3\ mol^{-1}$		
EAM + NMP	-1.37	0.60	0.14	0.36	0.0003	-0.343±0.001	-2.195±0.003	-0.280±0.003
EAP + NMP	-0.74	0.02	0.20	0	0.0002	-0.185±0.003	-0.562±0.005	-0.531±0.005
EAB + NMP	-1.61	-0.69	0	0	0.001	-0.403±0.007	-0.923±0.006	-2.300±0.006

Table IV.3

Values of the coefficients, c_i, obtained from the RK equation, excess molar enthalpies at equimolar composition, $H^E_{x=0.5}$, excess partial molar enthalpies at infinite dilution for each component, $\overline{H}_k^{E,\infty}$, and associated uncertainties, u.

System	c_0	c_1	c_2	c_3	c_4	c_5	$H^E_{x=0.5} \pm u$ /J mol^{-1}	$\overline{H}_1^{E,\infty} \pm u$ /kJ mol^{-1}	$\overline{H}_2^{E,\infty} \pm u$ /kJ mol^{-1}
EAM + NMP	0.58	-1.38	-1.11	0	0	0	-858±5	-1.6±0.2	-3.9±0.1
EAP + NMP	0.98	0.09	-0.52	-0.57	-0.13	0	56±10	25±11	-1.42±0.09
EAB + NMP	0.98	0.35	-0.21	-0.40	0	0	218±8	22±6	-0.3±0.05

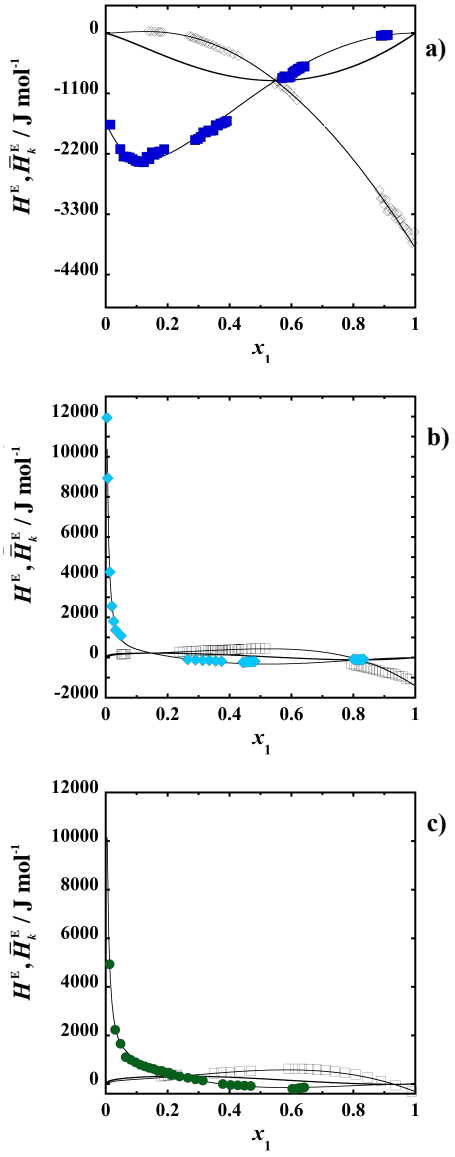

Figure IV.3. Molar excess enthalpies, H^E, and excess partial molar enthalpies, $\overline{H}_k^E$, for the binary mixtures EAX (1) + NMP (2) as a function of x_1, the mole fraction of component (1), at 298.15 K and 0.1 MPa. $\overline{H}_1^E$, full symbols: ■, EAM; ♦, EAP; ●, EAB; and $\overline{H}_2^E$, □, NMP. Curves fitting are calculated with the parameters of the RK equation reported in Table IV.3.

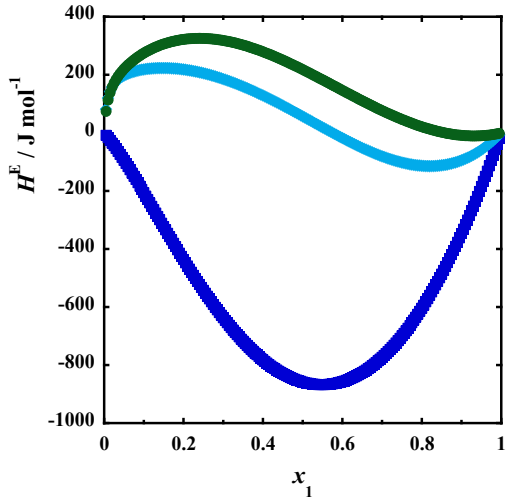

Figure IV.4. Molar excess enthalpies, H^E, for the binary mixtures EAX (1) + NMP (2) as function of x_1, the mole fraction of component (1), at 298.15 K and 0.1 MPa. Symbols: ■, EAM; ♦, EAP; ●, EAB.

REFERENCES

(1) Ludwig, R. Water: From Clusters to the Bulk. *Angew. Chemie Int. Ed.* **2001**, *40*, 1808–1827.

(2) Scatena, L. F.; Brown, M. G.; Richmond, G. L. Water at Hydrophobic Surfaces: Weak Hydrogen Bonding and Strong Orientation Effects. *Sci.* **2001**, *292* , 908–912.

(3) Conrad, M. P.; Strauss, H. L. Nearly Free Rotation of Water and Ammonia in Alkanes and Other Weakly Interacting Solvents. *J. Phys. Chem.* **1987**, *91*, 1668–1673.

(4) Backx, P.; Goldman, S. Water/water-d2 Solubility Isotope Effects. An Estimate of the Extent of Nonclassical Rotational Behavior of Water, When Dissolved in Benzene or Carbon Tetrachloride. *J. Phys. Chem.* **1981**, *85*, 2975–2979.

(5) Attri, P.; Venkatesu, P.; Kumar, A.; Byrne, N. A Protic Ionic Liquid Attenuates the Deleterious Actions of Urea on A-Chymotrypsin. *Phys. Chem. Chem. Phys.* **2011**, *13*, 17023–17026.

(6) Greaves, T. L.; Weerawardena, A.; Fong, C.; Krodkiewska, I.; Drummond, C. J. Protic Ionic Liquids: Solvents with Tunable Phase Behavior and Physicochemical Properties. *J. Phys. Chem. B* **2006**, *110*, 22479–22487.

Acknowledgments

I would like to express my gratitude to everyone who supported me throughout my PhD project. In particular, I express my warm thanks to my brilliant supervisor dr. Silvia Porcedda for her support and guidance during my PhD, and for her helpful teachings and comments. I would also like to sincerely thank my special "unofficial" supervisors, dr. Flaminia Cesare Marincola and dr. Francesca Mocci, for useful teachings and invaluable supervision in NMR experiments and MD Simulations, respectively. I am thankful to all of them for their truthful guidance, constructive advices, and their friendship during these years. I would also like to give a heartfelt, special thanks to prof. Bruno Marongiu for his supervision during my first PhD year.

Special thanks also go to prof. Ruggero Caminiti for sharing his illuminating views on a number of issues related to the project.

I am sincerely grateful to dr. Enrico Matteoli for insightful calorimetric comments and to the Istituto per i Processi Chimico-Fisici (IPCF-CNR) of Pisa, for allowing the use of calorimetric instrumentations and methods within the collaboration agreement between the Department of Chemical and Geological Science and IPCF.

My sincere thanks to prof. Kenneth R. Seddon and dr. Natalia V. Plechkova for the acceptance in Queen's University Ionic Liquid Laboratories (QUILL) during the Erasmus PlaceDoc, for their guidance, and for helpful discussions.

I gratefully acknowledge Sardinia Regional Government for the financial support of her PhD scholarship (P.O.R. Sardegna F.S.E. Operational Program of the Autonomous Region of Sardinia, European Social Fund 2007-2013 - Axis IV Human Resources, Objective l.3, Line of Activity l.3.1.).

In addition, these acknowledgements would not be complete if I did not mention my colleagues and friends Federica and Matteo. Thank you for your encouragement, support and most of all your humor. You both kept things light and me smiling. I wish you good luck and all the best.

Last but not least, I would like to thank my family and in particular my husband for their moral support throughout my life.

Marianna